Production of radioactive molecular beams for CERN-ISOLDE

Produktion radioaktiver molekularer Strahlen für CERN-ISOLDE
vom Fachbereich Physik der Technischen Universität Darmstadt zur Erlangung des Grades eines Doktors der Naturwissenschaften (Dr. rer. nat.) genehmigte
Dissertation von Dipl.-Phys. Christoph Seiffert aus Bad Nauheim
Juni 2015 — Darmstadt — D 17

TECHNISCHE UNIVERSITÄT DARMSTADT

Fachbereich Physik
Institut für Kernphysik, AG Kröll

Production of radioactive molecular beams for CERN-ISOLDE
Produktion radioaktiver molekularer Strahlen für CERN-ISOLDE

Dem Fachbereich Physik der Technischen Universität Darmstadt zur Erlangung des Grades eines Doktors der Naturwissenschaften (Dr. rer. nat.) genehmigteDissertation von Dipl.-Phys. Christoph Seiffert aus Bad Nauheim

1. Gutachten: Prof. Dr. Thorsten Kröll
2. Gutachten: Dr. Thierry Stora

Tag der Einreichung: 15.12.2014
Tag der Prüfung: 04.02.2015

Darmstadt — D 17

Erklärung zur Dissertation

Hiermit versichere ich, die vorliegende Dissertation ohne Hilfe Dritter nur mit den angegebenen Quellen und Hilfsmitteln angefertigt zu haben. Alle Stellen, die aus Quellen entnommen wurden, sind als solche kenntlich gemacht. Diese Arbeit hat in gleicher oder ähnlicher Form noch keiner Prüfungsbehörde vorgelegen.

Darmstadt, den 02.12.2014

(C. Seiffert)

Abstract

ISOLDE, the Isotope Separation On-Line facility, at CERN is a leading facility for the production of beams of exotic radioactive isotopes. Currently over 1000 different isotopes with half lives down to milliseconds can be extracted with beam intensities of up to 10^{11} ions per second. This variety is achieved by permanent investigations resulting in sophisticated target materials, target setups and ion sources. Although many isotopes are available at ISOLDE, the extraction of refractory elements is challenging. The high boiling points of these elements require the extraction in molecular form.
Carbon and boron, the subjects of this thesis, belong to the group of elements that are difficult to extract. Up to now reproducible extraction of exotic carbon isotopes ^{9}C and $^{17-20}$C is not successful. Furthermore beams of radioactive boron ^{8}B were never extracted at ISOLDE or any other ISOL facility. Hence there is a strong demand for beams of these isotopes.
Many different phenomena are involved in the extraction process from ISODLE target units and thus determine the beam intensity and purity. Radioactive isotopes are produced by impact of the 1.4 GeV proton beam on the target. After the production parts of the isotopes diffuse to the surface of the bulk material where evaporation or molecular formation takes place. During the migration from the target to the ion source chemical losses with the environment can occur.
Besides ionization to $q = +1$ ions, molecules can dissociate in the ion source. In some cases the cross section for the dissociation exceed the cross section for direct ionization by orders of magnitude.
To maximize the beam intensity each process has to be optimized by selection of target materials, target setup and operational conditions.
The goal of this thesis is to determine the hindering processes during extraction of exotic isotopes and identify target material and setup combination that will allow the production of radioactive ion beams of short lived carbon and boron in the future.
Therefore the diffusion of boron in target materials was studied. Stable boron was implanted into target material samples and later on irradiated with thermalized neutrons. Alpha particles occurring from the $^{10}\mathrm{B}(\mathrm{n},\alpha)^{7}\mathrm{Li}$ reaction allowed to monitor the amount of boron before and after heat treatment of the samples. This study lead to a choice of target material from which the release of ^{8}B was tested during the online period 2014.
The same implantation method was used for the production of samples which will serve the characterization of neutrons, emitted from the liquid lithium target (LiLiT) at the SARAF facility in Israel.
To identify target setups that allow an efficient formation and extraction of carbon oxide and boron fluoride, the chemical equilibrium with target materials and structural materials was calculated. The results of these calculations were experimentally tested at the ISOLDE off-line mass separator. The experimental setup consisted of a modified ISOLDE target unit that allowed the injection of reactive gases into the target container. In this way the dependency of the formation and release of carbon oxides and boron fluorides on temperature and materials present in the container was tested. Furthermore, the setup allowed studies of the ionization characteristics of these gases.
To complement the knowledge on the adsorption of carbon monoxide and carbon dioxide on target materials, the adsorption enthalpies on Yttria and Alumina were measured within a collaboration with the University of Pardubice, CZ.
The approach of extracting refractory elements as molecules was used for the production of a titanium fluoride beam. A sample of radioactive ^{44}Ti, produced at the Paul Scherrer Institute in Villigen, was inserted into an ISOLDE target unit. Injection of CF_4 allowed the formation and extraction of titanium as volatile $^{44}TiF_3^{+}$.

Zusammenfassung

ISOLDE, die Isotope Separation Online facility, am CERN ist eine führende Anlage für die Produktion radioaktiver Teilchenstrahlen. Derzeit können mehr als 1000 Isotope mit Halbwertszeiten bis zu wenigen Millisekunden und Strahlintensitäten von bis zu 10^{11} Ionen pro Sekunde extrahiert werden. Diese Vielzahl an möglichen Strahlen kann nur erreicht werden durch andauernde Verbesserungen von verwendeten Targetmaterialen, Targetaufbauten und Ionenquellen. Obwohl eine Vielzahl verschiedener Isotope bei ISOLDE verfügbar ist, ist die Extraktion refraktiver Elemente nach wie vor nicht in allen Fällen möglich. Der hohe Schmelzpunkt dieser Elemente erfordert die Extraktion als flüchtigere Molekuele. Die Elemente Kohlenstoff und Bor, das Thema dieser Arbeit, gehören zur der Gruppe der schwer zu extrahierenden Elemente. Bisher ist es nicht möglich, zuverlaessig Strahlen aus kurzlebigen neutronarmen ^{9}C sowie neutronreichen $^{17-20}$C herzustellen. Des Weiteren konnten bisher keine Strahlen aus radioaktivem ^{8}B bei ISOLDE oder einer anderen ISOL Anlage hergestellt werden. Folglich existiert ein grosser Bedarf an Strahlen bestehend aus diesen Isotopen.

Die Intensität und Reinheit mit welcher ein Isotop aus einem ISOLDE Target extrahiert werden kann hängt von einer Vielzahl von Prozessen ab. Nach der Erzeugung des Isotopes durch Wechselwirkung des 1.4 GeV Protonenstrahls mit dem Targetmaterial müssen diese vom Ort der Erzeugung zur Oberfläche des Targetmaterials diffundieren. Dort können Isotope verdampfen, oder im Falle von refraktiven Elementen, mit anderen Elementen zu Molekülen reagieren. Während der anschliessenden Migration zur Ionenquelle können Verluste durch chemische Reaktionen mit den umgebenden Materialen stattfinden. Im molekularen Fall können neben der Ionisation zu $q = +1$ Ionen Verluste durch Aufbruch der molekularen Bindung stattfinden. In manchen Fällen ist der Wirkungsquerschnitt für die Aufspaltung eines Moleküls um Grössenordnungen höher als die Ionisation. Um den resultierenden Teilchenstrom zu maximieren müssen all diese Prozesse optimiert werden. Dies geschieht durch geschickte Wahl von Targetmaterialen, des Targetaufbaus und Betriebsparametern. Das Ziel dieser Arbeit ist es, die Gründe zu identifizieren, welche bislang die verlässliche Extraktion von kurzlebigem Kohlenstoff und Bor verhinderten und Targetkombinationen zu finden, die es in Zukunft ermöglichen, Strahlen dieser Isotope für Experimente bei ISOLDE zur Verfügung zu stellen.

Dafür ist es notwendig die einzelnen Prozesse der Extraktion getrennt zu untersuchen. Um die Diffusion von Bor in Targetmaterialien zu untersuchen wurde stabiles ^{10}B mit Hilfe des ISOLDE Off-line Massenseparators in Proben von Targetmaterialien implantiert. Der hohe Neutroneneinfangs Wirkungsquerschnitt von $\sigma = 3840$ barn erlaubt, die Position und Teilchenzahl des implantierten Bors mittels der Reaktion $^{10}\mathrm{B}(\mathrm{n},\alpha)^{7}\mathrm{Li}$ zu untersuchen. Die Ergebnisse dieser Messungen führten zur Wahl des Targetmaterials für einen Online Experiment 2014, bei welchem die Extraktion von kurzlebigem ^{8}B erstmalig getestet wurde. Mit der gleichen Methode wurde ^{10}B in Aluminiumfolien implantiert. Diese werden in Zukunft benutzt um emittierte Neutronen des Liquid Lithium Targets (LiLiT) an der Saraf facility in Israel zu charakterisieren. Zur Identifikation von Targetmaterialien und strukturellen Materialien, welche die Formation und Extraktion von Kohlenstoffoxiden und Borfluoriden erlauben, wurde das chemische Gleichgewicht dieser Materialien berechnet. Die Ergebnisse dieser Berechnungen wurden experimentell am ISOLDE Offline Massenseparator getestet. Dafür wurde ein standard ISOLDE Target mit einer zusätzlichen Gasinjektion ausgestattet welche es erlaubt, Gase in den Targetcontainer zu injizieren und damit Extraktionseffizienzen zu bestimmen. Mit diesem Experiment wurde die Abhängigkeit der Bildung und Extraktion von Kohlenstoffoxiden und Borfluoriden von Temperatur und verwendeten Targetmaterialien untersucht. Darüber hinaus wurde die Ionisation dieser Moleküle sowie verschiedener Edelgase in der verwendeten VADIS Ionenquelle untersucht. Im Zuge einer Kollaboration mit der Universität Pardubice, CZ, wurden Adsorptionsenthalphien von Kohlenstoffmonoxid und Kohlenstoffdioxid auf Ytrriumoxid und Aluminiumoxid bestimmt.

Die Konzepte, welche für Kohlenstoff und Bor erarbeitet wurden konnten auf andere refraktive Elemente angewendet werden. Dies erlaubte die erfolgreiche Extraktion von radioaktivem Titan ^{44}Ti als $^{44}TiF_3{}^+$.

List of abbreviations and symbols

Abbreviation	Unit	Definition
A		Mass number of atom
CERN		European Organization for Nuclear Research
CNT		Carbon Nano Tubes
D	$m^2 \cdot s^{-1}$	Diffusion coefficient
D_0	$m^2 \cdot s^{-1}$	Diffusion pre-exponential factor
ϵ_0	F/m	Vacuum permittivity
ϵ_{diff}		Efficiency for the diffusion of an isotope to the surface of the target material
$\epsilon_{\text{Formation}}$		Efficiency for molecule formation
ϵ_{Ion}		Ionization efficiency
$\epsilon_{\text{Transport}}$		Efficiency taking into account chemical losses during effusion
ERAWAST		Exotic Radionuclides from Accelerator WAste for Science and Technology
FEBIAD		Forced Electron Beam Induced Arc Discharge (ion source)
f_{extr}		Extraction efficiency
ΔG	J	Gibbs free energy
ΔH_0	kJ/mol	Adsorption enthalpy
ISOLDE		Isotope Separator On Line DEvice
I_p	eV	Ionization potential
J	$mol/m^2 s$	Flux of diffusing isotope
k_B	$m^2 \cdot kg/s^2$	Boltzmann constant
K_c		Equilibrium constant for chemical reaction
λ_f	$1/s$	Fast decay constant
λ_s	$1/s$	Slow decay constant
λ_r	$1/s$	Rise time constant
N		Number of extracted isotopes
N_A	$1/mol$	Avogadro number
n_e	$1/cm^3$	Electron density
n_n	$1/cm^3$	Neutral atom density
N_0		Number of produced isotopes
m	kg	Mass
M	g/mol	Molar mass
MWCNT		Multi Walled Carbon Nano Tubes
P		Ionization probability
PSI		Paul Scherrer Institute
ϕ	mol/m^3	Concentration profile
Q	eV	Activation energy for diffusion
R	$eV/K \cdot mol$	Universal gas constant
RIB		Radioactive Ion Beam
RILIS		Resonance Ionization Laser Ion Source
ρ_A	g/cm^2	Areal density
SARAF		Soreq Applied Research Accelerator Facility
σ	$mbarn$	Production cross section
σ_{Ion}	$mbarn$	Ionization cross section
T	K	Temperature
τ	s	Residence time for single hit
t_{ads}	s	Total adsorption time
t_{diff}	s	Diffusion time

Continued on next page

t_{eff}	s	Migration time
U	V	Voltage
v	m/s	velocity
VADIS		Versatile Arc Discharge Ion Source
V_{Source}	cm^3	Ion source volume
W	eV	Work function
ξ		Extend of reaction

Contents

1 Radioactive Ion Beam Production and Phenomena

While an element and its chemical properties are defined by its number of protons and electrons, the number of neutrons in the nuclei can vary. Nuclei with the same number of protons but varying number of neutrons are called isotopes of an element. Certain combinations of protons and neutrons are known as the stable matter surrounding us. Other combinations where the number of neutrons is higher or lower than in the case of stable matter are unstable with half lives reaching up to billions of years. All known nuclei are listed in the nuclear chart where the stable isotopes form the so called valley of stability (see figure 1.1). Isotopes on the left or right side of the valley of stability decay via a variety of possible channels towards the valley of stability and eventually end up as a stable nuclei.

Since decades radioactive isotopes are used by researchers for manifold investigations. The study of nuclei and their properties is crucial for the understanding of processes in our universe such as the formation of matter or supernovae. But besides interest from nuclear physics and fundamental astrophysics other fields such as solid state physics show high interest in radioactive nuclei. Here radioactive nuclei are used as probes to investigate material properties and give an insight into the material.
Furthermore radioactive nuclei find an increasing number of applications in the field of medical physics and patient treatment. Besides using short lived isotopes as probes for imaging (e.g. positron emission tomography (PET) imaging with ^{18}F), radioactive isotopes are used for cancer treatment. Therefore suited isotopes (typically α or β^+ emitter) are attached to vectors which tend to accumulate in cancer cells, where these isotopes decay and deposit the energy locally. Hence less damage is caused to surrounding healthy tissue compared to conventional (γ) radiation therapies. The first approved alpha emitting radio-pharmaceutical drug uses $^{223}RaCl_2$ and targets prostate and bone cancer [1].
While some of the commonly used radioisotopes for medical applications can be produced via (p,n) reactions (e.g. $^{18}O(p,n)^{18}F$) using small cyclotrons with relatively low energy ($\geq 15MeV$), the production of most exotic isotopes requires sophisticated facilities. Historically these facilities are divided into two classes, depending on the applied technique for radioactive isotope production: the so called in-flight method and the Isotope Separation Online(ISOL) method. Although the methods are different, both techniques are based on a primary high energy beam hitting a so called target. The formation of radioactive isotopes takes place by spallation, fragmentation or fission of either the primary beam or the target nuclei. After the production, the desired isotopes need to be separated from the huge background at the interaction point. This process needs to be fast, efficient and highly selective in order to deliver pure beams of high intensity and assure the success of an experiment.
Depending on the nature of the isotope either the in-flight or the ISOL method are better suited.

1.1 Facilities for Radioactive Beam Production

In-Flight Method

The in-flight method is characterized by a primary ion beam hitting a thin target (100 nm to few cm) consisting of a light element (e.g. Be, C). The nature of the primary beam varies depending on the facility and desired production from light noble gases to heavy elements. The dominating process is the fragmentation of the projectile nuclei and therefore the production of isotopes lighter than these.

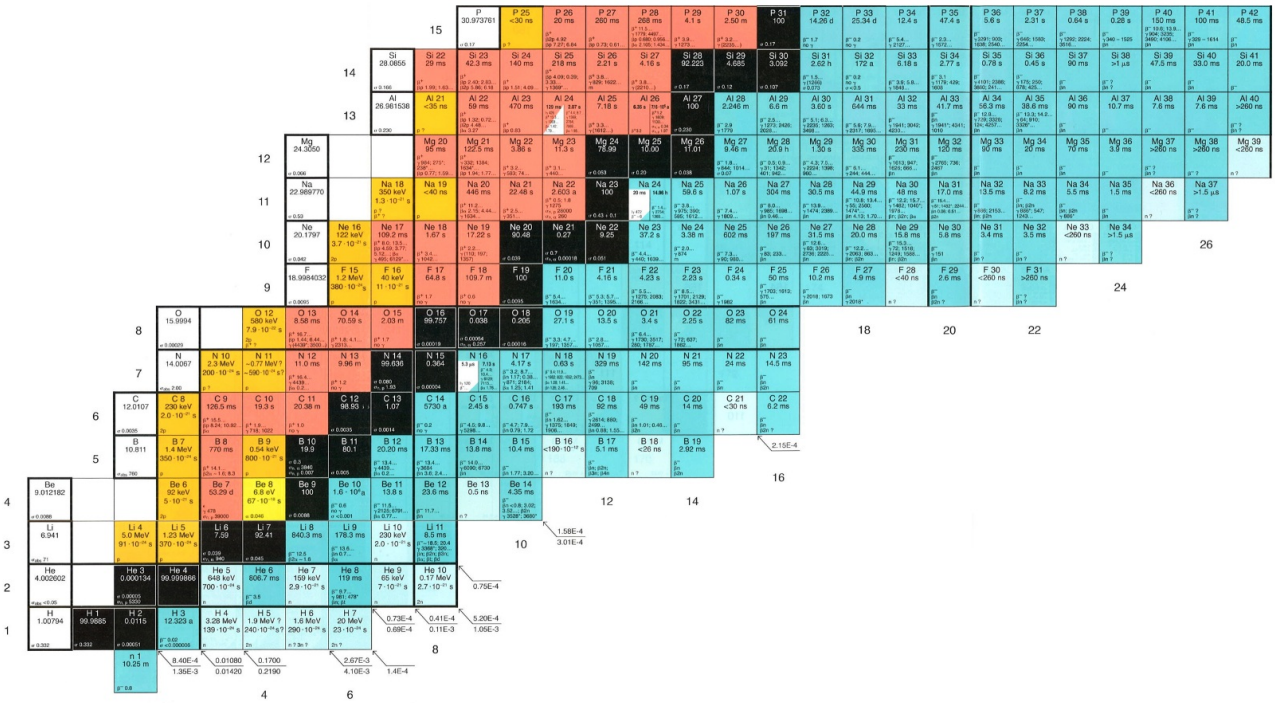

Figure 1.1.: Lower part of the nuclear chart showing light elements up to phosphorus. Each line represents one element with a fixed number of protons and varying number of neutrons. The stable isotopes are marked in black.

Different from the ISOL method (see next section) isotopes which are produced by the in-flight method don't need to be extracted from a target container, and therefore losses due to long transportation times are negligible. The delay from production to delivery of the isotope to the experiment is caused by the separation process and the time of flight. With energies of the secondary beam of more than 50 $\frac{MeV}{u}$ this time typically lies in the order of μs. This allows the study of very short lived isotopes. The extraction of the isotope of interest from the target happens due to the recoil energy itself and thus the in-flight method is not chemically dependent. This allows the equal extraction of chemically very reactive or refractory elements. A disadvantage of the In-flight method is the large emittance of the secondary beam. This is due to the random recoil momentum and angular distribution of the fragments coming from the target. Furthermore extractable yields are limited by the low production rate of this method and therefore experiments which require high amounts of isotopes are often not feasible. However this can be addressed with an increased intensity of the primary beam. Examples for currently operating facilities using the in-flight method are GSI (will be FAIR) in Darmstadt - Germany, RIKEN in Japan or NSCL/MSU (will be FRIB) in the United States [2].

ISOL Method

In ISOL facilities a thick target (ISOLDE: $l = 20$cm, $r = 1$ cm) is bombarded with an intense high energy beam of charged particles e.g. protons or heavier ions. The target usually consists of a heated metal container filled with a target material. The choice of target material depends on the desired isotopes and other parameters which will be discussed later. The particle beam penetrates the container over its whole length or is stopped towards the end of the container and produces a large set of isotopes along its path by interacting with the target material. Due to the large thickness of the target a high production rate of radioactive isotopes can be achieved. Different from the in-flight method, isotopes need to be extracted thermally out of the target material and the container. For the extraction containers are connected via a transfer line to an ion source. Here the species are ionized and extracted by an applied electrical field

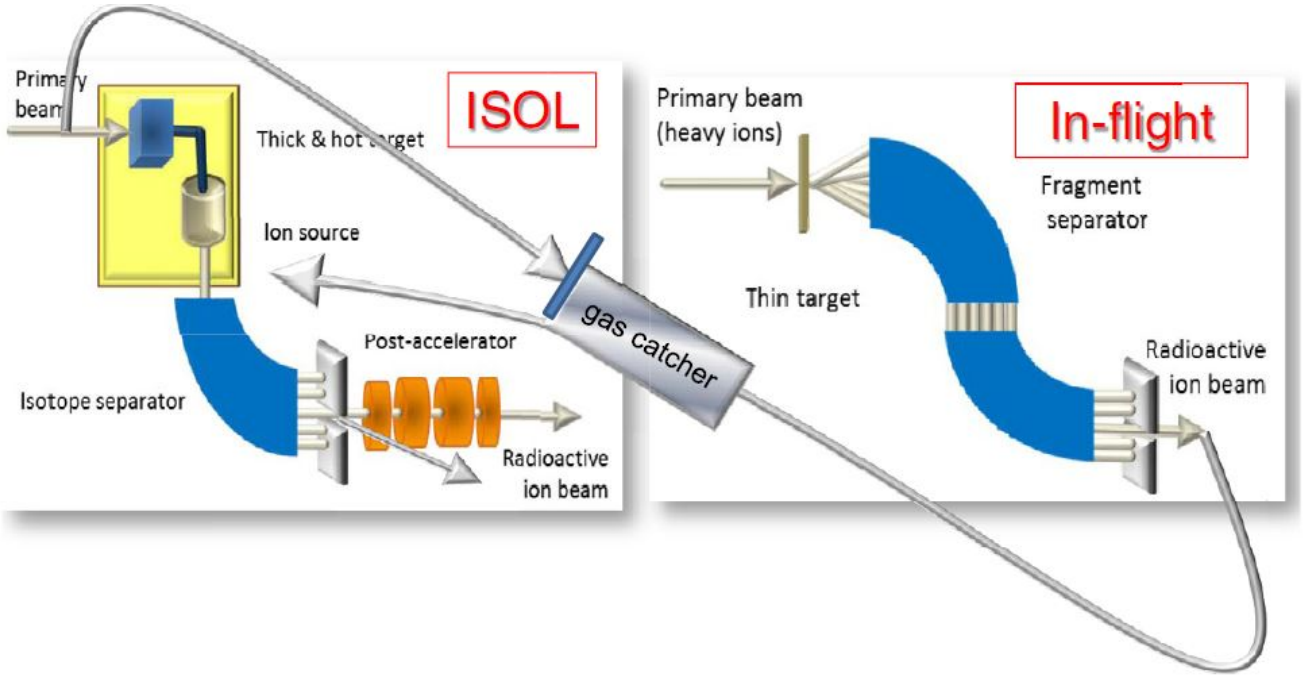

Figure 1.2.: Schematic drawing of the different techniques for radioactive ion beam production: ISOL, In-flight and hybrids. Picture taken from [2].

of typically 10 kV to 60 kV. The process of extraction from ISOL targets is delayed by diffusion in the target material and affected by chemical losses. Therefore short-lived isotopes with a reactive nature are typically difficult to extract and thus often only available in reduced quantities. However if the choice of target material and target setup allows the extraction of a species, high rates with current of up to 10^{11} pps can be achieved.

Besides these principal techniques that are used by the majority of the radioactive ion beam facilities other techniques can be found that lie somewhat in between ISOL and In-flight. An example is IGISOL, developed at the University of Jyväskylä in Finland.
The IGISOL method (Ion Guide Isotope Separation Online) separates radioactive isotopes from a thin target using a stream of noble gas. For the IGISOL method the target is located in a chamber filled with a noble gas (He or Ar). Here the ion is slowed down and thermalized [3].
Stopped ions are transported in the stream of helium or argon to an exit hole where separation of noble gas and ions takes place. If the applied flux of the noble gas is high enough extraction can take place faster than ms. Similar to the in-flight method the chemical nature of the element has no impact on the extraction. Hence refractory and very reactive elements can be extracted with high intensity ($\approx 10^5$ ions per sec of e.g. Mo, Rh, Tc)[4].

Future Facilities

In the near future a new generation of RIB[1] facilities will be available for the scientific community. The upgrade of existing facilities like HIE[2]-ISOLDE at CERN, FRIB[3] at MSU in Michigan and FAIR[4] at GSI in Darmstadt will provide beams of yet unmatched intensity and quality. Furthermore new facilities

1 Radioactive Ion Beam
2 High Intensity and Energy
3 Facility for Rare Isotope Beams
4 Facility for Antiprotons and Ion Research

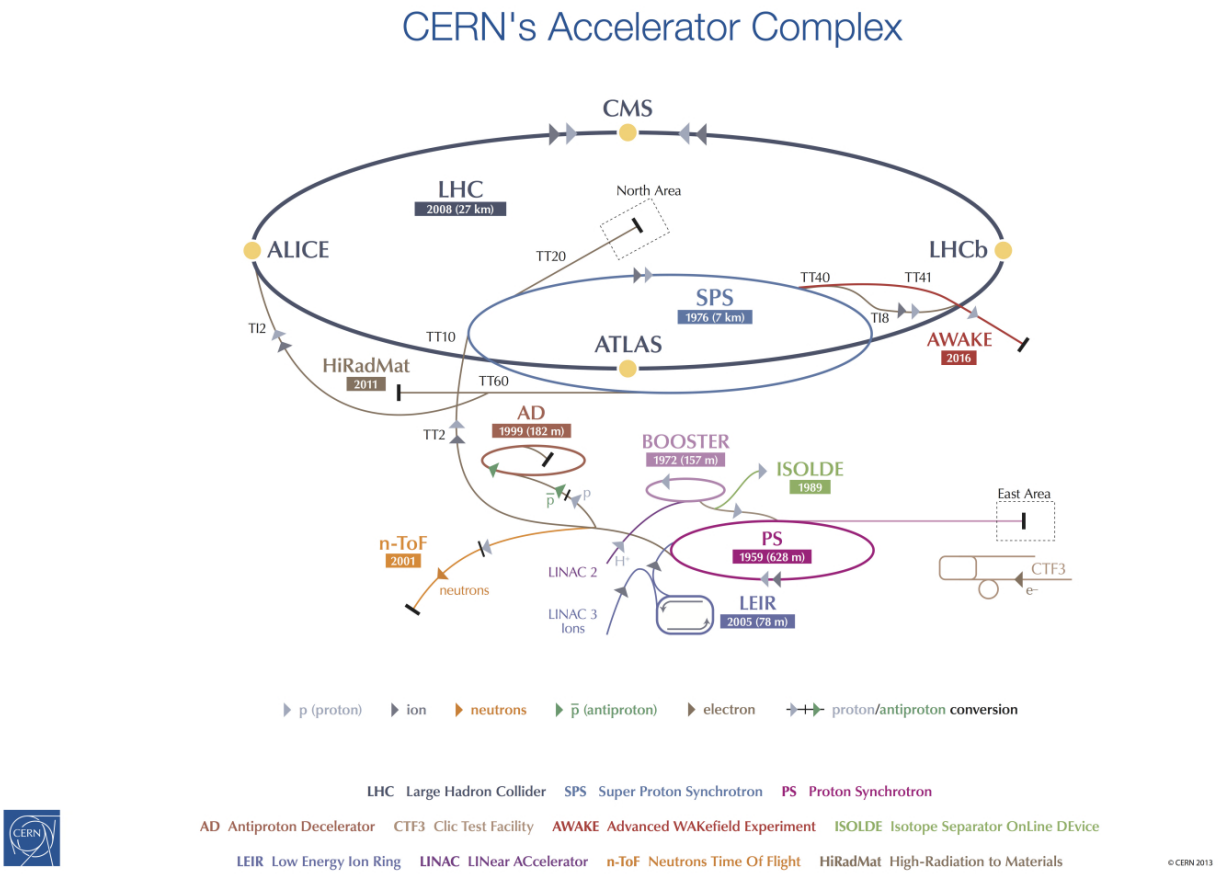

Figure 1.3.: ISOLDE in the CERN accelerator complex. The Protons for ISOLDE are accelerated by the LINAC 2 and the Booster up to 1.4 GeV.

like EURISOL are in the planning.
The upgrade of ISOLDE to HIE-ISOLDE will improve the energy, purity and intensity of post accelerated beams. This happens by upgrading REX-ISOLDE with a superconducting 40 MV linac what will raise the energy of post accelerated beams from currently 3 $\frac{MeV}{u}$ to over 10 $\frac{MeV}{u}$ [5].
At FRIB stable isotopes are accelerated to up to 200 $\frac{MeV}{u}$ and beam powers up to 400 kW by superconducting RF cavities. The beam will be directed on a thin (maximum thickness $\approx 50mm$ [6]) target and the resulting projectile fragment and fission products separated and post accelerated. The continuous power deposition on the target of up to 200 kW and the desired target life time of about one week requires the development of new target designs. One possible solution is a rotating graphite disc cooled by thermal radiation [6].
A similar target design will be used at FAIR in Darmstadt. Here a beam of up to 10^{12} $\frac{ions}{s}$ will impinge a rotating graphite target with a thickness of 1-8 $\frac{g}{cm^2}$. The primary beam will consist of all elements up to Uranium with energies up to few $\frac{GeV}{u}$, depending on the element. Fragmentation product will be separated within ns by the Super-FRS separator, allowing the extraction of most exotic isotopes.

1.2 RIB Production at ISOLDE

ISOLDE is part of the CERN accelerator complex. Located after the PS Booster [Fig 1.3] it receives protons with an energy of 1.4 GeV. The maximum frequency of this pulsed beam is one pulse every 1.2 seconds with up to $3 * 10^{13}$ protons per pulse. The theoretical maximum integrated current of protons

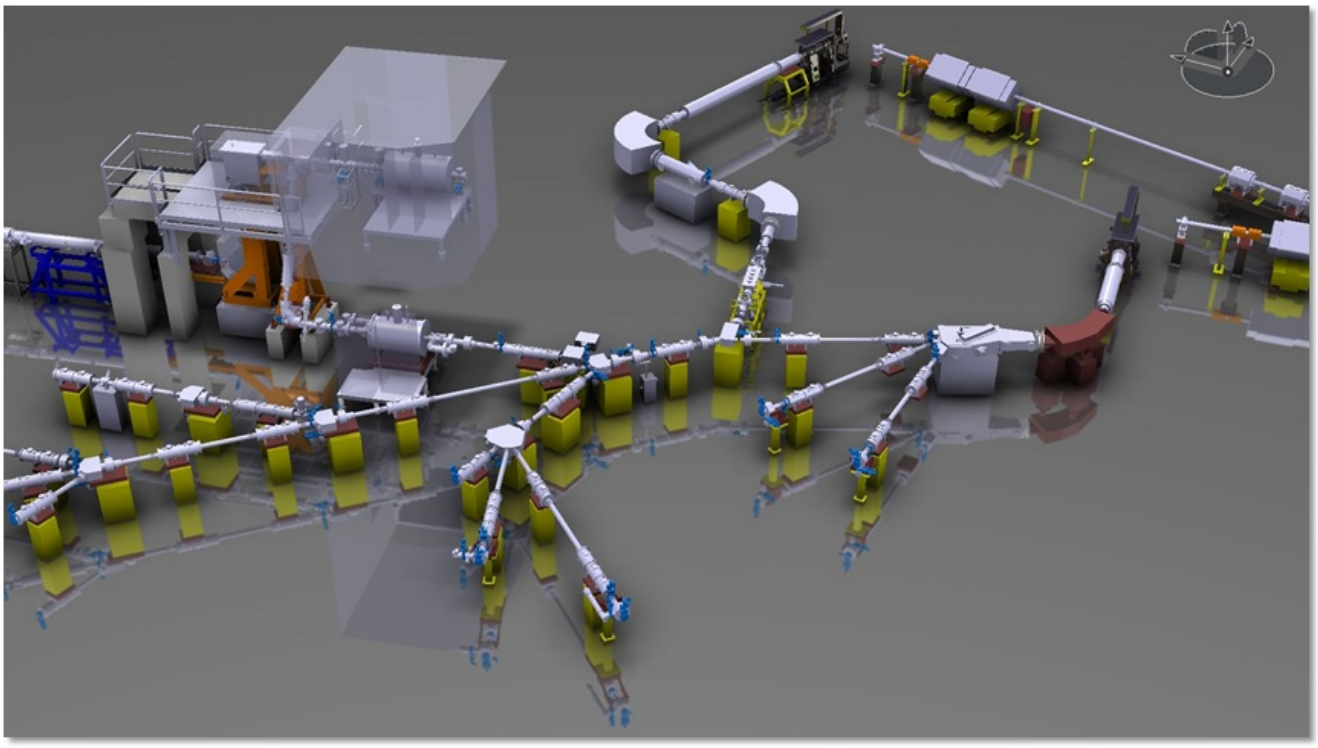

Figure 1.4.: Overview of the ISOLDE hall. The picture shows the two target stations GPS and HRS and the incoming proton beam lines (right side). Downstream, the separation magnets (two for HRS, one for GPS) and the lines for the secondary beam, leading to the different experiments, are shown.

is $4\mu A$. For reasons of radio protection the current is limited to $2\mu A$. At ISOLDE two targets can be connected simultaneously to the available mass separators: the general purpose separator (GPS) and the high resolution separator (HRS)[Fig 1.4]. After the extraction of radioactive ions from the target, the beam is mass separated and the requested isotopes guided to the experimental setups through beam lines.

Typical ISOLDE target units consist of a dome like container [Fig 1.5] which is evacuated to a vacuum of about $1 * 10^{-6}$ mbar. Inside one can find the target container which contains the target material of choice. For the production of radio nuclei this target container is bombarded by the proton beam and can be heated resistively up to 2100 $^{\circ}C$ in order to promote the extraction of isotopes. The produced isotopes are diffusing out of the material, through the transfer line into the ion source, where they are ionized and extracted via an applied electric field of 10 kV-60 kV. Depending on the nature of the desired isotopes several options are available for the choice of target material, ion source and transfer line.

From the initial produced number N_0 of an isotope inside the target material, to the point of extraction isotopes undergo a variety of interactions with the target environment where several physical and chemical processes are involved.

After the production, isotopes have to diffuse to the surface of the bulk material. This is happening within a characteristic time t_{diff}. Assuming that no secondary diffusion back into the target material at a different location is happening the isotope starts to migrate through the target and eventually reaches the ion source. During the migration losses due to chemical reaction with the surrounding material can occur. The lost fraction is taken into account by $\epsilon_{transport}$. Furthermore the migration can be delayed by a time t_{Ads} due to adsorption phenomena on the surfaces of target and structural material. In case the extraction of a desired isotope happens as a molecule this molecule has to be formed prior to the migration through the setup. Depending on the conditions (temperature, pressure) and present reaction partners inside the target formation of different molecules can take place. For instance carbon can react

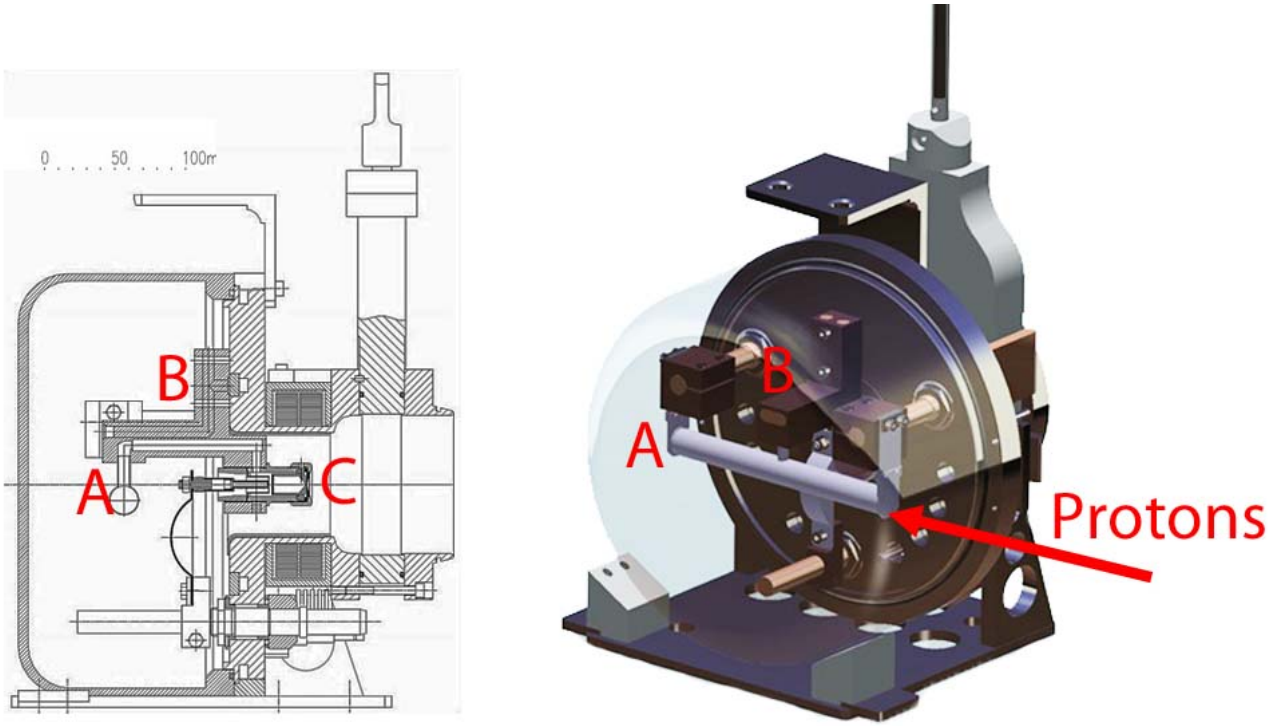

Figure 1.5.: One possible set-up of an ISOLDE target unit. To see here with a standard target container (A), a cold copper transfer line (B) and a Febiad ion source (C).

with present oxygen to form carbon monoxide and carbon dioxide. In most cases the formation of one species is thermodynamically favored under the given conditions. Hence this process can be characterized with an efficiency $\epsilon_{formation}$.
Eventually the species will be ionized with an efficiency ϵ_{ion} and the ion extracted to the experiment. In a first order approximation these processes can be assumed to be independent from each other and are happening sequentially. Taking these different processes into account the extracted number of ions can be described as:

$$N = N_0 \cdot exp(-\lambda \cdot t_{diff} + t_{Ads} + t_{eff}) \cdot \epsilon_{diff} \cdot \epsilon_{transport} \cdot \epsilon_{formation} \cdot \epsilon_{ion} \tag{1.1}$$

The goal of the thesis is to separately investigate the factors involved in equation 1.1 for the extraction process of carbon and boron from ISOLDE target units.
Reproducible extraction of carbon isotopes with half lives shorter than 200 ms is not successful up to now. Furthermore, radioactive beams of boron have not been produced at ISOLDE or other ISOL facilities. To identify the hindering processes and allow the extraction of radioactive isotopes of these elements in the future the results of several experiments carried out within this work were combined with theoretical results.
Namely the diffusion of boron in target materials ϵ_{diff} , molecular formation of carbon oxides and boron fluorides $\epsilon_{formation}$, transport processes through the target container and ion source $\epsilon_{transport}$, $t_{Ads} + t_{eff}$ and the ionization behavior of the molecules ϵ_{ion} were studied.

The availability of beams of short lived isotopes of carbon and boron would allow a number of experiments to be feasible. Beams of exotic ^{9}C ($t_{1/2} = 123$ ms) are requested for elastic resonance scattering experiments to investigate low lying states of ^{10}N. Due to the limited availability little is known about neutron rich isotopes $^{17-19}$C. Therefore experiments are interested in the study of basic properties such as half lives, decay and excitation of the nuclei.

Beams of ^{8}B ($t_{1/2} = 770$ ms) would serve the study of the proton halo of ^{8}B and resonant elastic scattering experiments on protons to investigate low lying states of ^{9}C. Furthermore ^{8}B is required to investigate the behavior of boron as a dopant in semi conductors using alpha emission channeling.

Hereinafter the different parts of ISOLDE units together with the relevant phenomena involved in equation 1.1 are introduced.

1.2.1 Target Materials and Transfer Lines

The choice of the target material is made to maximize the intensity of the beams of isotopes which are requested by the experiments. Production cross sections for the particular isotope are the first important parameter that needs to be considered. Furthermore characteristics of the target material such as structure, density, mechanical and thermal resistance, melting point and electrical conductance have to be taken into account. Uranium carbide is the preferred target material for many isotopes. This is due to its high production cross section for many neutron rich isotopes and good release characteristics[7]. For the production of light isotopes other materials like CaO, Y_2O_3, TiO_2 or HfO_2 [8], [9]are used. These materials are usually present in powder or fiber form and pressed to pills before they are inserted into the target container.
The release characteristics of the desired element from the target material is a second important parameter. To assure a fast extraction, diffusion and transport have to take place as fast as possible[10]. Delays due to slow diffusion in the bulk material or long residence time on surfaces due to adsorption lead to decay losses of short lived isotopes. Hence the powder, used for the production of the target pills, should consists of small grains. The small size assures short diffusion paths to the surface[11]. Once an isotope reaches the target materials surface it can evaporate or react with other species in order to form volatile molecules. To assure a fast extraction of isotopes which are formed deeper in the target material a high open porosity of the target material pill is desired.
After extraction, the volatile species can migrate through the transfer line towards the ion source.
This migration is an important parameter which needs to be controlled.
Depending on the element and therefore chemical and physical properties the choice of the transfer line can either hinder or promote the transport. For elements with a high boiling point and little reactivity towards the transfer line material a hot transfer line [fig 1.10] is the best choice. Similar to the target container the hot transfer line consists of tantalum and can be operated up to $2100°C$. These high operational temperatures assure that isotopes don't condensate on the walls and minimizes residence times on the surface due to adsorption. For elements for which a hot tantalum surface is not suited or if boiling points are low like it is the case for noble gases cold transfer lines are available. These water cooled copper lines [fig 1.9] reach temperatures of around $50°C$. Besides the fact that the low temperature combined with the chemically less reactive copper avoids the formation of chemical bonds, the extraction of isobaric contaminants with a higher boiling point is suppressed due to condensation and adsorption. The latter effect is used as an advantage in a special arrangement where a quartz tube is inserted into a kinked heated transfer line [12]. Since the adsorption enthalpy is different for each element and the residence time depends on the temperature and adsorption enthalpy [see eq. 1.6], the release for a particular element can be controlled by adjusting the temperature of the transfer line. Therefore the release of isobaric contaminants with a higher adsorption enthalpy can be suppressed and hence the extracted beam purified.

Isotope Production

At ISOLDE a proton beam of 1.4 GeV hits a thick ($l = 20$cm, $r = 1$ cm) target. Depending on the nature of the target material different processes can lead to the production of radioactive isotopes. These

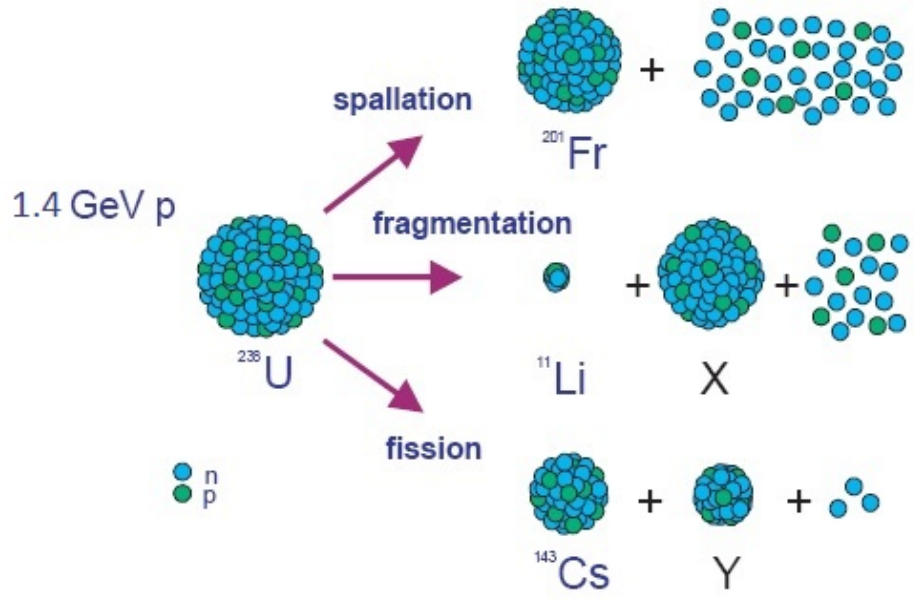

Figure 1.6.: Processes for isotope production at ISOLDE. The incoming beam of 1.4 GeV protons can undergo spallation, fragmentation and fission reactions with the target material.

processes are mainly spallation, fission and fragmentation (fig 1.6). The number of produced isotopes N_0 in 1.1 can be calculated as

$$N_0 = \sigma * N_p * \rho_A \tag{1.2}$$

where σ is the cross section for the production of a particular isotope, N_p the number of protons hitting the target and ρ_A the the number of target nuclei in the material per cm^2. Production cross sections can be calculated using advanced codes such as ABRABLA [13], EPAX [14] or Fluka [15].

Spallation

If a projectile, in the case of ISOLDE protons, with an energy higher than 100 MeV hits a target nucleus spallation can occur [16],[17]. Typically spallation of a target nucleus is a two step process. The first step of the process is the interaction of the projectile with single neutrons and protons of the target nuclei. This leads to an emission of secondary neutrons and protons which then interact with other nuclei in the same way. This process forms a cascade inside the target material. The interaction of the projectile with the target leaves a highly excited nucleus behind where the energy is equally distributed over all constitutes. This nucleus can then in the second process evaporate further neutrons and protons, leading to the final nucleus. Since the mass of the resulting nucleus is close to the mass of the target nuclei, this process is important for the production of heavy isotopes.

Fragmentation

If a high energy hadronic projectile hits heavy nuclei fragments with $6 \leq A \leq 40$ [18] can be produced by nuclear fragmentation. The cross section for this process are small for low energies and raise with the energy of the projectile up to 10 GeV where it stabilizes. Fragmentation is the important process for the production of light nuclei.

Fission

Fission takes place if an incoming particle e.g. neutron, proton is absorbed by the target nuclei. If the additional binding energy due to the absorbed particle is high enough the target nucleus can be excited to a state where fission occurs. The excited nucleus separates in two, sometimes three secondary nuclei and additional neutrons and protons. For cold fission, which takes place for low energy projectiles (e.g. thermal neutrons on ^{235}U), the resulting nucleus typically obtain 1/3 and 2/3 of the mass of the primary nuclei. For fission induced by high energy neutrons or protons (hot fission) the resulting distribution of nuclei strongly depends on the target material and the projectile energy. Fission takes place if the resulting nuclei are energetically more stable. Hence it is a process merely observed for heavier elements.

1.2.2 Diffusion

Diffusion describes a transport phenomena in a bulk material, based on the statistical movement of particles due to their thermal energy. Diffusion of a species in the host material occurs if the concentration of the diffusing species along the host material is not homogenous. Then the system evolves to an equilibrium state with homogeneous distribution. Even when this state is reached, diffusion still takes place, but without any net change of the concentration.
Depending on the nature of the host material and the diffusing species, diffusion can take place in different ways, vacancy diffusion, interstitial diffusion and substitutional diffusion [19]. Vacancy diffusion occurs if the solid has vacancies so atoms can exchange their positions with vacant positions. The rate with which this process takes place depends on the number of vacancies in the material and the activation energy needed to overcome energy barriers for atomic motion.
Interstitial diffusion occurs for species which are small in comparison to the crystal lattice of the solid. In this case atoms diffuse in between the atoms of the solid. The later process is in general much faster than the vacancy diffusion as energy barriers are lower.

If the diffusion is steady, it is proportional to the concentration gradient in direction of the diffusion and described by Fick's first law [20]:

$$J = -D\frac{\delta\phi}{\delta x} \tag{1.3}$$

Here J $[\frac{mole}{m^2 s}]$ is the flux of the diffusing species, D the diffusion coefficient $[m^2/s]$ and ϕ $[\frac{mole}{m^3}]$ the concentration profile in direction of x.
The diffusion coefficient D is specific for each combination of host material and diffusing species and given by

$$D = D_0 * exp(-\frac{Q}{RT}) \tag{1.4}$$

where Q is the activation energy, R the universal gas constant and T the temperature.
The more general case of non-steady diffusion is described by Ficks's second law:

$$\frac{\delta\phi}{\delta t} = D\frac{\delta^2\phi}{\delta^2 x} \tag{1.5}$$

Here local differences in concentration and time dependent processes are taken into account. Exact solutions of these differential equations are dependent on the boundary and initial conditions and thus specific for each system.

In the case of isotope extraction the diffusion of produced isotopes to the surface of the target material is important. Once an isotope reaches the surface it can either evaporate or react with a second species to become more volatile and then be extracted. As migration through open pores is much faster than the diffusion in the material it is desired to have short diffusion paths. Therefore the grain size of the used target materials should be as small as possible ($\approx$ nm).
The diffusion of produced isotopes can be influenced due to radiation damage induced vacancies in the material [21].

1.2.3 Adsorption

When an atom or molecule hits a surface it will remain with a certain probability for a certain time on the surface. The process of attaching to the surface is called adsorption, its reverse process, the detachment from the surface, desorption. The force with which the adsorbate is attracted to the adsorbent is characterized by the so-called adsorption enthalpy ΔH_0 [kJ/mole]. The sticking probability and the adsorption enthalpy depend on the combination of adsorbent and adsorbate. Normally one distinguishes between physisorption and chemisorption[22].
Physisorption is characterized by the fact that the adsorption on the surfaces is weak, reversible and usually the adsorbent is found in a mono layer or few layers. The cause of the interaction is the Van-der-Waals force [22]. The electron structure of the adsorbed species is not changed significantly.
In the case of chemisorption the bonding is often dissociative, irreversible and present in multilayer. A molecule which chemisorbs on a surface would often break the bond between its atoms and either undergo a chemical reaction with the adsorbent or remains as an unbound fraction of the molecule. The binding is often of covalent nature. As an orientation the absolute value of ΔH_0 can be considered in order to distinguish between physisorption and chemisorption. Adsorption as physisoprtion takes place if the adsorption enthalpy is below $\Delta H < 10$ kJ/mole and chemisorption for values bigger than $\Delta H > 10$kJ/mole. However this can't be regarded as a universal rule.
Some examples for values of adsorption enthalpy are $\Delta H = 16$kJ/mole for CO on Y_2O_3, $\Delta H = 153$kJ/mole for CO on ZrO_2 (compare sec 2.5). The time an atom remains on the adsorbent is dependent of temperature and adsorption enthalpy and given by

$$\tau = \tau_0 * exp(\frac{\Delta H_0}{k_B * T}) \tag{1.6}$$

where $\tau_0 = 1/\nu_m$ is given by the maximum theoretical phonon frequency for a material with ν_m the Debye frequency. This material specific time constant typically lies in the order of $\tau_0 = 10^{-13} - 10^{-15}$ s. k_B is the Boltzmann constant and T the temperature. For a molecule or atom hitting a surface multiple times, the residence time for a single hit has to be multiplied by the number of hits n. This leads to the total adsorption time for a surface:

$$t_{ads} = n * \tau = n * \tau_0 * exp(\frac{\Delta H_0}{k_B * T}) \tag{1.7}$$

The residence time at room temperature for an adsorption enthalpy of approximately $\Delta H = 100$kJ/mole is in the order of 10^{-4} seconds for a single hit. Hence for isotopes with half lives of less than one second adsorption becomes a determining factor if the number of hits equals to the reciprocal of the residence time for a single hit.
The number of hits n on the surface has to be simulated with specific codes e.g. RIBO[23]. For simple geometries it can be calculated with semi empirical formulas[24], derived from Monte Carlo simulations.

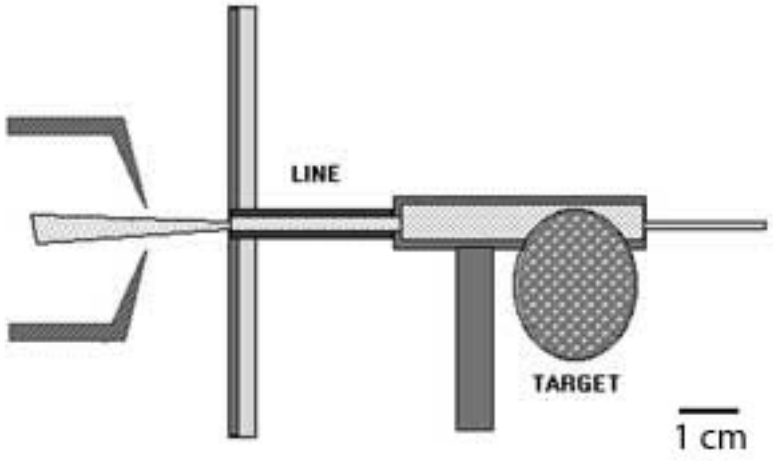

Figure 1.7.: The picture shows a cross section of a target arrangement using a surface ion source. The heated tube is connected in the center of the target container. Protons impinge the target container perpendicular to the drawing plane.

The sum of all adsorption times for all present materials together with the flight time of the molecule gives the total time needed for effusion t_{eff}:

$$t_{eff} = t_{flight} + \sum_i t_{ads_i} \tag{1.8}$$

The time of flight can be estimated with the kinetic energy of the gas atom. This energy depends on the mass and the average temperature $\overline{T}$ of the gas and follows a Maxwell-Boltzmann distribution with an average velocity $\overline{v}$

$$E_{kin} = \frac{1}{2} m \overline{v}^2 = \frac{3}{2} k_b \overline{T} \tag{1.9}$$

$$\overline{v} = \sqrt{\frac{3 k_b \overline{T}}{m}} \tag{1.10}$$

Obviously adsorption on surfaces is a crucial factor that needs to be controlled in order to be able to successfully extract short-lived radioactive isotopes as molecules. Both, a long total adsorption time due to multiple hits on a surface and an irreversible adsorption due to high adsorption enthalpies lead to losses during extraction.

1.2.4 Ion Sources

The Surface Ion Source

The surface ion source has the simplest design of all ion sources used at ISOLDE. Different from other ion sources, the ionization takes place on the surface of the transfer line and the additional ionizer tube[fig 1.7][25]. The surface ion source consists of a refractory metal with a high work function like tantalum or rhenium which is operated at around $2000°C$. Roughly, ionization of an element takes place if the work function of the ion source material is higher or close to the ionization potential of the

Element	ϕ_i [eV]	Element	ϕ_i [eV]
Li	5.39	Be	9.32
Na	5.13	Mg	7.64
K	4.34	Ca	6.11
Rb	4.17	Sr	5.69
Cs	3.89	Ba	5.21
Fr	3.83	Ra	5.27

Table 1.1.: First ionization potentials of alkali and earth alkali metals [27]

Material	W [eV]
Re	4.85
Ta	4-4.8
W	4.32-5.22
LaB_6	2.07

Table 1.2.: Work function of used materials for surface ion sources

element. With typical work functions of rhenium and tantalum between 4 eV and 5 eV this ion source is capable of ionizing alkali and some earth alkali metals. The degree α of ionization for a given element at temperature T is given by the Saha-Langmuir equation [26]:

$$\alpha = \frac{g_0}{g_i} * e^{(W-\phi_i)/k_B T} \tag{1.11}$$

where g_0 and g_i are the statistical weights of the atomic and ionized states, W the work function of the metal and ϕ_i the ionization potential of the element. The efficiency of ionization is given by

$$\epsilon_{surface} = \frac{1}{1+1/\alpha} \tag{1.12}$$

Tables 1.1 and 1.2 show ionization potentials of alkali and earth alkali metals and work functions of materials used for surface ion sources

Ionization probabilities P are close to 100% for some element-ion source combinations: P(Cs on W at 1500 K)=0.99. [26]. At ISOLDE the temperature of surface ion sources is typically kept at $2000°C$.

The Resonance Ionization Laser Ion Source (RILIS)

The RILIS [28] ion source is used in approximately 50% of the on-line runs at ISOLDE. A system of lasers, which are specifically tuned on the desired element, are directed into the hot cavity of the surface ion source. During the migration time of the atom through the cavity the atom is interacting with the lasers. By adjusting the wavelengths of the lasers to the energies of the electronic transitions in the atomic shell it is possible to excite the outer electron to the ionization energy of the particular element or even isotope. If isobars are not ionized on the hot surface, purification of the beam can be achieved as each laser scheme is specifically matched to a particular element. Figure 1.8 shows the schematic setup of a surface ion source in combination with resonant laser ionization. At ISOLDE, RILIS is used for the extraction of about 31 different elements [29]and more to come.

The FEBIAD Ion Source

Due to its versatility FEBIAD (Forced Electron Beam Induced Arc Discharge) ion sources are widely used at ISOLDE. In FEBIAD ion sources a heated cathode emits electrons which are accelerated in a little chamber by an anode [31]. The atoms or molecules in this chamber, coming from the target container or injected via a dedicated gas system are ionized via electron impact ionization by electrons flying towards the anode. Besides $q = +1$, ions with higher charge states can be produced, although with lower cross sections.

The modern FEBIAD ion source used at ISOLDE is the so called VADIS (Versatile Arc Discharge Ion

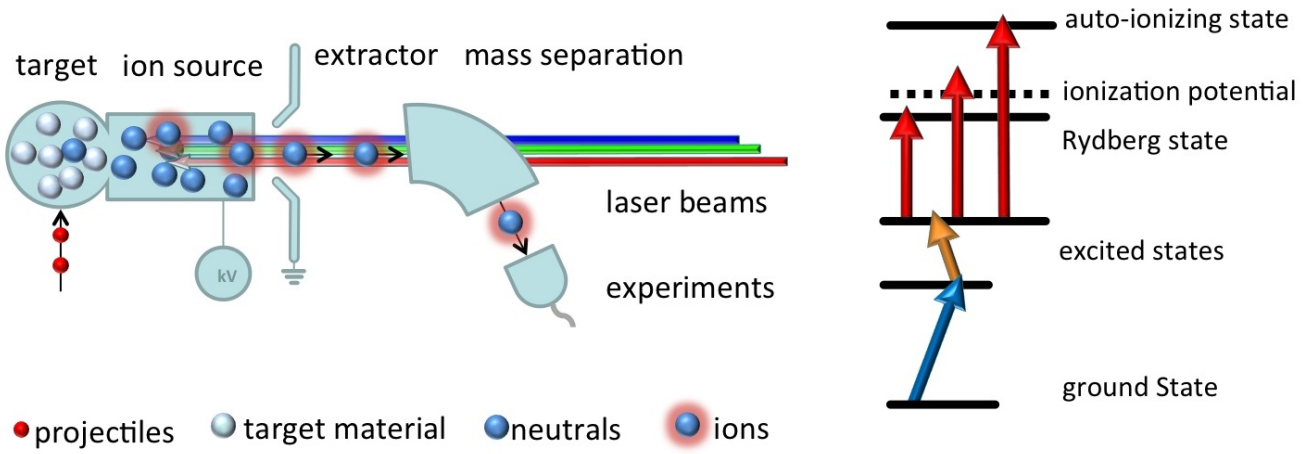

Figure 1.8.: Principle of RILIS ion source: Different lasers, matching a specific energy scheme of an element, are directed into the hot tubular cavity of the ion source. Here the elements valence electrons are stepwise excited and eventually ionized. Figure taken from [30]

Element	Ionization efficiency ϵ [%]
He	1.4
Ne	6.7
Ar	26
Kr	38
Xe	47
Rn	62

Table 1.3.: Measured ionization efficiencies of the VADIS ion source for first ionization of noble gases [32]

Source) [32] ion source. VADIS ion sources are typically operated with anode voltages of $120V - 250V$ at a temperature of $T = 2000°C$.

The adjustment of the anode voltage and with that the electron energy offers the opportunity to tune the ion source to the maximum of the ionization cross section for the desired element. The efficiency for ionization ϵ_{ion} is described by the following theoretical model:

$$\epsilon_{ion} = \frac{n_e * n_n * \sigma_{ion} * v_{rel} * V_{source} * f_{extr}}{I_{n_{in}}} \tag{1.13}$$

where n_e is the electron density in the source, n_n the neutral atom density, σ_{ion} the ionization cross section, v_{rel} the relative velocity of electrons to atoms, V_{source} the source volume, f_{extr} the extraction efficiency of ionized species and finally $I_{n_{in}}$ the current of species entering the source.
Table 1.3 shows ionization efficiencies for noble gases. Fig 1.9 shows the profiles of a setup using a FEBIAD ion source. In this setup the target container is connected to the ion source via a cold copper transfer line.

The radio frequency (RF) Ion Source

A major disadvantage for the extraction of some elements is the fact that the electron emission in FEBIAD and surface ion sources relies on hot metal surfaces. Depending on their chemical nature some elements tend to form stable bonds with tantalum, molybdenum or other refractory metals used in ion

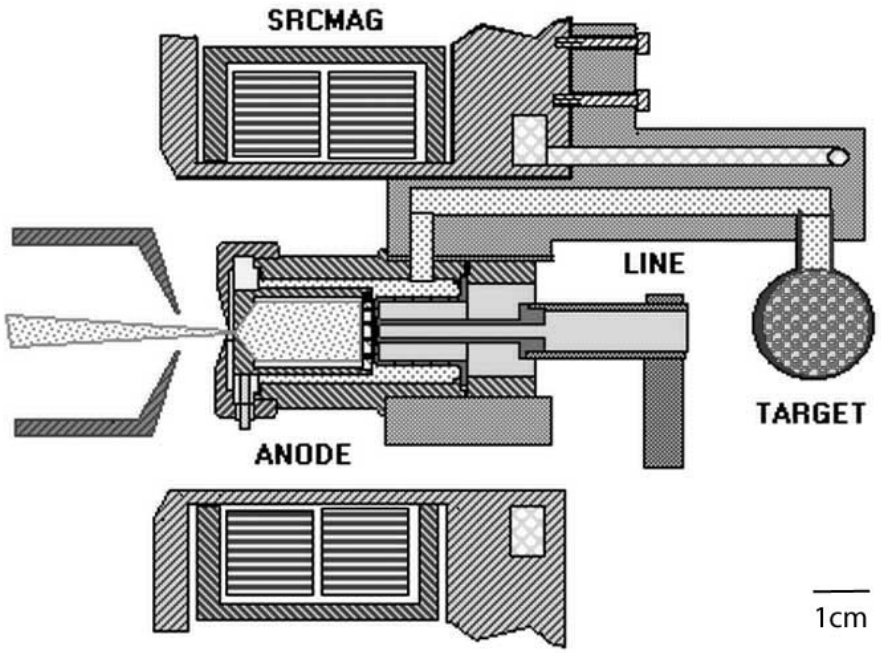

Figure 1.9.: FEBIAD ion source with cold transfer line: The target container is connected via a water cooled copper transfer line to the ion source. During operation the ion source reaches temperatures of approximately 50 $°C$.

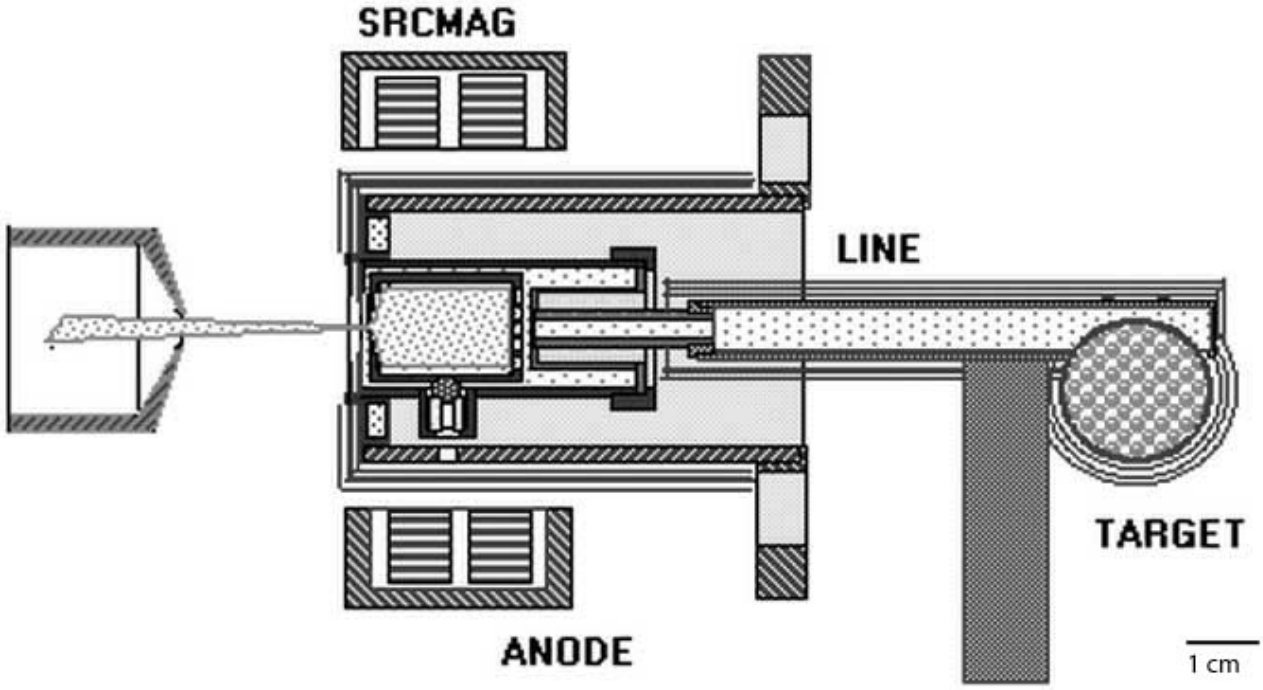

Figure 1.10.: FEBIAD ion source with heated transfer line: The target container is connected via a resistively heated tantalum transfer line to the ion source. Similar as the target container the transfer line can be heated to 2100 $°C$.

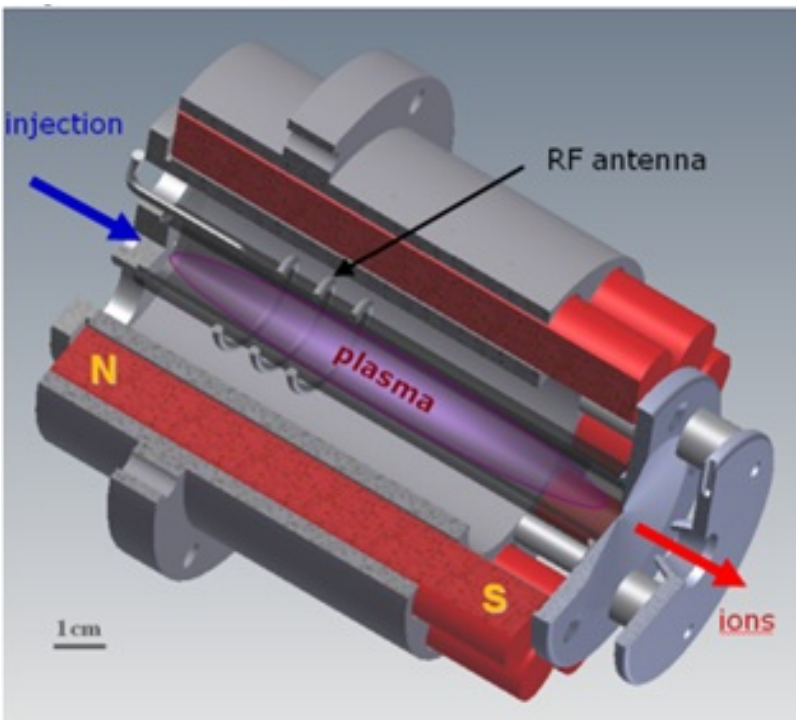

Figure 1.11.: Helicon ion source from [33]

sources. This is in particular the case for carbon and boron that are studied in this thesis. Therefore an ion source based on RF technology [33] with the goal to minimize the use of hot metal surfaces was developed. Fig 1.11 shows the setup of the ion source: a quartz tube is surrounded by permanent magnets and a RF coil. Inside this quartz tube the RF coil induces a RF discharge, ionizing the injected buffer gas (He, Ne, Ar,..) and the volatile species coming from the target container. Formed ions are extracted via a two step extraction system. During operation ionization efficiencies of 3.9% for argon and 2.5% for carbon monoxide were achieved.

For the case of gaseous species and molecules FEBIAD and RF ion sources are the ion sources of choice. In FEBIAD ion sources the energy of the electrons can be adjusted by tuning the accelerating voltage. Typically these values vary between 120 V and 300 V and therefore lead to energies up to 300 eV. This allows to adjust the electron energy to the maximum of the ionization cross section of a particular species. For the case of RF ion sources the electron energy is lorentzian distributed around smaller energies of typically 1eV - 10eV. The energy needed to ionize an atom or molecule is called ionization potential. Typical values are around 15eV for most gases with a maximum for helium of 24.6eV. While the ionization potential is the minimal energy required for (direct) ionization, the maximum of the cross section is usually found for electron energies three to four times the ionization potential. The ionization can take place by direct or stepwise ionization due to electron-electron interaction, ion-electron or laser-electron interaction.

Direct ionization by electron electron impact

Direct ionization of neutral unexcited atoms or molecules can occur if an incident high energy electron interacts with a valence electron. If the transferred energy ϵ [eV] exceeds the ionization potential I_p [eV]

of the species, ionization occurs. The cross section for an energy transfer of $\epsilon \geq I_p$ can be estimated by the Thomson Formula:

$$\sigma_i = \frac{1}{(4\pi\epsilon_0)^2}\frac{\pi e^4}{\epsilon}\left(\frac{1}{\epsilon} - \frac{1}{I_p} + \frac{2\epsilon_v}{3}\left(\frac{1}{I_p^2} - \frac{1}{\epsilon^2}\right)\right) \tag{1.14}$$

Where ϵ_v [eV] describes the kinetic energy of the valence electron and ϵ_0 the vacuum permittivity [F/m].

For the case of diatomic molecules non-dissociative direct ionization can be described as

$$AB + e^- \rightarrow AB^+ + e^- + e^-$$

Since some parts of the energy of the incident electron can be transferred into molecular vibration this process requires a little more energy than the corresponding process for atoms. After direct ionization the molecule can often be found in an excited state $(AB^+)^*$. If the energy transfer from the incident electron was high enough this can result in a dissociation of the molecule with the excited molecule as an intermediate state

$$AB + e^- \rightarrow (AB^+)^* + e^- + e^- \rightarrow A + B^+ + e^- + e^-$$

For the case of CO and CO_2 the cross sections for ionization are significantly higher than for dissociation [34], [35], [36].

Stepwise ionization by electron-electron impact

For the case that the energy of the electrons in a plasma is distributed around lower values (like it is the case in RF sources) and therefore direct ionization by high energy electrons is not likely, stepwise ionization becomes the dominant process. Here a neutral species is excited stepwise until the valence electron has enough energy to escape its boundary. In comparison with direct ionization this process can be $10^3 - 10^4$ times faster. Since the time scale for direct ionization is in the order of 10^{-16} to 10^{-15} seconds the time needed for ionization does not contribute to delays in the extraction process. [36]

1.2.5 Chemical Equilibrium

Chemical processes play two roles in the extraction of radioactive isotopes from a target. On one hand the chemical reactivity of the desired element with the present materials has to be considered. Formation of molecules with the hot tantalum of the target container (e.g. TaC_2) or the target material itself can take place. These bonds might lead to irreversible losses.
On the other hand formation of volatile molecules is desired in order to extract less volatile elements like carbon, boron or titanium from target units. Therefore one has to assure that elements necessary for the formation (e.g. oxygen for CO, fluorine for BF_x, TiF_x) are present in the target unit and available for the formation. This can be achieved by the choice of target material (e.g. an oxide for CO or a fluoride for BF_x) or the additional injection of a gaseous species during operation (e.g. SF_6, CF_4).
In order to estimate the reactions taking place inside the target container the chemical equilibrium of a system can be considered. This allows (with some limitations) to evaluate under which conditions and combination of materials in the target the extraction of desired species is favored.

A chemical reaction 1.15 is called to be in equilibrium if the concentration of products (C and D) and reactants (A and B) remains constant and the system has no tendency to change in one direction.

Usually both reactions still happen but without any net change of the concentration of any component. [20]

$$\alpha A + \beta B \underset{k_-}{\overset{k_+}{\rightleftharpoons}} \gamma C + \delta D \tag{1.15}$$

A reaction like 1.15 can be divided into forward and backward reaction with reaction rate coefficients k_+ and k_-:

- Forward reaction: $k_+ A^\alpha * B^\beta$
- Backward reaction: $k_- C^\gamma * D^\delta$

If a system is in equilibrium the rates of forward and backward reaction are equal: $k_+ A^\alpha * B^\beta = k_- C^\gamma * D^\delta$.

The ratio of these rate constants is called the equilibrium constant and specific for each reaction and temperature:

$$K_c = \frac{C^\gamma * D^\delta}{A^\alpha * B^\beta} = \frac{k_+}{k_-} \tag{1.16}$$

Thermodynamically a system is considered to be in equilibrium where the reaction Gibbs energy of the system for constant pressure and temperature plotted against the extent ξ of reaction has a minimum. Therefore:

$$\Delta_r G = \left(\frac{\delta G}{\delta \xi}\right)_{p,T} = 0 \tag{1.17}$$

As illustrated in figure 1.12 a system with a reaction Gibbs energy different from zero tends to migrate spontaneously towards the equilibrium point:

- $\Delta_r G < 0$: forward reaction is spontaneous
- $\Delta_r G > 0$: backward reaction is spontaneous

In order to estimate the phase coexistence in ISOLDE target units the software HSC 7 [37] was used. This software uses the Gibbs free energy minimization method to calculate equilibrium compositions[38]. Unfortunately these calculations do not consider the kinetics with which this reaction is happening. Hence it is possible that from a thermodynamic point of view the production of a species takes place under the conditions given, that however the process takes much longer than the half life of the isotope or typical extraction times found at ISOLDE. The extraction time is defined as the time between production of the isotope by impact of the proton beam on the target and the point in time when the isotope is extracted by the applied electrical field after ionization.

1.3 Release from ISOLDE Targets

All the previously mentioned effects (fig 1.13) after the production of the isotopes lead to a characteristic release for each element in combination with the set-up of the target unit and choice of target material. To determine the performance of a target unit and to document the release, each target unit is tuned and the release characteristics are measured at the beginning of an online run. These characteristics are absolute ion yield, level of isobaric contaminants and the time structure of the release. Besides a strong interest from the experiment side these measurements help to understand the impact of changes of the

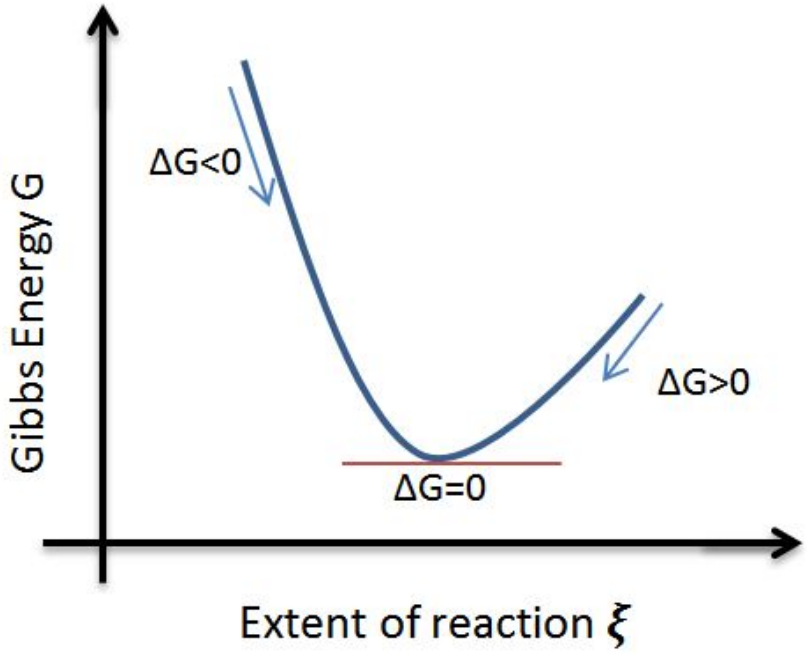

Figure 1.12.: Reaction Gibbs energy

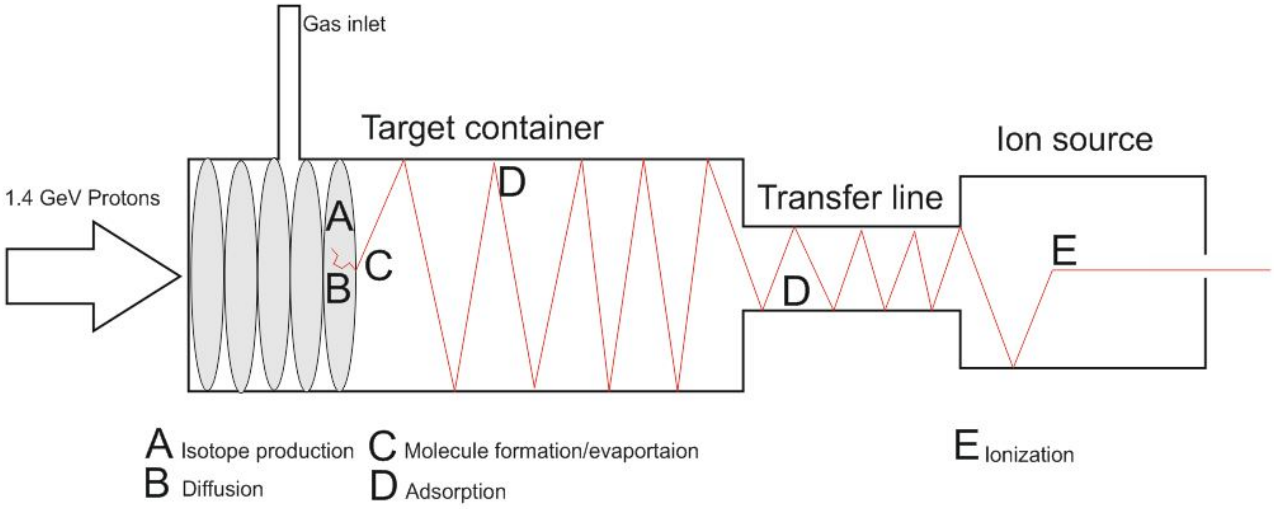

Figure 1.13.: Scheme of a target setup including the target container, transfer line and ion source. The relevant phenomena are shown .

target set-up on the online performance and determine the direction of further developments.

For the measurement the radioactive ion beam is directed to a so called tape station [39] that allows to measure β and γ radiation and thus allows to determine the ion current and to distinguish the isotope of interest from possible isobars.
The time window between arrival of the pulsed primary proton beam and release of secondary ions from the target is increased step-wise in order to determine the time characteristics of the release.
For the description of the measured release a modified version of equation 1.1 can be used [40]. In this approach the diffusion and effusion processes are described by probabilities $p_\mu(t)$ for diffusion and $p_\nu(t)$ for effusion. The probability that a produced isotope diffuses to the surface of the target material and effuses through the target system before it decays can be described by

$$P(p_\mu, p_\nu, \lambda) = e^{-\lambda \cdot t} \cdot p_\mu(t) \otimes p_\nu(t) \tag{1.18}$$

Solutions for the diffusion probability p_μ can be calculated with Fick's law and depend on the characteristics of the target material. The diffusion probability in a foil with infinite length and thickness d can be described by

$$p_\mu(t) = \frac{8\mu_0}{\pi^2} \cdot \sum_{n=0}^{\infty} e^{-\mu_0(2n+1)\cdot t} \tag{1.19}$$

where $\mu_0 = \frac{\pi^2 \cdot D}{d^2}$ with D $[m^2/s]$ the diffusion constant of the element in the material.

The probability for effusion can be described by considering the conductance of the tubular system. Assuming a gas filled tube that is emptied through a small hole at its end, the probability that gas molecules effuse through the hole can be described by

$$p_\nu(t) = \nu \cdot e^{-\nu \cdot t} \tag{1.20}$$

For the more complex geometry of an ISOLDE target container the effusion is described more accurately if a second time dependent term is added to equation 1.20. This leads to

$$p_\nu(t) = (1 - e^{-\nu_1 \cdot t}) \cdot e^{-\nu_2 \cdot t} \tag{1.21}$$

Integration of $P(p_\mu(t), p_\nu(t), \lambda)$ gives the released fraction:

$$\epsilon_{release} = \int_0^\infty P(p_\mu, p_\nu, \lambda) d\tau = \int_0^\infty e^{-\tau \cdot \lambda} \cdot p_\mu \otimes p_\nu d\tau \tag{1.22}$$

With equation 1.22 equation 1.1 can be described as

$$N = N_0 \cdot \epsilon_{release} \cdot \epsilon_{formation} \cdot \epsilon_{ion} = N_0 \cdot \int_0^\infty e^{-\tau \cdot \lambda} \cdot p_\mu \otimes p_\nu d\tau \cdot \epsilon_{formation} \cdot \epsilon_{ion} \tag{1.23}$$

This function can be fitted to the resulting graph of number of ions versus time after arrival of the protons on the target in order to determine e.g. diffusion constants. However due to the complexity of the model this is in many cases not possible.
The typical shape of release curves with a steep rise with a following decay can be described by a function containing of three exponential factors. This description was suggested in [40] and [41]:

$$R(t, \lambda_r, \lambda_f, \lambda_s) = A * (1 - e^{-t\lambda_r})(\alpha * e^{-t\lambda_f} + (1 - \alpha) * e^{-t\lambda_s}) \tag{1.24}$$

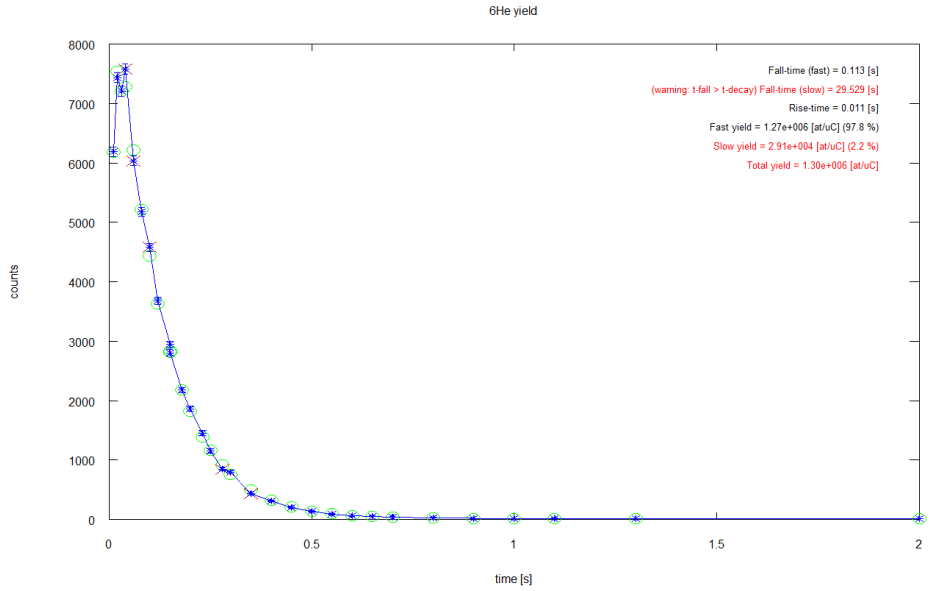

Figure 1.14.: Release of ^{6}He measured during an online experiment within this thesis. The curve shows a typical behavior: a steep rise within ms after the arrival of the proton pulse, followed by a decay with two time constants. In this case the fast decay time is 113 ms. The displayed measurement was taken with a unit using Carbon nano tubes as a target material, operated at $1600°C$. The code, used to determine the parameters was developed by Tim Giles, CERN.

where A is a normalization factor to the released ion current, λ_r the rise time constant, λ_f the fast decay constant and λ_s the slow decay constant. The value of α $(0 < \alpha < 1)$ determines the fraction of the released ions in the fast and slow part of the release. Figure 1.14 shows an example for a release curve measured during an online run. In this case the release of ^{6}He from carbon nano tubes was measured.

1.4 Extraction of Molecular Beams

Although ISOL facilities deliver a wide range of isotopes some elements are still not available or only in low intensities. This applies in particular for refractory elements or those with a very reactive nature. With some exceptions (Hf, Y, Lu, Ta, Ti) [42] the extraction of refractory metals of group 3b to 5b was not successful to this point. This is also the case for some non metals. These are boron, carbon (which are the subject of this thesis), phosphorus and sulfur. These elements share that due to their reactive nature stable bonds with the surrounding materials like tantalum, molybdenum or even the target material itself, are formed and thus extraction is difficult. In the case of carbon longer lived isotopes ($t_{1/2} \geq 500ms$) can be extracted as CO^{+} from ISOL units. However extraction times are often a multiple of the half live of short lived isotopes like ^{9}C, $^{17-20}C$ and thus extraction is difficult.
Already in the early years of ISOL facilities the extracting of refractory elements in molecular sidebands was discussed [43]. The possibility of extraction as halides, oxides, hydrates or combinations is suggested and displayed in fig 1.15.

First extractions of BaF^{+} with fluorine coming from the used target material ($ThF_4 \cdot LiF$) were reported by Ravn et al. [44]. Formation of chlorides was tested but due to the higher reactivity of chlorine towards the structural materials extraction as fluorides was preferred [45]. Furthermore fluorine has the advantage that only one stable isotope exists which allows a higher extraction efficiency during mass separation.
With the fluorination method beams of Sr, Ba [46], Ga, Y, Zr,In, Sn [45], V [47] and Ti, Zn, Sb [48] have

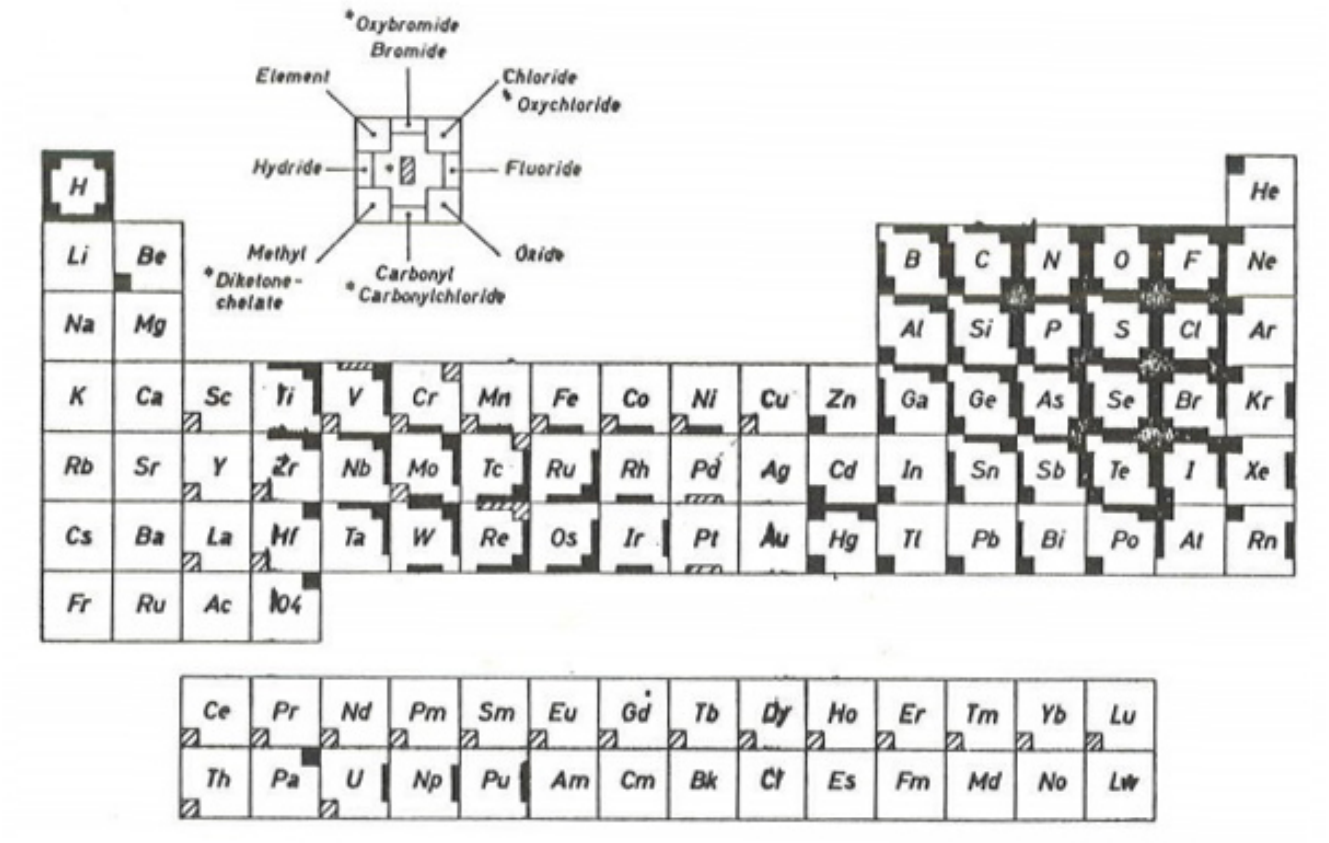

Figure 1.15.: Periodic table with suggestions on how refractory elements can be extracted by formation of molecules. Taken from [43]

been extracted.
Oxygen was used to produce beams of CO, COSe [9] and Lanthanides [49]. Furthermore a vapor of stable aluminum was used to form molecules with radioactive halides AlI and AlBr [45].

1.5 Beam development

To match the demand for high intensity and high purity beams of exotic radioactive ion beams the development of new target techniques, target materials and ion sources is required. As introduced in section 1.2 species undergo a variety of interaction with the environment during the extraction process. For the development of a new beam at ISOLDE these interactions have to be investigated. Classically beam development involves investigation of the in-target production of the desired isotope, diffusion characteristics in the target material, adsorption on present surfaces and the ionization of the species.

For carbon and boron, which have to be extracted in molecular form, the list of investigations has to be expanded. To promote the formation of molecules, the chemical equilibrium of carbon and boron with target materials has to be considered.
Furthermore the ionization of molecules is more complex in comparison to atoms. Besides additional degrees of freedom like vibrational and rotational states, the dissociation of the molecule into its components might influence the overall extraction efficiency.
An example which will be discussed in detail later in this thesis is the extraction of boron as boron fluorides. While calculations of the chemical equilibrium of boron with fluorides suggest a dominant production of BF_3, ion beam composition is such that the current of BF_2^+ is 100 fold higher than the current of BF_3^+. Comparing this observation with literature showed, that the ratio of measured currents can be explained by the high dissociation cross section of BF_3 in comparison to the direct ionization.

In this work aspects of classical beam development for carbon and boron and in some extend for other species are investigated. These investigations cover in-target production as well as adsorption and diffusion characteristics with materials present in target units. Molecule specific investigations focus on the calculation of the chemical equilibrium and ionization characteristics in the utilized VADIS ion source.

2 Extraction of Short-Lived Carbon Isotopes

2.1 Introduction

The technique of extracting carbon isotopes as an oxide molecular sideband from ISOLDE targets was suggested many years ago [50] and extensively studied ever since [51]. While extraction of longer lived isotopes is very successful (e.g. $7.7 \cdot 10^8 \frac{1}{\mu C}\ ^{11}C$ [52]), reliable beams of short lived isotopes with half lives shorter than 500 ms are not available in requested amounts for sufficient periods of time. Table 2.1 shows currents of different carbon isotopes extracted at ISOLDE. This chapter will describe properties of carbon relevant for the extraction of carbon from ISOLDE targets such as diffusion and adsorption, chemical equilibrium with surrounding and target materials and ionization characteristics.
Knowledge available in literature and former investigations at ISOLDE (mainly [51]) will be summarized and supplemented with results achieved within this thesis. These results allowed a deeper understanding of former online runs and identified the problems occurring during the extraction of radioactive carbon isotopes from ISOLDE targets.

Neutron deficient ^9C is requested for the investigation of low lying states in the unbound ^{10}N via elastic resonance scattering of ^9C on protons [55].
Beams of neutron rich isotopes of ^{17}C to ^{19}C would allow to study basic properties of these nuclei like beta decay, excitation and half-life. Due to the difficulty in producing these beams generally little is known about the heaviest carbon isotopes. For feasible experiments, extracted yields have to be in the order of $5 * 10^4\ 1/\mu C$.

As introduced in section 1.2, the number of released isotopes from thick ISOLDE targets can be described by formula 1.1:

$$N = N_0 \cdot exp(-\lambda \cdot (t_{diff} + t_{Ads} + t_{eff})) \cdot \epsilon_{diff} \cdot \epsilon_{transport} \cdot \epsilon_{formation} \cdot \epsilon_{ion} \tag{2.1}$$

Some of the factors in formula 1.1 have been studied at ISOLDE in the past [51] or can be found in literature. In order to achieve a more complete understanding of the processes involved in the release of carbon and to identify the hindering process, a series of investigations have been performed within this thesis. These investigation involve simulations of the chemical equilibrium between carbon and both structural and target materials. This allows to estimate under which conditions desired carbon oxides are formed ($\epsilon_{formation}$) or where losses occur ($\epsilon_{transport}$). The results of these calculations are shown in section 2.4. Furthermore measurements of the adsorption enthalpy ΔH_0 of carbon oxides on Alumina (Al_2O_3) and Yttria (Y_2O_3) are performed within a collaboration between CERN-ISOLDE and the group

Isotope	Half life [s]	extracted yield [$1/\mu$C]	Target Material	Ion Source	Ref
^9C	0.123	$1 * 10^3$	Y_2O_3	Minimono	[53]
^{10}C	19.3	$7 * 10^5$	CaO	VD7	[54]
^{11}C	1222.22	$7.7 * 10^8$	LiF:NaF	VD5	[52]
^{15}C	2.45	$1.5 * 10^5$	CaO	VD7	[54]
^{16}C	0.747	$8.9 * 10^1$	CaO	HELICON	[33]
^{17}C	0.193	$8 * 10^0$	HfO_2	HELICON	[33]

Table 2.1.: Some carbon isotopes and yields at ISOLDE

of R. Bulanek University of Pardubice, Czech republic. The obtained results allow a deeper analysis of former on-line runs during which Yttria was utilized as a target material. The measured adsorption enthalpy for CO on Yttria has been found to be low ($\Delta H_0 = -16$ kJ/mole) and thus making Yttria a very interesting candidate for extraction of short-lived carbon isotopes. The results together with other known adsorption enthalpies are analyzed in section 2.5.
In order to understand where, and to which degree, losses of carbon oxides during the extraction from the target container and ion source take place a dedicated experiment has been set-up. This setup allows to study efficiencies ($\epsilon = \epsilon_{transport} \cdot \epsilon_{ionization}$) and time structures of the release of carbon oxides depending on present materials and target temperature. The obtained results are compared to calculations of the chemical equilibrium of carbon oxides with materials used in ISOLDE target systems.
The experimental set-up together with the obtained results are shown in section 2.6.
As the final step in the extraction of radioactive isotopes the ionization of carbon oxides in a VADIS ion source was studied. The results are shown in section 2.7 and compared to theoretical cross sections for ionization.

In summary the following factors of formula 1.1 are studied within this chapter:

- N_0
  - Calculation of in-target production of carbon isotopes, using EPAX and ABRABLA
- $\epsilon_{formation}$
  - Calculation of chemical equilibrium between carbon and target materials
- $\epsilon_{transport}$
  - Calculation of chemical equilibrium between carbon and structural materials
- t_{ads}
  - Measurement of adsorption enthalpy of CO and CO_2 on Al_2O_3 and Y_2O_3
- $\epsilon_{ionization}$
  - Study of ionization behavior of CO and CO_2 in Febiad ion source - dependency of $\epsilon_{ionization}$ on U [V] and comparison with theoretical cross sections
- $\epsilon_{transport} \cdot \epsilon_{ionization}$
  - Study of release of injected $^{13}CO_2$ as $^{13}CO_2{}^+$ and $^{13}CO^+$ from target and ion source system depending on temperature and material composition

2.2 Isotope Production from Target Materials

In order to predict the initial production of isotopes inside the target, simulations of the production cross section have been carried out using the ABRABLA [13] and EPAX [14] code. The chosen materials are oxides of calcium (CaO), hafnium (HfO_2), yttrium (Y_2O_3), aluminum (Al_2O_3) and titanium (TiO_2). Calcium oxide, hafnium oxide and yttrium oxide have been used as target materials for carbon beam production during online experiments. The good material properties of Alumina in terms of adsorption make this material a possible candidate for online experiments. The isotope production cross section was calculated for each of the constituents of the material separately. The resulting cross section is calculated by combining the result for each component. The resulting cross section of a compound A_mB_n is given by:

$$\sigma_{A_mB_n} = m * \sigma_A + n * \sigma_B \tag{2.2}$$

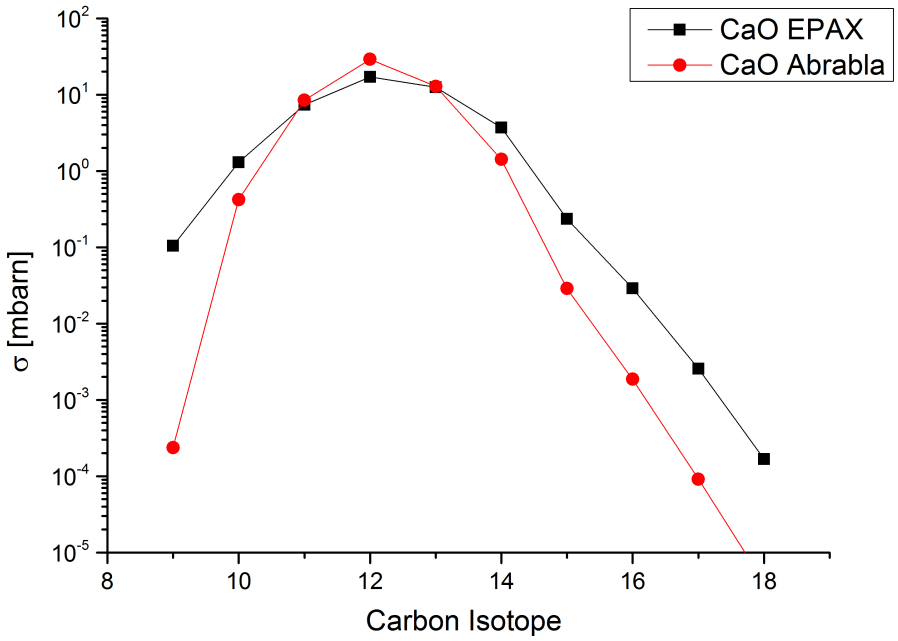

Figure 2.1.: Comparison of simulated isotope production cross sections for carbon isotopes using ABRABLA and EPAX.

The calculated cross sections from ABRABLA and EPAX show significant differences for radioactive isotopes. Former estimations for the in-target production of exotic isotopes were based on the results from calculations using EPAX [51].
Results from calculation with the ABRABLA code suggest that the current of ^{9}C can be expected to be 2 to 3 orders of magnitude lower than formerly believed.
Figure 2.1 shows the cross sections for isotope production from calcium oxide obtained with the different codes. Results for other target materials can be found in appendix A.1.

The amount of produced isotopes per proton pulse can be calculated with a thin target approximation via

$$N = \sigma_{A_mB_n} * N_p * N_{A_mB_n} = \frac{\sigma_{A_mB_n} * N_p * V_{target} * \rho * N_A}{M} \tag{2.3}$$

where $\sigma_{A_mB_n}$ is the production cross section, N_p the proton density per pulse $[1/cm^2]$, $N_{A_mB_n}$ the number of particles of the material, ρ the density of the material, N_A the Avogrado constant, V_{target} the target volume and M the molar mass of the used species. The densities and molar masses used for the calculation are compiled in table 2.2. The densities of the actual target material is usually smaller than the nominal density due to the desired porosity. Figure 2.2 shows the cross sections obtained with the ABRABLA code and the resulting in-target production derived with formula 2.3.

2.3 Diffusion

As discussed in 1.2.2 the diffusion of isotopes to the surface of the target material's is a major factor for the speed and efficiency of extraction. Target materials for the production of exotic radioactive carbon isotopes usually consist of powders or fibers of metal oxides. Depending on whether neutron rich or deficient isotopes are desired, heavier (e.g. Hf) or lighter (e.g. Al, Ca) metals are chosen. As shown before, the production cross section for neutron deficient carbon isotopes does not vary much with the

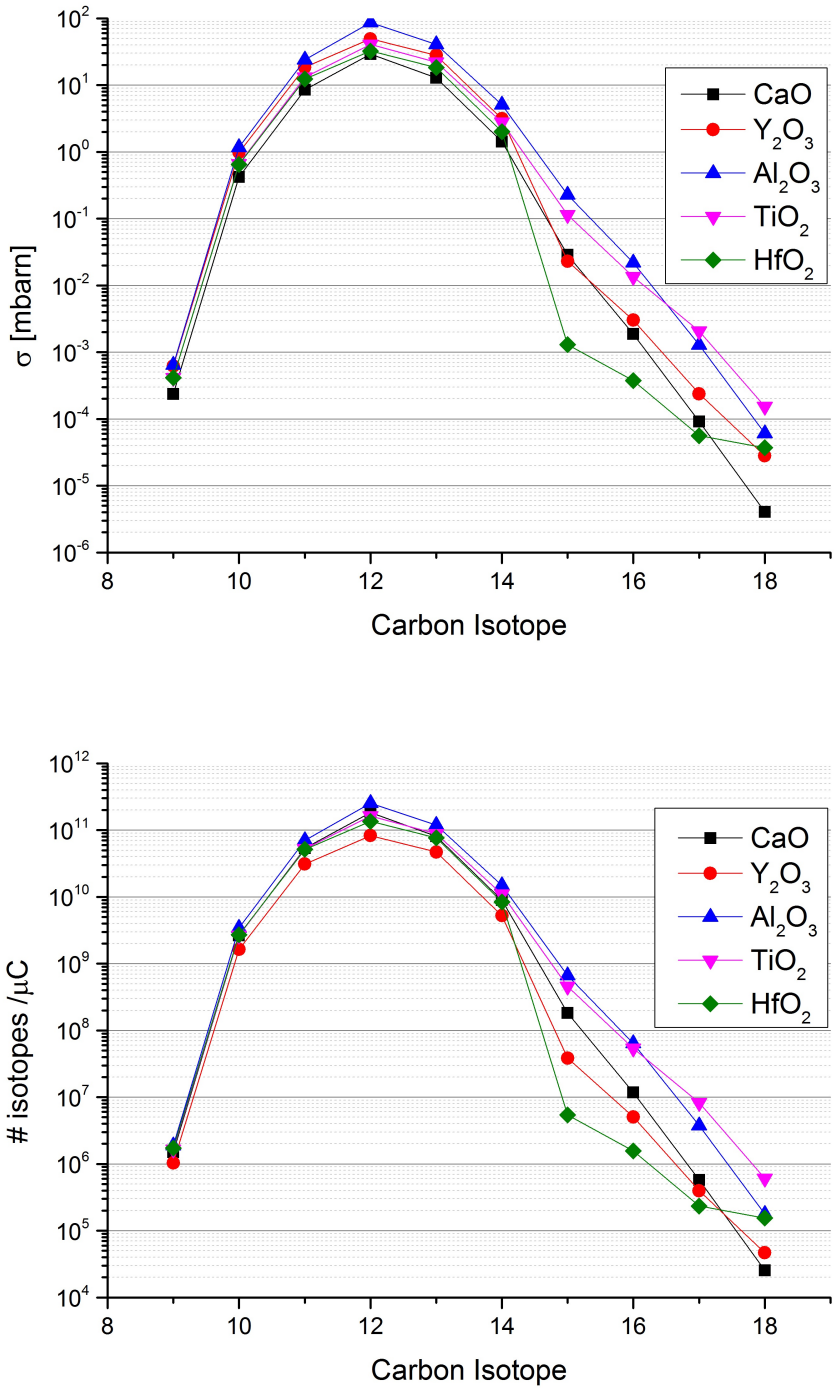

Figure 2.2.: Simulated isotope production cross section (upper figure) and in-target production (lower figure) for different potential target materials. The numbers were derived using the ABRABLA code [13].

Material	M $[g/mole]$	Nominal density $[g/cm^3]$
CaO	56	3.35
Y_2O_3	225.8	5.01
Al_2O_3	101.96	3.95
TiO_2	79.86	4.23
HfO_2	210.49	9.68

Table 2.2.: Nominal densities and molar masses of target materials. The lower densities of the actual target material have to be taken into account to calculate the isotope production

choice of the metal cation, as the production is dominated by oxygen. More important than the choice of the actual material is the structure and chemical behavior of the material.
In general, release is favored if the target material has a high open porosity and a small grain size [≈ nm]. In this case the path from the production point to the surface is short. The high open porosity assures that the isotope can migrate quickly in between the grains. Since in most cases the movement of a gaseous substance in open space is much faster than the diffusion through a solid material this will support a fast release.
As diffusion and effusion are dependent on the temperature target units are usually operated at a high temperature of 700 $°C$ to 2100 $°C$.
Studies on i.e. CaO [54] show that high temperatures can be adverse for the target material to maintain grain size and porosity. If a target material is operated at too high temperature small grains will sinter to bigger sizes and the open porosity gets lost. This sintering process is faster the smaller the initial grain size is [56]. This so called aging of the material explains in some cases why exotic species can be seen for a short time when target temperatures are raised but then suddenly disappear.
Studies on the release of carbon from metal oxides have been performed at ISOLDE [51],[19]. During an online experiment at GANIL it was found that the release from pressed fiber pellets is faster than from those made of pressed powder [51]. The results are shown in figure 2.3. The same work studied the release of implanted radioactive ^{11}C from pellets of MgO, TiO_2 and HfO_2. For implantation, carbon was extracted during online operations and implanted at 60 keV and 260 keV energy respectively. In order to promote diffusion, samples were heated afterwards for 10 minutes for each temperature step and the remaining activity was measured. These measurements show that in the case of MgO and TiO_2 90 % of the implanted ^{11}C was released at 1200 $°C$. To release the same fraction from HfO_2 the temperature had to be 1300 $°C$ -2000 $°C$.

As operational temperatures of the target should be kept at relatively low temperatures in order to maintain the target material properties, materials that show a higher diffusion rate at these temperatures such as MgO and TiO_2 are favorable.
Measurements of the diffusion properties of carbon in CaO and Y_2O_3 are still pending and should be object of future investigations.

2.4 Chemical Equilibrium of Carbon Oxides with Target Materials

After the production and the diffusion of an isotope to the surface of the grain, the formation to a more volatile molecule has to happen in the case of refractory elements like carbon and boron. Besides a high boiling point, these elements share high reactivity with many materials. In order to find conditions (temperature) and combinations of used materials under which the formation of a desired molecule and its extraction is as efficient as possible, the chemical equilibrium of carbon with materials present in the target system is calculated here.

In former tests it was found, that in the case of extraction of carbon from oxide target materials the molecules with the highest abundances are carbon monoxide and carbon dioxide. Typically cur-

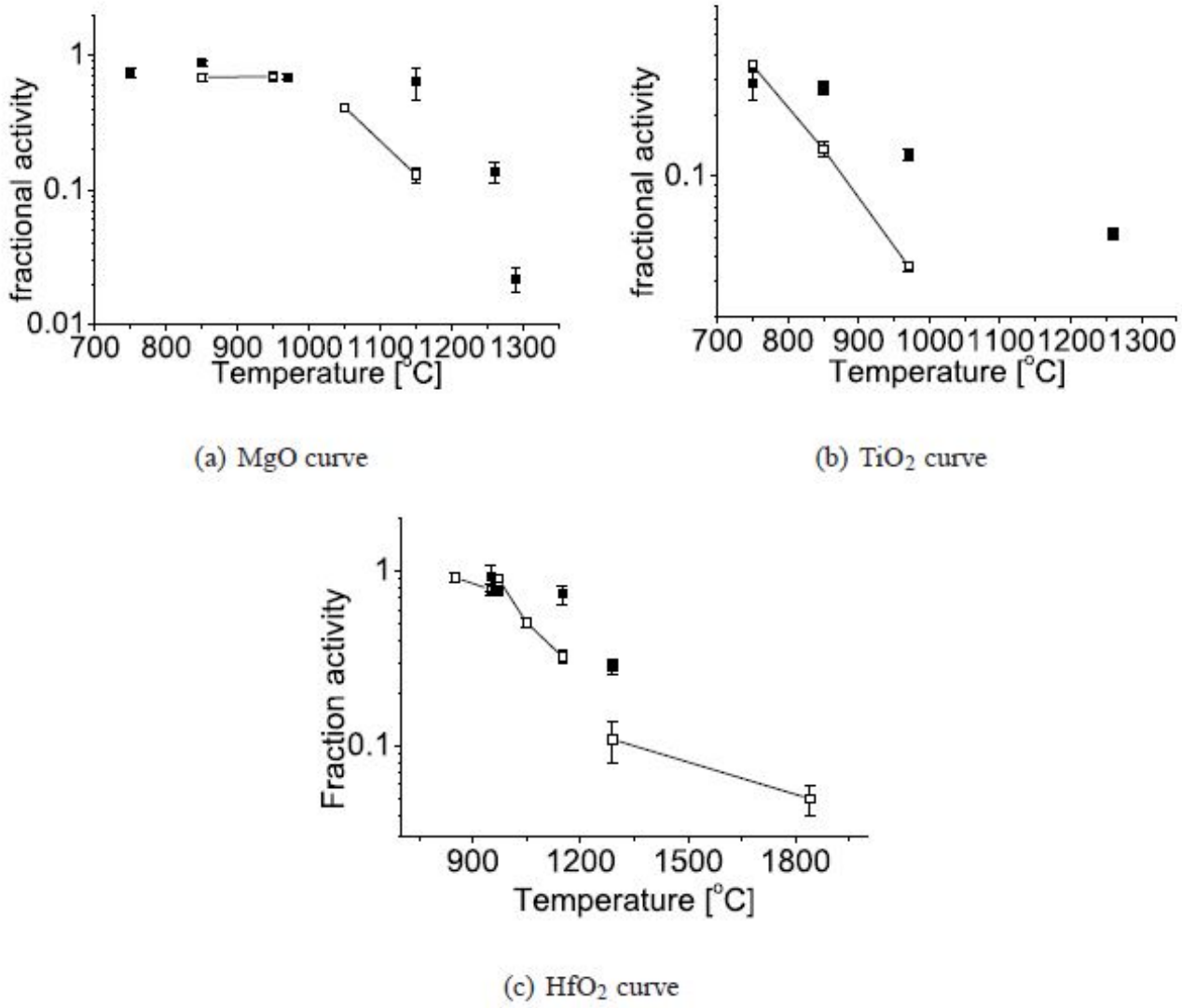

(a) MgO curve

(b) TiO_2 curve

(c) HfO_2 curve

Figure 2.3.: Diffusion studies from different target materials. Open markers show results from implantation with 60 keV, solid markers from implantation with 260 keV. Results and figure taken from [51]

rents of stable as well as radioactive CO^+ is measured with a factor of ten to hundred more than $CO_2{}^+$.

Other molecules like COF, CF_n or CH_4 are also volatile at temperatures present in targets but either extracted currents are not as high as for CO, CO_2 or the provision of a reaction partner (e.g. hydrogen for the formation of CH_4) comes along with safety issues. Hence calculations performed in this section concentrate of the extraction of carbon as an oxide. For simplicity the formation of the carbon oxide and its extraction are considered separately.

One aspect in choosing a suited target material for the production of carbon beams is the supply of available oxygen from the target material at operational temperatures. A sufficient supply of oxygen is necessary in order to assure an efficient formation of carbon oxide molecules.
Typically characteristics of the target materials that are important for an efficient extraction, such as grain size and porosity can be maintained for a longer period if the operational temperature is maintained below material dependent thresholds. Therefore it is advantageous, if the target material provides oxygen for the formation of carbon oxides at relatively low temperatures. In order to identify in which temperature region the production of carbon oxides is favored the equilibrium of carbon with different target materials has been calculated (see section 2.4.2).

In the same way the chemical equilibrium between CO and structural materials present in the target (Ta,Mo, Re, Cu) was calculated. The results of these calculations allow to estimate where losses during the migration of the formed carbon oxide to the ion source might occur. The results are shown in section 2.4.1.

In both cases the calculation of the chemical equilibrium was carried out using the HSC 7 code [37]. The ratios used in the calculations of the chemical equilibrium of carbon or carbon oxide and the investigated material is 1:10. In reality the ratio of produced carbon to the target material is orders of magnitude smaller. However performing the results with a ratio of 1:10 does not change the resulting composition but allows for more comfortable usage of the figures. The temperature region for which the equilibrium is calculated is 25 $^\circ C$ to 2500 $^\circ C$ at a pressure of 10^{-3} mbar. Typical operational values for ISOLDE targets are temperature between 800 $^\circ C$ and 2100 $^\circ C$ with pressures of $p \approx 10^{-3} - 10^{-6}$ mbar. Calculating the chemical equilibrium with lower or higher pressure shifts the occurrence of a species to higher or lower temperatures but does not change the ratios of present species. Hence results present a general tendency of a system to form one or the other species. Figure B.1 in appendix B illustrates the pressure dependency. The kinetics of the formation of desired species and the optimum conditions have to be determined experimentally.

2.4.1 Extraction of Carbon Oxides

Figure 2.4 shows the results of the calculation of the chemical equilibrium between carbon monoxide and structural materials (Ta, Re, Mo, Cu).
In the case of tantalum, the formation of tantalum carbide and tantalum oxide is thermodynamically favored at all temperatures. Hence losses are to be expected if the molecule gets in direct contact with the hot tantalum surfaces in the target. The formation of carbides and oxides with tantalum is known and has been studied in many cases (e.g. [57]).
In the case of molybdenum, the formation of molybdenum carbides takes place up to temperatures of approximately 1600 $^\circ C$. At higher temperatures the formation of carbon monoxide is dominant.
With rhenium no reaction with carbon oxide is expected up to approximately $1300^\circ C$. At higher temperatures rhenium forms solid solutions with the stoichiometry of $Re_2(CO)_{10}$.
Tantalum, rhenium and molybdenum are typically operated at temperatures between $800^\circ C$ and 2100 $^\circ C$, where these reactions become important for the release of carbon oxides. Typical operational tem-

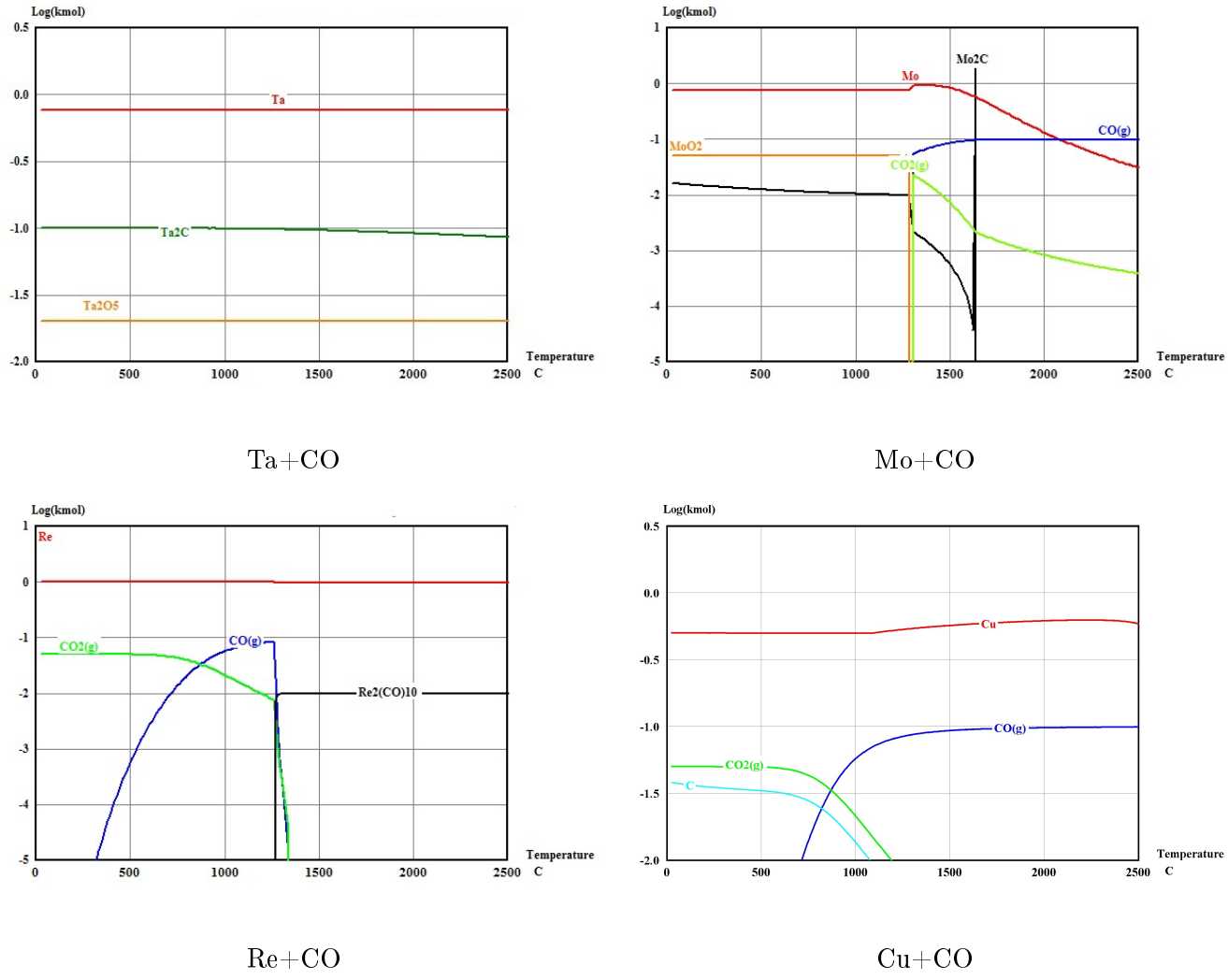

Figure 2.4.: Chemical equilibrium of CO with structural materials found in ISOLDE target units. The calculation were performed with a ratio of 1:10 of CO to the particular material.

peratures of copper are approximately 50 $°C$. The low operational temperature combined with the chemical inertness of copper towards carbon oxides makes copper a good material for the extraction of CO. However due to its low melting point it can be only utilized for cold parts of the target.

Figure 2.5 shows the results of the calculation of the chemical equilibrium of carbon monoxide with target materials. Investigated materials were either used as target materials in the past or show promising properties for a successful extraction of carbon as carbon oxide. The investigated materials are CaO, MgO, Y_2O_3, Al_2O_3, TiO_2 and HfO_2.
For the case of MgO, Y_2O_3, Al_2O_3 and HfO_2 no reactions between carbon oxide and the material occure up to 2500 $°C$. Hence no losses of formerly formed carbon oxide is expected. In the case of CaO an additional provision of oxygen occurs from 800 $°C$. If oxygen is present in a surplus CO reacts to CO_2. At lower temperatures calcium oxide reacts with carbon dioxide and forms $CaCO_3$. A similar behavior can be observed for TiO_2. At temperatures lower than 600 $°C$ carbon monoxide is reduced to carbon. For temperatures between 600 $°C$ and 1000 $°C$ formation of carbon monoxide is favored. At higher temperatures additional oxygen is provided, leading to an oxidation of CO to CO_2.

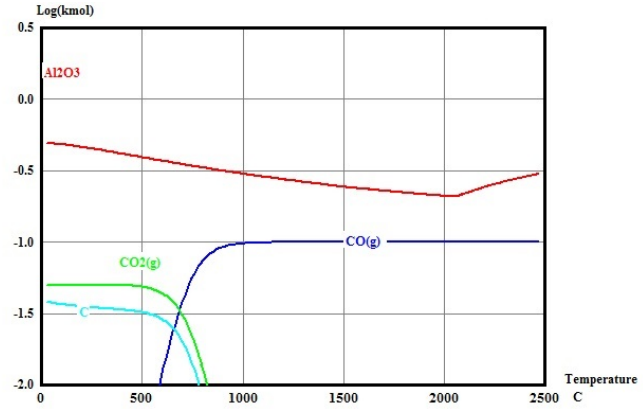

Al_2O_3+CO

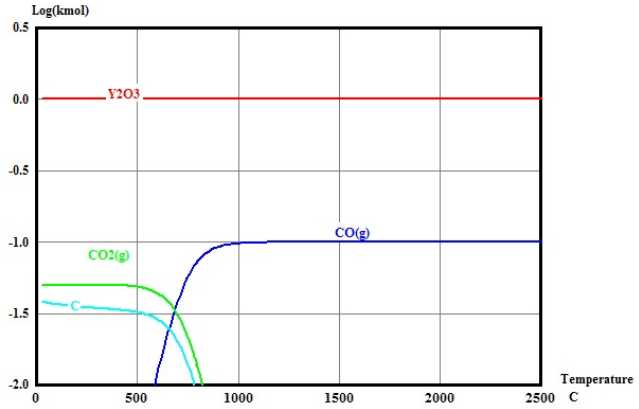

Y_2O_3+CO

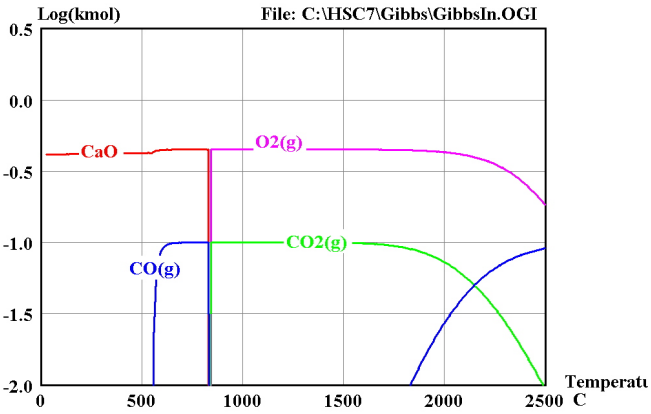

CaO+CO

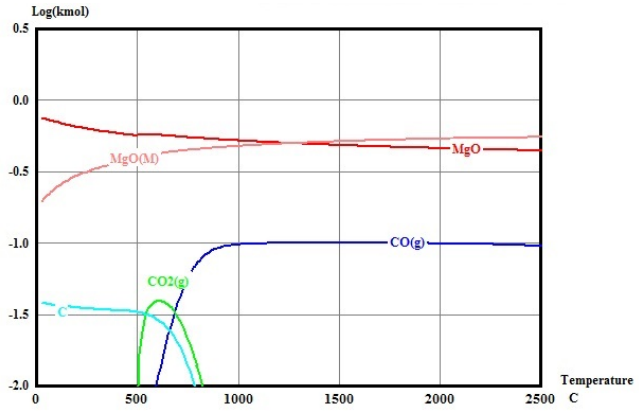

MgO+CO

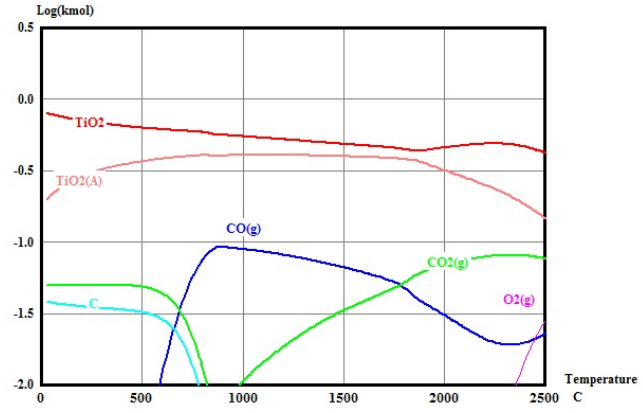

TiO_2+CO

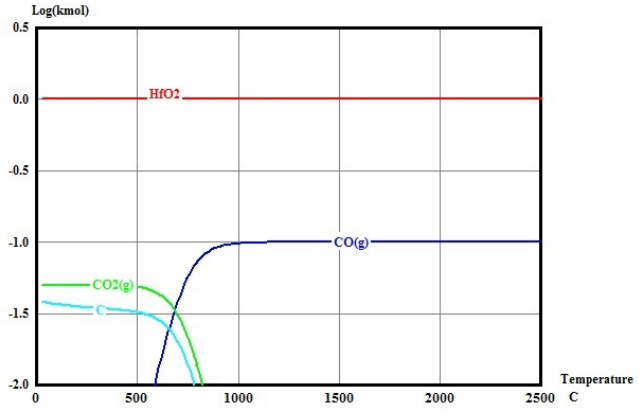

HfO_2+CO

Figure 2.5.: Chemical equilibrium of CO with possible target materials. The calculations were performed with a ratio of CO to the particular material of 1:10.

2.4.2 Formation of Carbon Oxides

For an efficient formation of carbon oxides it is crucial that a surplus of oxygen is present in the target container. In the past the supply of oxygen was believed to be assured by using an oxide as a target material. Calculations of the chemical equilibrium of carbon with used target materials show that this is not the case for some of the materials.
Instead the formation of carbon oxides only occurs at temperatures higher than temperatures these materials have been operated at in the past (e.g. Operational temperatures for Y_2O_3: T= $1100°C$ and HfO_2: T= $1450°C$; Formation of carbon oxides expected from Y_2O_3: T= $2000°C$ and HfO_2: T= $1600°C$)
.
The results of the calculations are shown in figure 2.6. In the case of Alumina (Al_2O_3), Magnesia (MgO) and HfO_2, carbon monoxide is formed from approximately 1600 $°C$. In the case of Titanium oxide (TiO_2) and calcium oxide (CaO) oxygen is provided from temperatures around 800 $°C$.

The results suggest that chemical reactions in the target container are more complicated than believed. Most of the discussed target materials have been used for the extraction of carbon as CO at operational temperatures between 800 $°C$ and 1500 $°C$. According to the chemical equilibrium formation of CO is not expected in some cases.
The fact that CO is released nevertheless means that a supply of oxygen is not only given by the material. Possible sources of oxygen might be

- Contamination that might be present in much higher amounts than C and influence the equilibrium
- Target materials are rarely present in theoretical stoichiometries and crystal lattice. Hence oxygen might be present in the structure and be slowly released
- Chemical bound is destroyed by proton beam

The exact analysis of the origin of oxygen requires a deeper insight into the chemical equilibrium and phase coexistence of target materials in the target container environment and is beyond the scope of this work.
If the availability of oxygen is one of the limiting factors in the formation and extraction of carbon as carbon oxide it is possible to change the chemical equilibrium in the target by injection of additional gases. According to equilibrium calculations Ta_2O_5, Y_2O_3 and Al_2O_3 form fluorides while releasing oxygen if fluorine is present. In the case of tantalum, present fluorine might also suppress the formation of tantalum carbides and therefore provision of fluorine might enhance the release of carbon as carbon oxide in these two ways.

2.5 Adsorption

On its way through the pores of the target material and on the path through the target container a previously produced atom or molecule experiences many hits with the surrounding surfaces. As described in 1.2.3 the particle will stick with a certain probability S on the surface. This causes a delay of $\tau = \tau_0 * \exp \frac{\Delta H_0}{k_B * T}$ each time the particle sticks to the surface. The total delay caused by one adsorption has to be multiplied by the total number of hits n. Simulations show [24] that n is in the order of 10^2 for the transport through the target structure. Comparing the ratio of tubular length and radii of the target container to a nano structural target material leads to an estimated number of hits of at least 10^6 inside the material.
In order to guarantee a similar delay for both materials the adsorption enthalpy of the species on the target material has to be 10 times smaller than the adsorption enthalpy of the structural material.
Parts that are resistively heated to temperatures up to 2100 $°C$ such as transfer line, target container and ion source inside ISOLDE target units are made from refractory metals. While the container and the

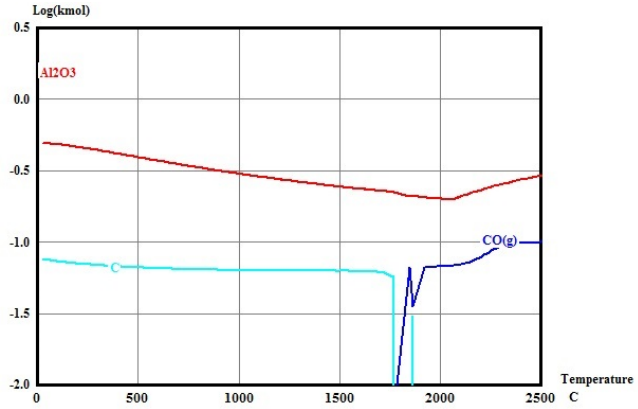

Al_2O_3+C

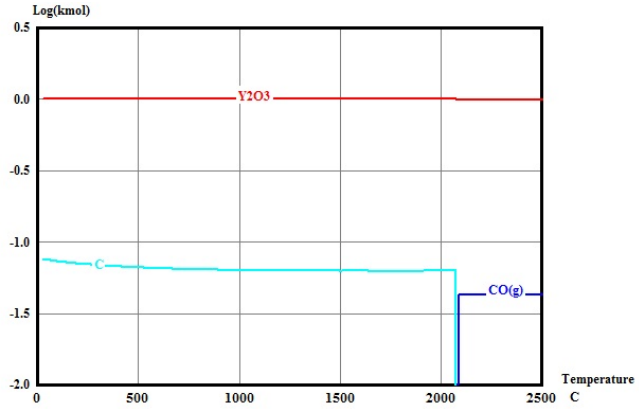

Y_2O3+C

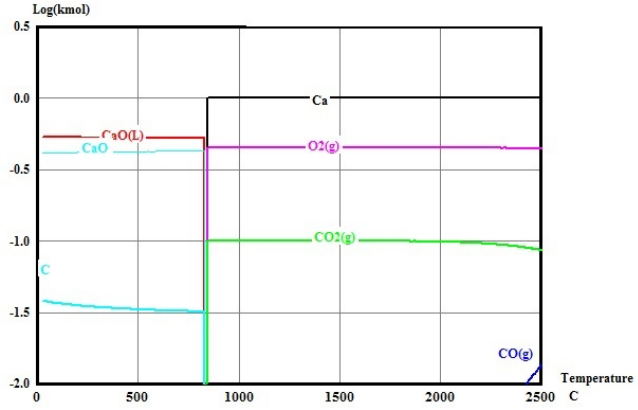

CaO+C

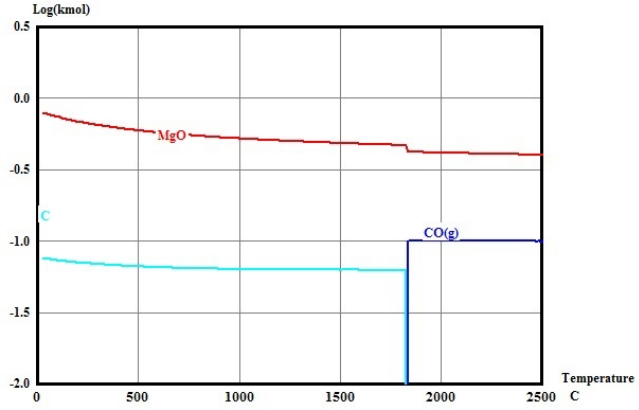

MgO+C

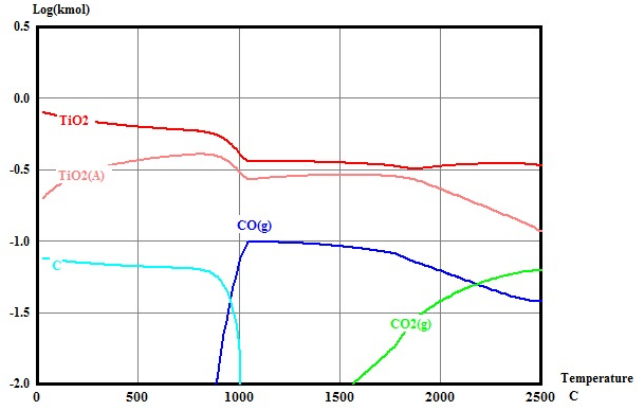

TiO_2+C

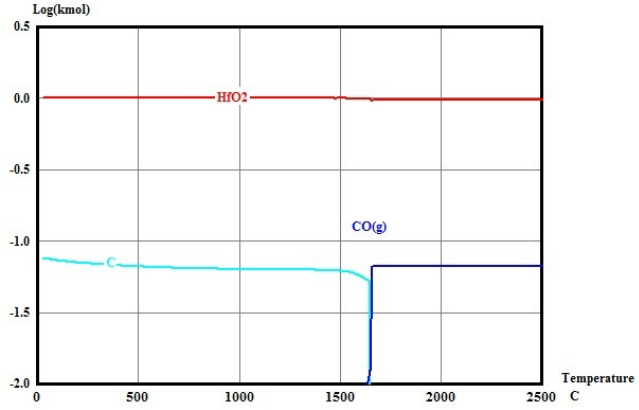

HfO_2+C

Figure 2.6.: Chemical equilibrium of C with target materials. The results show the temperature region in which formation of carbon oxides can be expected (CO: dark blue line, CO_2: green line.

Adsorbent	ΔH_0 [kJ/mole] CO	Ref.	ΔH_0 [kJ/mole] CO_2	Ref.
Ta	-128	[68]		
Re	-96	[62]		
Mo	-60	[68]		
MgO	-131	[51]	-164	[51]
Y_2O_3	-16	this work	-80	this work
HfO_2	-66	[51]	-133	[51]
Al_2O_3	-35,-21	this work,[51]	-35,-65	this work, [51]
TiO_2	-61	[51]	-158	[51]
ZrO_2	-153	[51]	-177	[51]
SiO_2			-22	[51]

Table 2.3.: Adsorption enthalphies ΔH_0 for CO and CO_2 on target and structural materials.

transfer line (in case of a hot transfer line) are made of tantalum, the ion source can contain tantalum, molybdenum, rhenium, tungsten and carbon. Furthermore foils of rhenium are often inserted into the target container to carry the target material. Other materials used are copper, graphite, quartz and a large variety of target materials for isotope production. For light isotopes such as carbon, pills of pressed powder or fibers of metal oxides are the target material of choice. To extract carbon isotopes with high efficiencies the adsorption on each of these materials has to be considered separately. Most experimental studies that are investigating the interaction of gases with surfaces are carried out with highly directed structures. As materials for target production are usually polycrystalline, studies looking at such unordered and porous structures are of particular interest.
These studies show that most of the metals used in ISOLDE targets interact strongly with carbon and carbon oxides. This is in particular the case for tantalum [58], the main component of target units. While adsorption occurs already at lower temperatures, dissociative chemisorption of CO occurs from $T = 400\ ^\circ C$, bonding the oxygen on the surface while the carbon diffuses into the tantalum lattice [59] [60].
A similar interaction, although in different temperature regions, was found for rhenium [61]. Chemisorption of carbon monoxide occurs from room temperature. When heating to 500 $^\circ C$ the chemisorbed molecules partly desorb while the remaining molecules are dissociated. Heating the sample to 1060 $^\circ C$ causes a recombination and desorption of the dissociated CO.
If Re is exposed to CO and O/O_2 in same amounts, almost no dissociative chemisorption was observed. The order of exposure had no impact in this behavior [62]. On tungsten CO adsorbs at low temperatures ($T \approx -200^\circ C$ to $-173^\circ C$). Heating this sample to $T \approx 0-100^\circ C$ shows that 60% of the initially adsorbed CO desorbs. Even on elevated temperatures $T \approx 600-700^\circ C$ no dissociative chemisorption was observed in isotopic mixing experiments [63].
For the case of molybdenum non-dissociative chemisorption at room temperature was observed [64]. Desorption occurs from 500 $^\circ C$ with no evidence of further adsorption [65].
Studies on the adsorption of CO and CO_2 on proposed light metal oxides (Al_2O_3, MgO, CaO,Y_2O_3) are not as manifold as for the adsorption on metals. However some few investigations were performed [51]. It was found that MgO is a strong adsorbent for CO and CO_2. Investigations on CaO could not be carried out since CaO carbonizes in contact with air. Calcium and Magnesium belong to the same group and it can be assumed that the strength of interaction is comparable.
For the case of Alumina, Yttria and Hafnia adsorption enthalpies are lower and comparable (see table 2.3). The table also shows results from measurements carried out in the framework of this thesis. The adsorption enthalpy of CO and CO_2 on Al_2O_3 and Y_2O_3 was investigated by the group of R. Bulanek at the University of Pardubice using microcalorimetry. A detailed description of the technique can be found in [66] and [67].

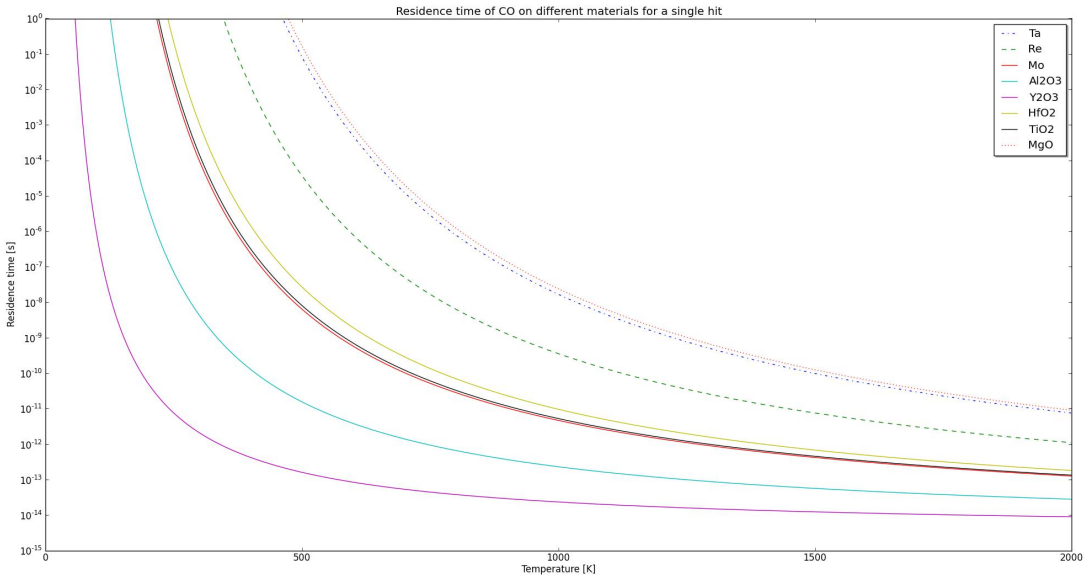

Figure 2.7.: Residence time of CO on target and structural materials for a single hit, assuming a sticking probability of 100 %.

Figure 2.7 and 2.8 show the residence time given by formula 1.6 for CO and CO_2 on different materials depending on temperature, calculated for one single hit on a surface assuming a sticking probability S of 100%.

2.6 Release Studies of Carbon Oxides from ISOLDE Targets

From release measurements taken during on-line runs it is often difficult and in many cases not possible to calculate single contributions of the total release efficiency or release time introduced in equation 1.1. Most of the time a combination of several efficiencies or even the total release efficiency or release time for a release can be derived. In order to investigate release parameters in more detail and to understand where losses occur a dedicated experiment has been set-up. An ISOLDE target unit was equipped with a cold transfer line that connects an empty tantalum container to a VADIS ion source.
Through a controllable valve, that is connected via a gas line to the target container, pulses of gas (e.g. CO, CO_2, noble gases) are injected into the target container and the resulting release from the ion source is monitored (see figure 2.9).
Via a second gas line that is connected to the transfer line additional gases can be injected into the target system and the impact on the release of the species injected through the pulsed valve studied.

As introduced in chapter 1.2 the release fraction from an ISOLDE target is described by

$$N = N_0 \cdot exp(-\lambda \cdot (t_{diff} + t_{ads} + t_{eff})) \cdot \epsilon_{diff} \cdot \epsilon_{transport} \cdot \epsilon_{formation} \cdot \epsilon_{ion} \tag{2.4}$$

The released fraction can also be described by the integral of the time depended current I(τ) which will be used later in this chapter.

$$N = \int_0^\infty I(\tau) d\tau \tag{2.5}$$

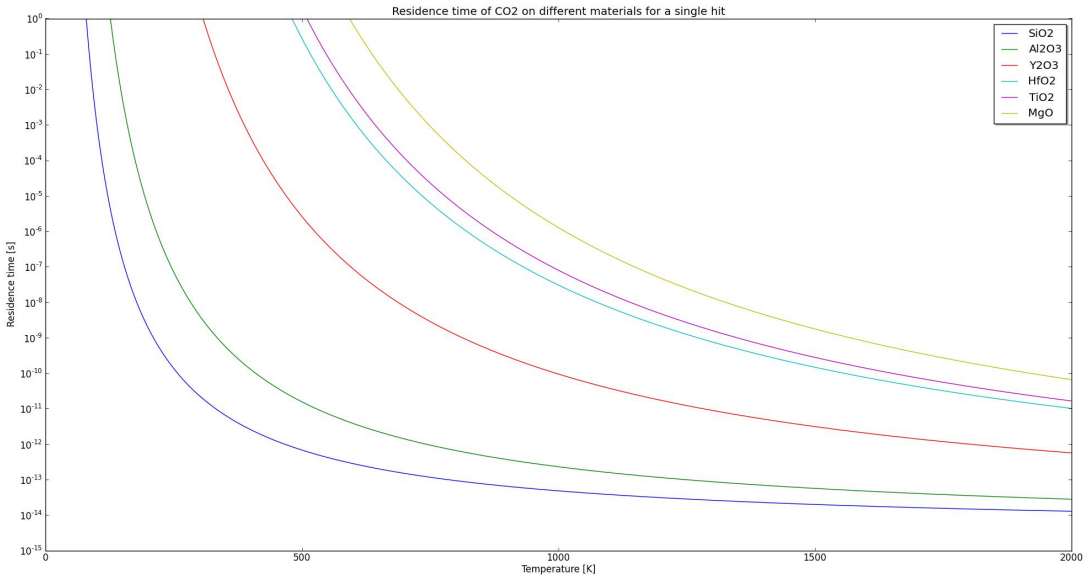

Figure 2.8.: Residence time of CO_2 on target and structural materials for a single hit on the surface, assuming a sticking probability of 100 %

For the measurements the gas to be studied (e.g. CO_2, Ar) is injected directly into the target container. Therefore diffusion from the target material and in case of molecules their formation is not required. Hence the diffusion efficiency ϵ_{diff}, the molecule formation efficiency $\epsilon_{formation}$ and the diffusion time t_{diff} in equation 1.1 are $\epsilon_{diff} = 1$, $\epsilon_{formation} = 1$ and $t_{diff} = 0s$. Then equation 2.4 simplifies to

$$N = N_0 \cdot exp(-\lambda \cdot (t_{ads} + t_{eff})) \cdot \epsilon_{transport} \cdot \epsilon_{ion} \tag{2.6}$$

Combining equation 2.6 with equation 1.22 under consideration that $\epsilon_{diff} = 1$ gives

$$N = N_0 \cdot \int_0^\infty e^{-\tau \cdot \lambda} \cdot p_v d\tau \cdot \epsilon_{ion} \tag{2.7}$$

where p_v is the probability for effusion out of a volume for a given geometry.

When noble gases are injected no losses due to chemical reactions or delay due to adsorption on surfaces are expected and hence $\epsilon_{transport} = 1$ and $t_{ads} = 0$. This allows to determine the ionization efficiency ϵ_{ion} and the effusion time t_{eff}.

For chemically reactive gases like CO_2 a delayed release time due to adsorption and losses due to chemical reactions with the target system are expected.

The goal of the experiment is to study the impact of operational temperature of the target container, different materials and chemical composition in the target on the release of carbon oxides. This is in order to identify materials and operational parameters that allow to maximize the extraction efficiency of produced radioactive carbon isotopes.

2.6.1 Experimental Setup

The setup was designed as a part of this thesis project. The gas of interest is injected into the target container via a dedicated gas system. This system consists of a calibrated leak with a leak rate of $5 * 10^{-5} \frac{mbar}{l*s}$ (for air) through which a reservoir is filled. Downstream of the reservoir a rapid valve

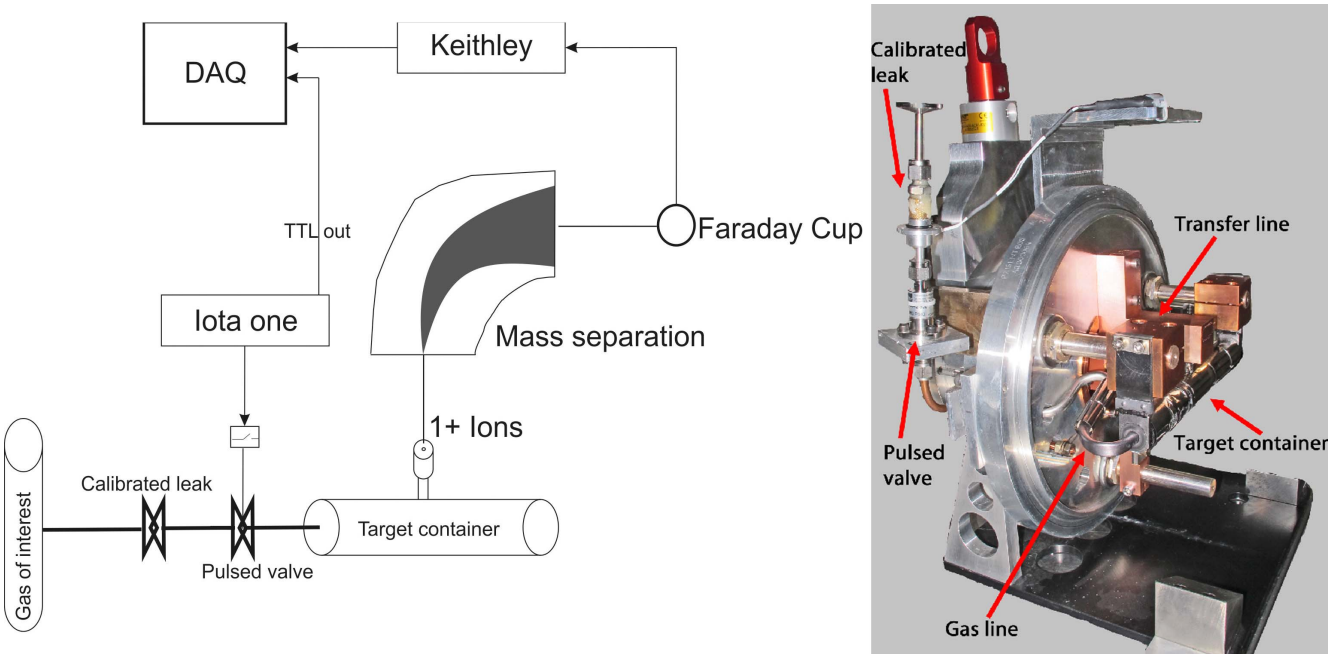

Figure 2.9.: Setup for release measurements. The gas of interest (e.g. CO, CO_2, Ne, Ar,..) is injected pulse by pulse via a pulsable high speed valve into the target container. Depending on the nature of the injected gas, adsorption or chemical reactions with the container materials can occur during the migration to the ion source. After the extraction, ions are mass separated and the current of +1 ions monitored via a Faraday cup.

(Parker 009-0442-900) is installed. Figure 2.9 shows the schematic setup of the experiment and a picture of the modified target unit.

After a closure time t_{close} of the valve during which the gas of interest accumulates in the reservoir a pulse generator opens the high speed valve for a period t_{open} during which the reservoir is emptied and the gas injected into the target container. The amount of gas injected can be calculated with

$$V = \frac{L \cdot t_{close}}{p} \cdot \sqrt{\frac{m_{air}}{m_{gas}}} \tag{2.8}$$

where L is the leak rate of the calibrated leak $[\frac{mbar \cdot l}{s}]$, t_{close} [s] the time the high speed valve is closed and p [mbar] the pressure of the gas applied on the calibrated leak. The $\sqrt{\frac{m_{air}}{m_{gas}}}$ term in formula 2.8 accounts for the fact that the leak rate is given for air and thus needs to be scaled to the mass of the injected gas. As soon as the valve is open a burst of gas migrates through the gas line into the target container and to the ion source where it is ionized and extracted.
The resulting stream of ions is mass separated and the current of the ion of interest monitored with a Faraday cup. The data acquisition is realized with a Keithley 6487 picoamperemeter and a labview® program running on the connected computer.

2.6.2 Measurements

To study release characteristics measurements with noble gases (Ne,Kr,Xe) and isotopicaly enriched $^{13}CO_2$ were performed. During each series of measurement the target container temperature was increased stepwise from room temperature to 2000 $°C$ for the case of the plain tantalum container and the container covered with rhenium foil and to 1400 $°C$ in the case of Al_2O_3. After each increase of temperature the target remained for 10 minutes in order to reach thermal equilibrium.

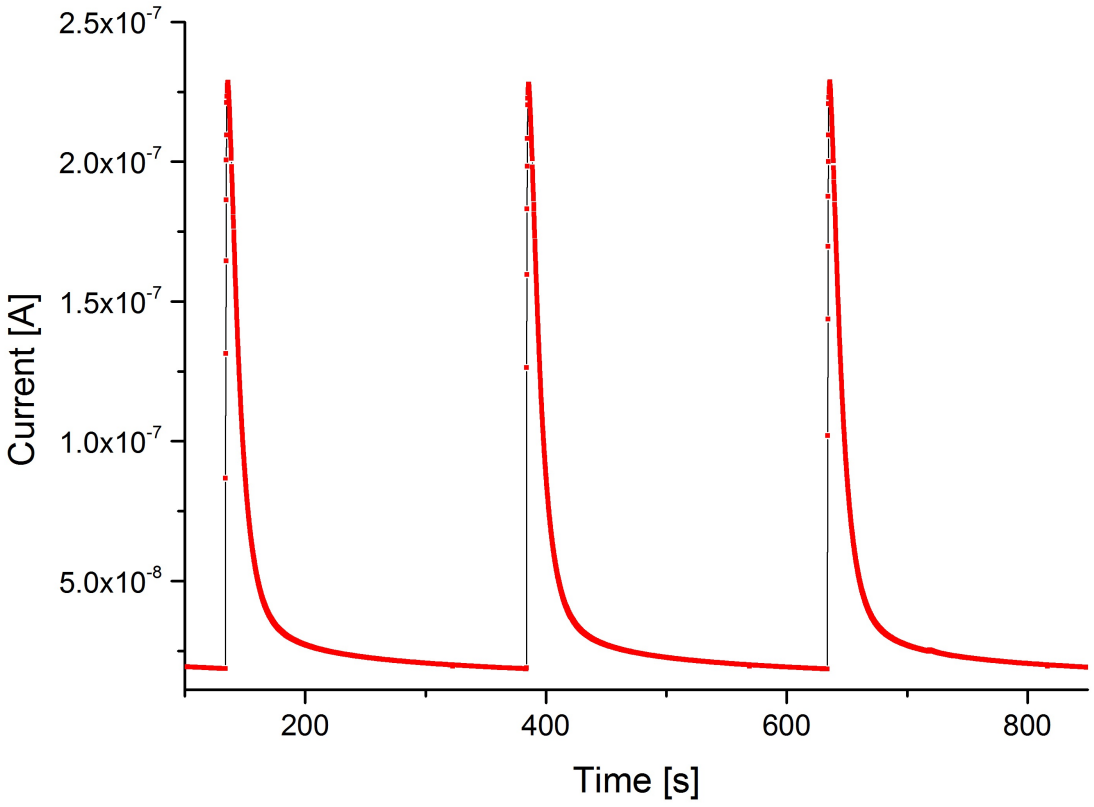

Figure 2.10.: Ion beam intensity of $^{13}CO^{+}$ after pulsed injection of $^{13}CO_2$ with a target temperature of $T = 1500\ °C$.

After that 8 pulses of the gas of interest were injected and the resulting release was monitored. In the case of noble gases the $q = +1$ ions and in the case of $^{13}CO_2$, $^{13}CO_2{}^{+}$ and $^{13}CO^{+}$ were monitored as dissociation is expected. Figure 2.10 shows a typical measurement.

To accumulate gas, the valve was closed for $t_{close} = 250$ s and opened for $t_{open} = 1$ s. When shorter opening times were chosen an increase of the peak height over time was observed what suggests that the reservoir could not be emptied entirely.

The measurements can be separated into two different parts:

1. Characterization of the system with noble gases
   - evaluation of release efficiency, here $\epsilon = \epsilon_{Ion}$
   - evaluation of dependency of rise time[1] to square root of mass $t \propto \sqrt{M}$ (see equation 2.9)
2. Injection of reactive species ($^{13}CO_2$) to study release time and release efficiency
   - release of $^{13}CO_2{}^{+}$ and $^{13}CO^{+}$ from plain tantalum container
   - release of $^{13}CO_2{}^{+}$ and $^{13}CO^{+}$ from tantalum container covered by i.e. Al_2O_3, Re

[1] The rise time is the time between the opening of the valve and the moment when the resulting ion current reaches it's maximum.

During the first part of the experiment different noble gases were injected into the container. These gases are neon, krypton and xenon. Due to their chemical inertness noble gases do not react with the surrounding material. This allows to characterize the system and determine the migration time independently of adsorption. Furthermore chemical losses do not occur which allows to determine the ionization efficiency. The average time a noble gas atom needs to migrate through the system is determined by the mass m of the species, the temperature T and the effective path length l through the system:

$$\begin{aligned} E = \frac{1}{2}m\overline{v}^2 &= \frac{3}{2}k_B\overline{T} \\ \overline{v} &= \sqrt{\frac{3k_B\overline{T}}{m}} \\ \overset{v=\frac{l}{t}}{\rightarrow} \overline{t} &= \sqrt{\frac{l^2 * m}{3k_B\overline{T}}} \end{aligned} \tag{2.9}$$

A linear correlation between the rise time t and the square root of the mass $\sqrt{m}$ is expected.
In this experiment the correlation between mass and release time was studied for noble gases. The results allowed to study release time characteristics of reactive species where $t_{ads} \geq 0$. Measurements showed that the rise time of the release offers the best way to study the time structure of the release. The rise time is defined as the time between the opening of the valve by the trigger pulse from the pulse generator and the point where the pulse reaches its maximum (see figure 2.11).
The goal when injecting $^{13}CO_2$ into the container is to understand the impact of surfaces of hot tantalum and other materials on the release time and release efficiency. When the container was covered with a Re foil and a tube of Al_2O_3 one expects different release efficiencies (see section 2.4) due to the chemical reaction of CO_2 with the surrounding material. Furthermore the release time is expected to be influenced by adsorption (see section 2.5) as shown in equation 2.4.

In order to analyze the release efficiency the measured peaks were averaged and the background subtracted (figure 2.11). Integrating the curve numerically results in the total amount of released gas N_{rel}. Comparing that number with the amount of injected gas N_{inj} that is determined by formula 2.8 allows to calculate the release efficiency ϵ in the case of carbon oxides or the ionization efficiency in the case of noble gases:

$$\epsilon = \frac{N_{rel}}{N_{inj}} \tag{2.10}$$

2.6.3 Calibration with Noble Gases

Figure 2.12 shows the results of ionization efficiency measurements for different noble gases at temperatures from 850 $^\circ C$ to 1900 $^\circ C$. As noble gases are chemically inert no losses due to chemical reactions with the target environment are expected.
Indeed measurements show that the ionization efficiency is independent from the temperature and constant.
The measured ϵ_{ion} and published efficiencies ϵ_{Vad} [32] are compared in table 2.4. The errors for the ionization efficiencies ϵ_{ion} are given by the standard deviation of the measurement, the errors of the quotient of expected efficiency ϵ_{Vad} and ϵ_{ion} follow from the propagation of this uncertainty.
While the quotients of measured ionization efficiency $\epsilon_{release}$ divided by published efficiency ϵ_{Vad} for

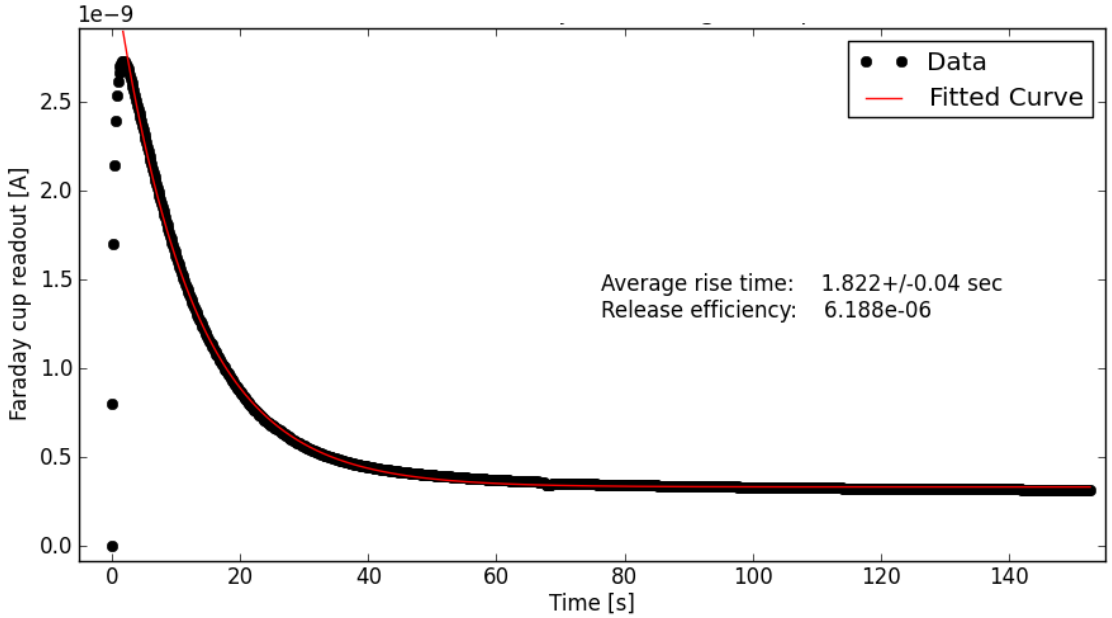

Figure 2.11.: Typical measurement of release of injected gas. In this case the release of $^{13}CO^{+}$ was monitored after the injection of $^{13}CO_2$ from a plain tantalum target container heated to 1500 $^{\circ}C$. The presented peak is an average of 82 injections.

Species	ϵ_{ion} [%]	ϵ_{Vad} [32] [%]	$\frac{\epsilon_{Vad}}{\epsilon_{ion}}$ [32]
Ne	0.42 ± 0.05	6.7	15.99 ± 1.38
Kr	1.43 ± 0.04	38	26.57 ± 0.72
Xe	1.93 ± 0.09	47	24.35 ± 0.76

Table 2.4.: Comparison of measured and published ionization efficiencies for noble gases, ionized in a Vadis [32] ion source.

xenon and krypton are in agreement, the ionization efficiency for neon appears to be too high compared to Kr and Xe respectively. This is most likely due to a contamination on mass 20 due to Ar^{2+} ions coming from injected argon.

In order to investigate the delay time a species experiences migrating through the target system, the time structure of the measured curves was analyzed. Here the rise time, the time between the opening of the valve and the point when the measured current reaches its maximum is considered.
As noble gases should not experience adsorption on surfaces the release time for a species should only depend on its mass and temperature. As shown in equation 2.9 a linear correlation between the square root of the mass and the release time is expected for a given temperature. Figure 2.13 presents the results for neon, krypton and xenon, where the linear correlation between $t_{release}$ and $\sqrt{m}$ is observed. The absolute values are in the order of seconds, compared to ms seen during online measurements. The reason for that appears to be the conductance of the used fast valve and the gas system. Hence the absolute release times are not representative. However as shown in the next section can a delayed release for reactive species be observed.

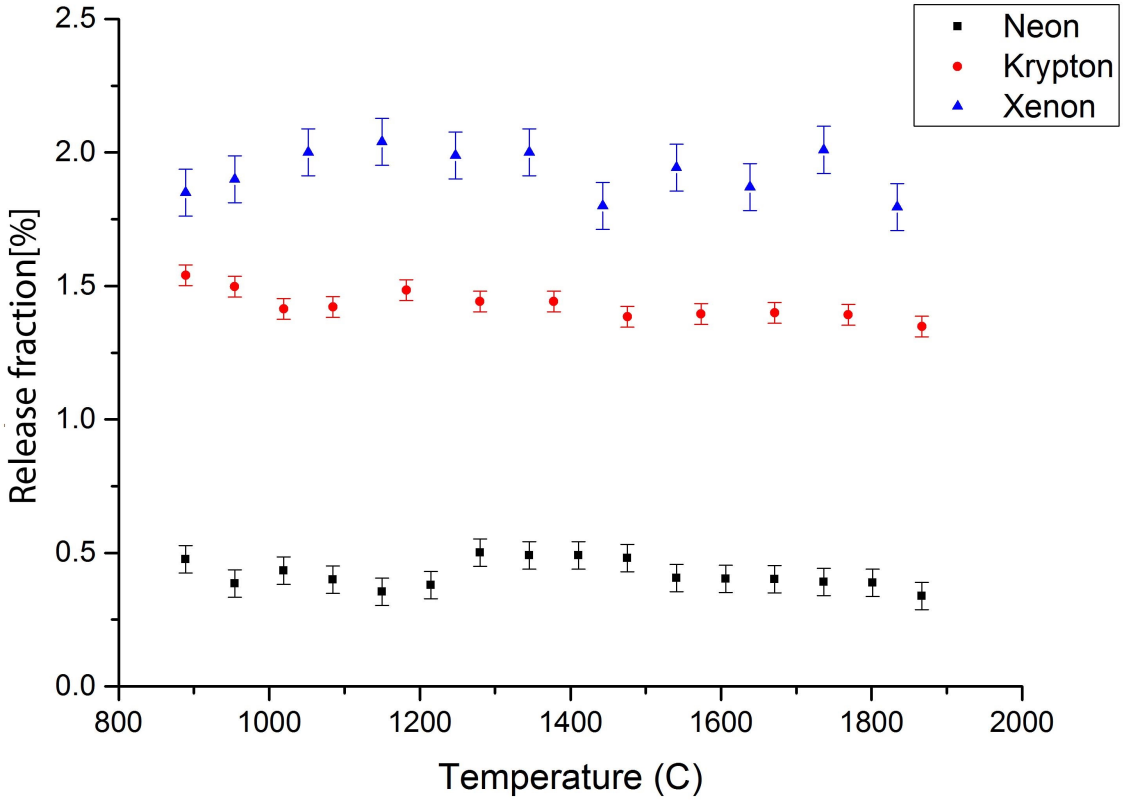

Figure 2.12.: Derived release fractions of neon, krypton and xenon depending on the target temperature. As expected for noble gases is the release fraction independent of the target temperature.

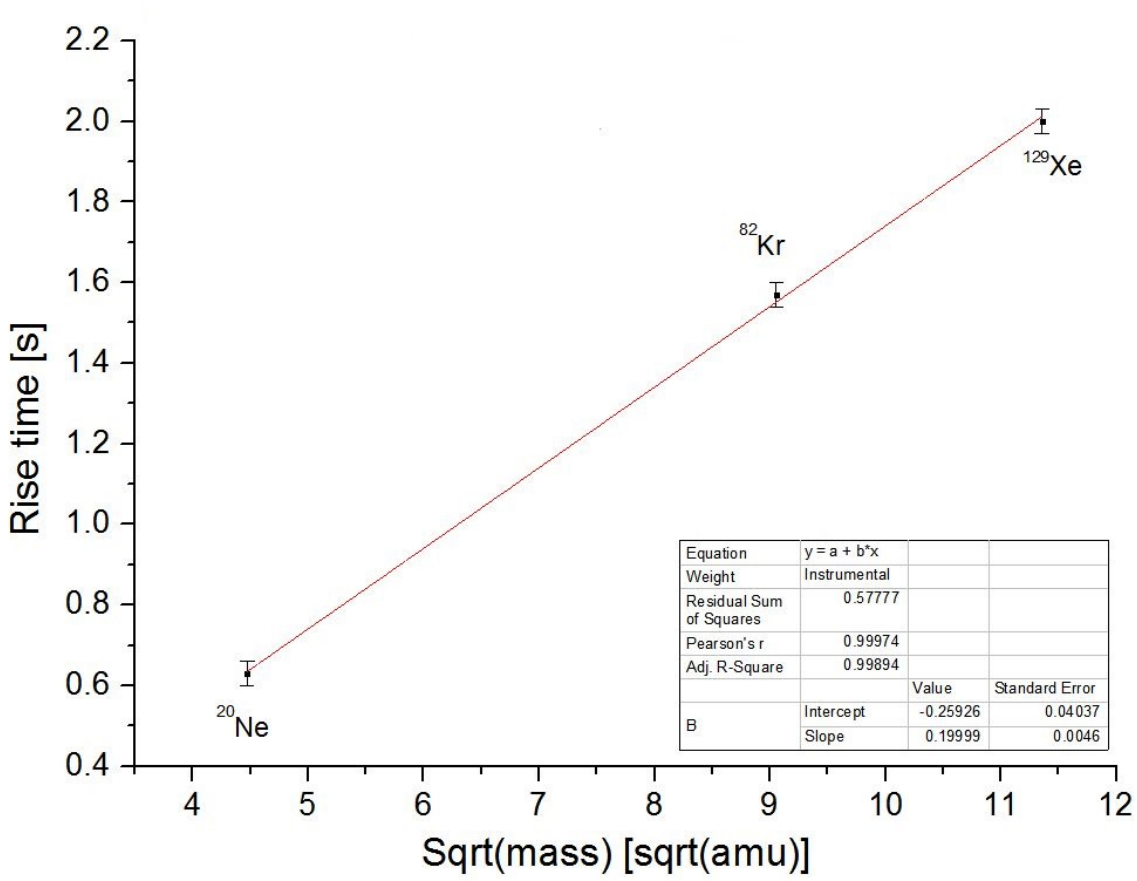

Figure 2.13.: The plot shows the linear correlation of rise time with the square root of the mass as shown in equation 2.9. Measurements were taken with $T_{target} = 800°C$ and $p_{gas} = 0.4bar$.

2.6.4 Release Measurement with $^{13}CO_2$ and Release Efficiency

In order to understand the release of carbon oxides, $^{13}CO_2$ was injected into the target container. This isotopically enriched gas was used in order to distinguish the injected $^{13}CO_2$, released as $^{13}CO_2^+$ and $^{13}CO^+$ from naturally occurring carbon oxides and other contaminants with the same mass (e.g. N_2 for mass 28).
As natural carbon occurs in the isotopic mixture 98.9% ^{12}C and 1.1% ^{13}C the background level of ^{13}C oxides was determined prior the injection of $^{13}CO_2$. As seen in section 2.7 is the majority of the injected $^{13}CO_2$ expected to occur as two different ions: $^{13}CO_2^+$ and $^{13}CO^+$. Hence the beam intensity of $^{13}CO^+$ and $^{13}CO_2^+$ was monitored after each injection.
The released $^{13}CO_2^+$ originates from direct ionization of $^{13}CO_2$ by electron impact. For the production of $^{13}CO^+$ three different scenarios are possible:

- Dissociative ionization of CO_2: $CO_2 \rightarrow CO^+ + O^+ + 2e^-$
- Thermal dissociation of CO_2 to CO and O with subsequent ionization of CO
- Dissociative adsorption or chemical reaction of $^{13}CO_2$ on surfaces with release of CO and subsequent ionization

Figure 2.14 and 2.15 show the results of the measurements. Both figures show the release from the plain Ta container and the same container covered with a rhenium foil and an Alumina tube.

In the case of carbon dioxide as $^{13}CO_2^+$ clear trends are observable, for $\epsilon_{release}$ we find that $\epsilon_{Al_2O_3} \geq \epsilon_{Re} \geq \epsilon_{Ta}$.
For temperatures up to 1400 $^\circ C$ the release efficiency from the alumina covered container where no reaction is expected is around 2 times higher than the release from a rhenium covered container and 4 times higher than the release efficiency from the plain tantalum container. Above 1400 $^\circ C$ the release efficiency from the plain container and the rhenium covered container drops by almost two orders of magnitude. However the release efficiency from the rhenium covered container is higher at all temperatures.
For rhenium a reaction with carbon oxides is expected from approximately 1400 $^\circ C$ as seen in figure 2.4 and indeed the release efficiency starts dropping at this temperature.
According to calculations of the chemical equilibrium no release of $^{13}CO_2^+$ is expected for the case of tantalum. This is reflected in the generally low release efficiency from the plain container.
The reason why $^{13}CO_2{}^+$ is released, in contrast to the predictions from chemical equilibrium calculations, can probably be found in effects induced by saturation of the surface, sticking probabilities smaller than 1 and the finite time the molecule spends in the container. In the later case the molecule might be release before equilibrium was reached.
In general it has to be noted that the coverage of the tantalum container was not perfect. Substitution of the tantalum as a container material is not possible as the design of the container heating requires a refractory metal. Therefore effects applying on the release of $^{13}CO_2{}^+$ and $^{13}CO^+$ from tantalum also apply to the measurements with alumina and rhenium, but to a smaller degree.

In the case of carbon monoxide differences in the observed release efficiency are not as high as in the case of $^{13}CO_2$. Measured efficiencies for all three materials are approximately the same for low temperature (up to 800 $^\circ C$). Again the release from rhenium drops in agreement with figure 2.4 while efficiencies from alumina and tantalum remain constant up to 1400 $^\circ C$.
The fact that release efficiencies for CO are approximately the same for all three materials leads to the conclusion, that the majority of produced CO comes from a reaction that is not taking place in the target container and hence independent of the inserted material. Therefore the transformation from CO_2 to CO must take place in the ion source.

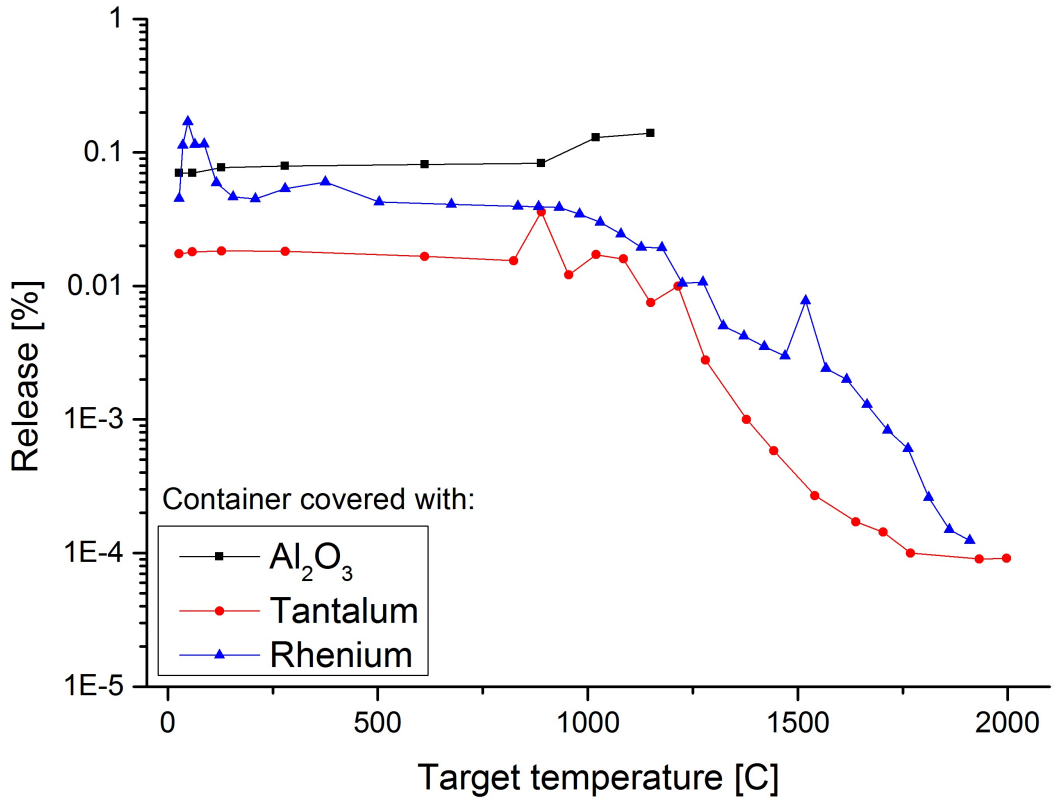

Figure 2.14.: Fraction of $^{13}CO_2$, released as $^{13}CO_2{}^+$

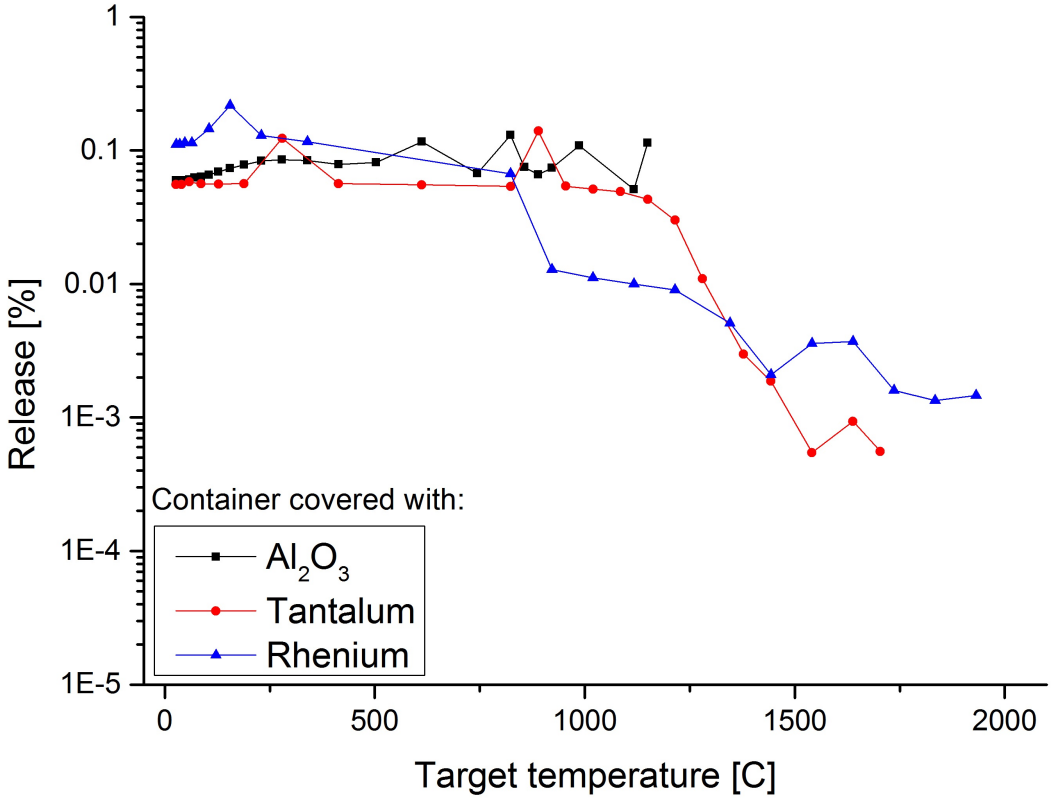

Figure 2.15.: Fraction of injected $^{13}CO_2$, released as $^{13}CO^+$

As dissociation cross sections of CO_2 to CO are much smaller than the direct ionization of CO_2 [35] the released CO must origin from a chemical reaction. Looking at the calculations of the chemical equilibrium between the ion source material molybdenum and CO shows, that for elevated temperatures ($T \geq 1500°C$) the formation of CO is favored. This means that a fraction of CO_2 that is arriving in the ion source reacts with the surrounding Mo to CO and gets extracted as CO^+. The remaining CO_2 is ionized immediately and extracted as $^{13}CO_2{}^+$.
If release times are considered additional evidence can be found (figure 2.16). From the release measurements of noble gases the dependency of the square root of the mass to the release time is known (see figure 2.13). For this particular setup at a temperature of 800 $°C$ the dependency is given by:

$$t(\sqrt{M}) = 0.19 \cdot \sqrt{M} - 0.259 \tag{2.11}$$

For $^{13}CO_2{}^+$ with a mass of $m(^{13}CO_2) = 45$ amu and $^{13}CO^+$ with a mass of $m(^{13}CO) = 29$ amu equation 2.11 gives release times of $t(\sqrt{45}) = 1.01$ s and $t(\sqrt{29}) = 0.76$ s. The experimentally measured release times of $^{13}CO_2{}^+$ and $^{13}CO^+$ are $t(\sqrt{45}) = 1.09 \pm 0.1$ s and $t(\sqrt{29}) = 1.81 \pm 0.1$ s (see figure 2.16). While the release of $^{13}CO_2{}^+$ happens withing the expected time, the release of $^{13}CO^+$ is delayed by a factor of 2.4. This delay probably occurs from the reaction of $^{13}CO_2$ to ^{13}CO on the ion source material.

2.6.5 Conclusion

From Calibration with noble gases:

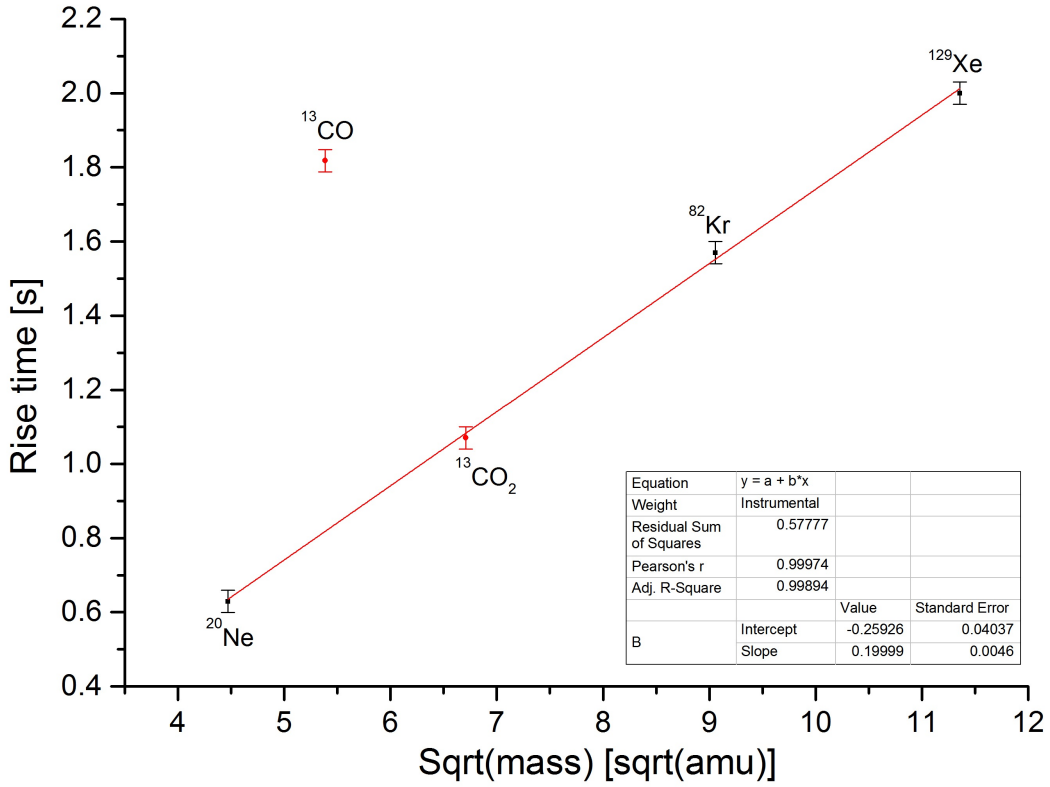

Figure 2.16.: Comparison of rise times of noble gases (Ne,Kr,Xe) with measured rise times found for $^{13}CO^{+}$ and $^{13}CO_2^{+}$

- The ion source performance for the used (conservative) settings was determined. The published [32] maximum ionization efficiency ϵ_{ion} for Kr and Xe is approximately 25 times higher than the measured ones. The ionization efficiency for neon is biased by the overlapping Ar^{2+} peak on mass A= 20 and is therefore not discussed further.

- The expected linear correlation between the release time and the square root of the mass of the species was confirmed: $t \propto \sqrt{m}$. This qualifies the setup for the investigation of reactive species.

From Release measurements with $^{13}CO_2$

- From the characterization with noble gases we learn, that if the combined efficiency $\epsilon = \epsilon_{trans} \cdot \epsilon_{ion}$ for $^{13}CO_2$ is limited by ϵ_{ion} an increase of up to 25 fold can be expected if the ion source is operated at best conditions.

- The combined efficiencies $\epsilon = \epsilon_{trans} \cdot \epsilon_{ion}$ of CO_2 as $CO_2{}^+$ are higher if the container is covered with alumina or rhenium than from the plain Ta container ($\epsilon_{Al_2O_3} \geq \epsilon_{Re} \geq \epsilon_{Ta}$). The efficiencies vary between $0.07 - 1 \cdot 10^{-4}$% for Ta, $0.03 - 1 \cdot 10^{-4}$% for Re and 0.07% for Al_2O_3 for the release of CO_2.

- The release of CO seems to be independent of the surface material for temperatures up to 1300 $°C$ ($\epsilon_{Al_2O_3} \approx \epsilon_{Re} \approx \epsilon_{Ta}$). This leads to the conclusion that the dissociation of CO_2 to CO does not take place in the container.

- Released CO originates from chemical dissociation of CO_2 to CO on the hot molybdenum surface in the ion source. This is in agreement with calculations performed in 2.4.1.

- The delayed release of CO in comparison to CO_2 is an additional indicator that CO is produced in a chemical reaction while the extracted part of CO_2 does not experience any delay. That means that CO_2 that gets in contact with hot tantalum surfaces is lost irreversibly.

- In the case of CO_2 efficiencies drop for Re and Ta as of $T \approx 1000$ $°C$. For Al_2O_3 more data needs to be collected for a conclusive interpretation.

2.7 Ionization Characteristics of CO_2 in a VADIS Ion Source

The last step in the extraction process is the ionization of the produced isotopes and molecules. In order to extract carbon oxides with high efficiencies, the impact of the ion sources parameters on the extracted current of CO^+ and CO_2^+ has been studied. After the emission from the hot cathode (see figure 2.17) electrons are accelerated by the applied anode voltage. The voltage of the commonly used VADIS [32] ion source can be varied between 0 V and 300 V. Without additional effects the energy of the electrons can be calculated by $E = e \cdot U$ [eV] where U is the applied voltage and e the elementary charge [32]. Due to their importance in environmental science CO and CO_2 have been intensively studied, including their ionization and dissociation cross sections σ_{ion}[34], [35],[36]. The precise knowledge of the energy dependent ionization cross section $\sigma_{ion}(E)$ allows to determine the average energy of electrons in the used VADIS ion source.

Enriched $^{13}CO_2$ (99,9%) was injected into the target container via a dedicated gas line while the target unit was mounted to the ISOLDE off-line separator. Here the release of $^{13}CO^+$ and $^{13}CO_2{}^+$ was monitored depending on the applied anode voltage. The error on the determination of the anode voltage originates from fluctuations of the anode power supply and is given by $\Delta U = \pm 3$ V.
After each change of anode voltage a mass scan was performed in order to determine the exact position and intensity of the peak maximum of $^{13}CO^+$ and $^{13}CO_2{}^+$. The measured ion current of $^{13}CO^+$ and

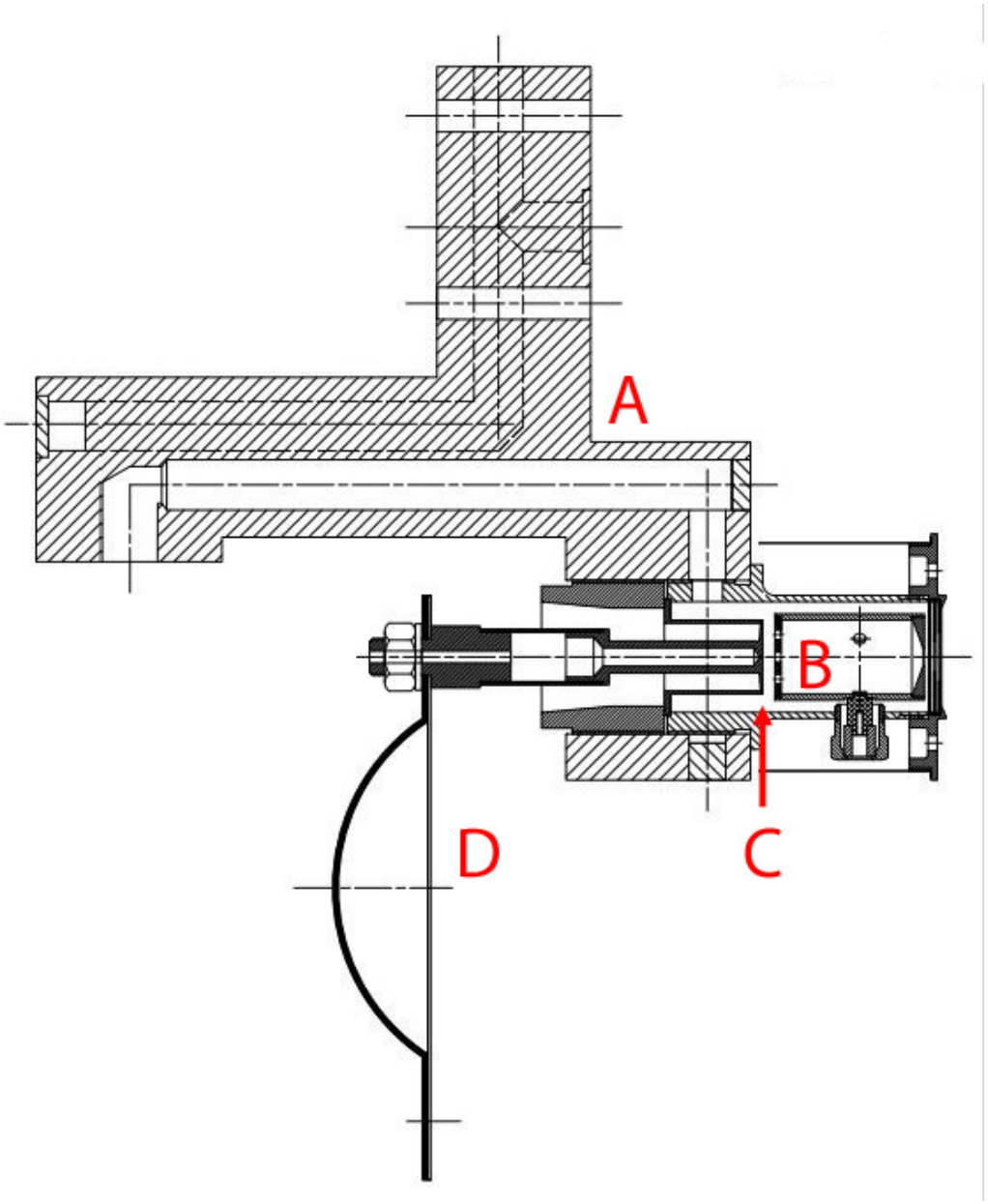

Figure 2.17.: Sketch of the VADIS ion source with a cold transfer line. A: Copper transfer line, B: Anode, C: Cathode, D: Connection for resistive heating.

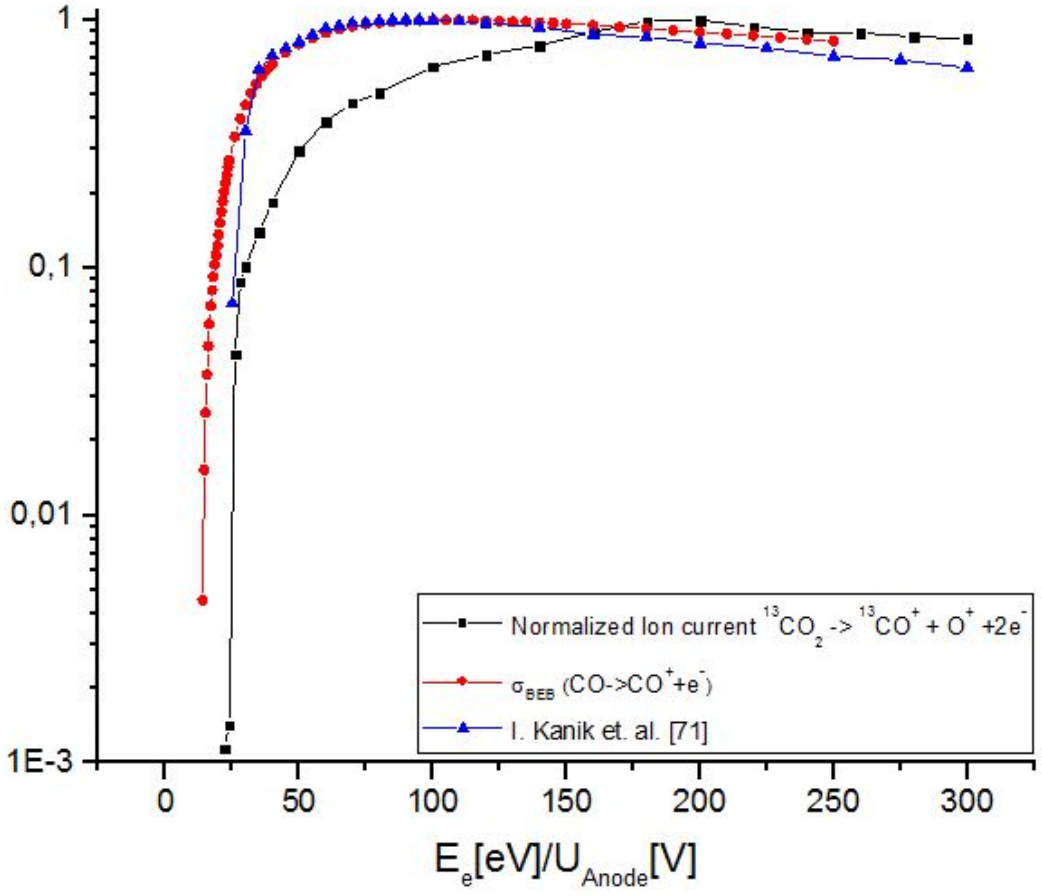

Figure 2.18.: Normalized yield of CO^+ and normalized ionization cross section $\sigma_{(CO \rightarrow CO^+ O^+ + 2e^-)}$

$^{13}CO_2{}^+$ and ionization cross sections are shown in figure 2.18 and 2.19. To ease comparison the measured yields and known cross section are normalized. Theoretical cross sections obtained with the BEB[2] model σ_{BEB} [69] taken from [70], experimentally obtained values for CO [71] and CO_2 [72] are shown.

While the theoretical [69] cross sections for CO and CO_2 and the one obtained in [71] and [72] are in good agreement, measurements taken here show systematic differences (see figures 2.18 and 2.19). Both the ionization potential I_p of CO and CO_2, and the maximum of the ionization are shifted towards higher energies. The ionization potential I_p is the value were ionization first occurs and was determined by fitting a linear function of the form $y = m \cdot x + b$ to the low energy part of the measurements and solving the obtained equation for $y = 0$ (the fitted measurements can be found in appendix C). The error is calculated with gaussian error propagation and given by the error of the fit:

$$\Delta I_p = \Delta x_0 = \sqrt{\left(\frac{1}{m}\right)^2 \cdot \Delta b^2 + \left(\frac{b}{m^2}\right)^2 \cdot \Delta b^2} \tag{2.12}$$

Table 2.5 shows the difference between expected and measured values for I_p and σ_{max}.

The reason for this difference is, that the electron energy is not purely given by the accelerating voltage and thus $E = a \cdot e \cdot U$ with $a \leq 1$, where a follows a distribution. The field distribution inside the ion

[2] BEB=Binary-encounter-Bethe: A theoretical model for electron impact ionization of atoms and molecules.

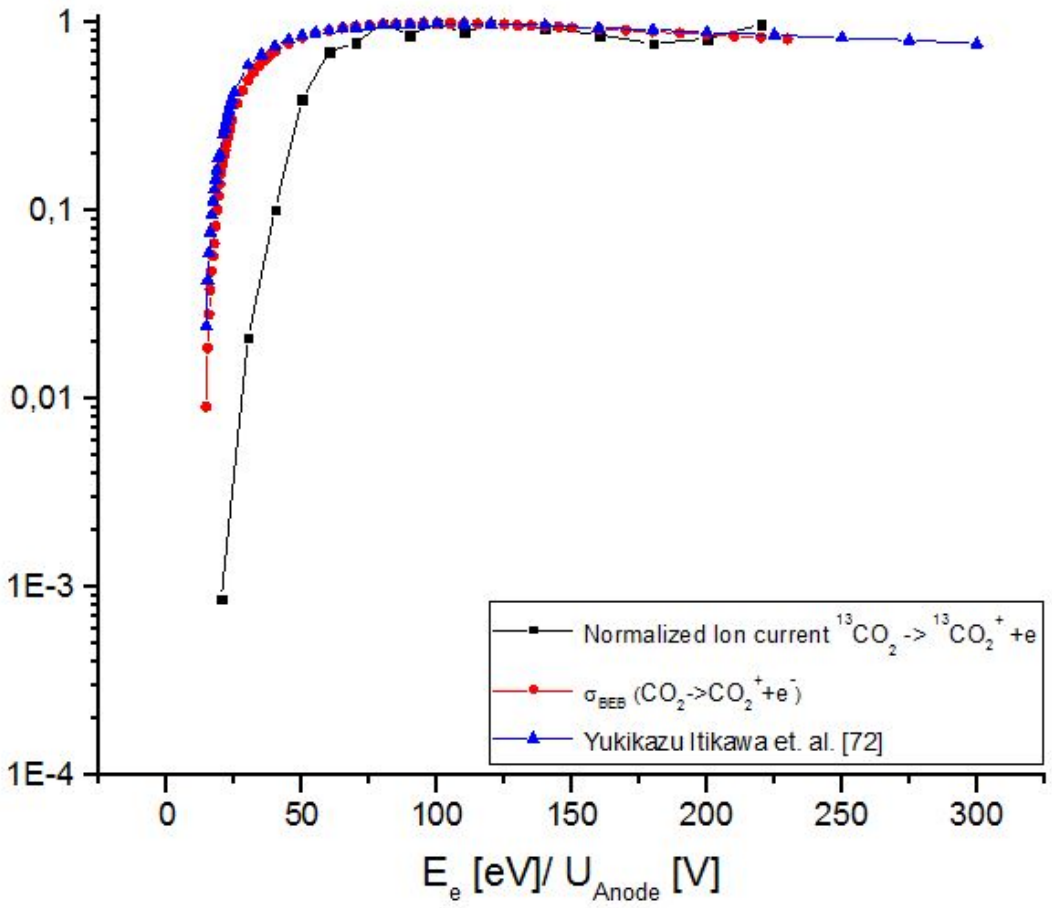

Figure 2.19.: Normalized yield of CO_2^+ and normalized ionization cross section $\sigma_{(CO_2 \rightarrow CO_2^+ + e^-)}$

Species	I_p theo [eV]	I_p exp [eV]	E(σ_{max}) theo [eV]	E(σ_{max}) exp [eV]
CO	14	20.7 ± 1.5	105	200
CO_2	14.5	31.1 ± 7.3	95	80-120

Table 2.5.: Comparison of measured and theoretical threshold of ionization I_p and electron energy with maximum cross section for CO and CO_2.

Unit	Material	Ion Source	$T_{target}[^\circ C]$	Yield $1/\mu C$	comment
123	CaO	MK7	1000-1100	$^9C : 5 \cdot 10^3$	humidity in target
425	Y_2O_3	VD7	1400-1600	$^9C : 1.5 \cdot 10^3$	O_2 inj, Cl cont
425	Y_2O_3	VD7	1400-1600	$^{10}C : 1.5 \cdot 10^4$	O_2 injection, Cl cont
469	CaO	VD7	687	$^{15}C : 1.3 \cdot 10^5$	nano material
469	CaO	VD7	687	$^{10}C : 6.1 \cdot 10^5$	nano material

Table 2.6.: List of online runs during which ^9C was successfully extracted or extraordinary high yields.

source was simulated in [32]. It was found, that the resulting field follows a distribution where in some regions the field is approximately 30% lower than the applied voltage. The ionization characteristics of the used VADIS ion source is further investigated in section 3.4.1, where measurements are extended to noble gases and boron fluorides.

2.8 Analysis of On-line Measurements

During on-line runs at ISOLDE the release of radioactive carbon from target units has been studied in several cases. Many combinations of target materials and ion sources were investigated but to this point it is not possible to extract requested yields of exotic carbon isotopes like $^{17-20}C$ or ^9C for an extended period of time, in a reproducible manner.
In some cases (target units #123, #371, #425, #459) extraction of the short-lived ^9C isotope was measured but either yields were too low or only available for a short period.
An exception is the online run using target unit #123 in 1999 (CaO, MK7) when yields of $5 \cdot 10^3$ $^1/_{\mu C}$ of ^9C were extracted over 3 days. However it was not possible to repeat this result using the same combination of material, ion source and target setup.

Figure 2.20 gives an overview over all documented extractions of carbon as CO^+, extracted from a range of different setups at ISOLDE. The ratio of carbon beam current extracted as C^+, CO^+ and $CO_2{}^+$ ions is usually 1:100:10. Therefore the focus of discussion is on CO^+.
The extracted yields from the different target units vary up to four orders of magnitudes for the same isotope. Generally yields from setups using a VADIS or the former MK7 ion source show higher yields compared to units using RF ion sources. Furthermore units with calcium oxide as a target material show good yields. This is especially true for unit #469 for which a sophisticated target material with nano-sized grains and high porosity was developed [54].

To analyze the factors of the origin of the low or high yields, three online runs were chosen. These target units are #123 utilzing CaO and a MK7 ion source. This unit is the only documented from which it was possible to extract ^9C for three days. The second target unit is #425 with Y_2O_3 as a target material and a VD7 ion source. During operation ^9C was seen as well, although for only a short period. This target unit is especially interesting as release times are the shortest ever observed for carbon oxides. The third unit #469 utilizing the above mentioned nano-structured calcium oxide as the target material and a VD7 ion source. Here very high currents of ^{10}C were extracted. The details of these runs are summarized in table 2.6.

In case of unit #425 where Yttria (Y_2O_3) was used as target material the absolute yield of extracted carbon as CO^+ was not very high. However during this run it was possible to extract short lived ^9C with $1.5 \cdot 10^3$ $^1/_{\mu C}$.
This was measured after increasing the target temperature to 1600 $^\circ C$ which might have caused additional release of oxygen. As seen in section 2.5 is the adsorption enthalpy of carbon oxides on Yttria with $\Delta H_0 = 16$ $^{kJ}/_{mole}$ very low. Hence the elevated temperature avoids long residence times on the surface. The fact that short-lived carbon was only measured after an increase of the temperature and the low observed yields of longer lived isotopes indicates a shortage of oxygen when Yttria is used as a target

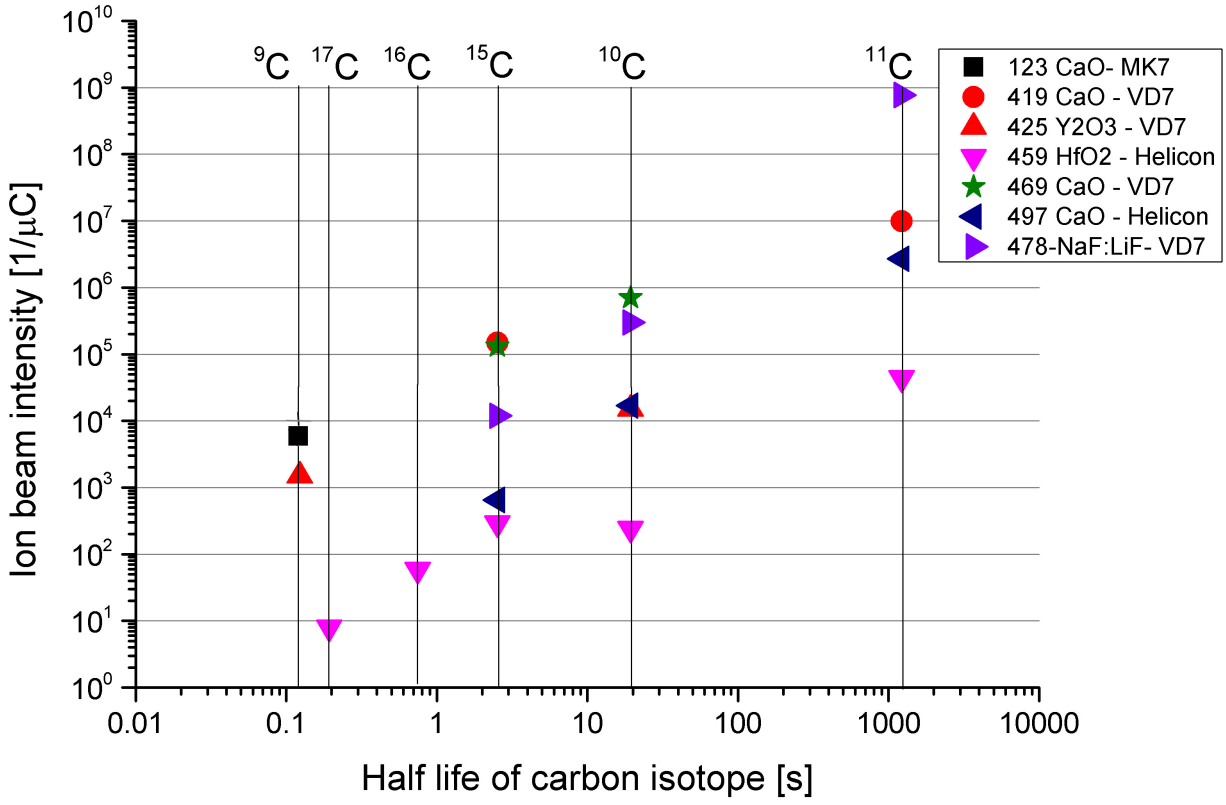

Figure 2.20.: Obtained yields of carbon isotopes extracted as CO^+ during online runs from different target units. The legend indicates the target unit number, the used target material and ion source.

material. This can also be seen by comparing the ratios of production cross sections of ^{9}C and ^{10}C with the ratio of extracted yields:

$$\frac{\sigma_{^{10}C}}{\sigma_{^{9}C}} \approx 300, \quad \frac{I_{^{10}C}}{I_{^{9}C}} \approx 10$$

Here the ratio is 30-fold smaller than expected from the production cross sections. If a surplus of oxygen was available for the formation of molecules both ratios should be of the same order. Hence only a small fraction of the produced carbon can react to carbon oxide and be extracted.

In comparison to Yttria, yields extracted from calcium oxide units are generally higher, with record yields from unit #469. Nevertheless it was not possible to extract very exotic isotopes.
According to chemical equilibrium calculations (shown in section 2.4) calcium oxide decomposes at temperatures above 700°C -900 °C and, in presence of carbon, formation of carbon oxides is taking place. This availability of oxygen can be seen when comparing ratios of production cross-section and extracted yield.

$$\frac{\sigma_{^{10}C}}{\sigma_{^{15}C}} \approx 11.8, \quad \frac{I_{^{10}C}}{I_{^{15}C}} \approx 4.7$$

Here the difference in the ratio is only a factor of 2.5, compared to a factor larger than 30 in the case of Yttria. The availability of oxygen combined with nano-metric grain size of the target material and the open porosity allowed the extraction of the highest yields. Furthermore the low target temperature is beneficial as seen in the experimental part of this chapter 2.6.
However the low operational temperature seems to be responsible for diffusion and adsorption times much longer than life times of exotic isotopes.
In contrast to that ^{9}C was extracted over a period of 3 days from target unit #123 utilizing CaO as a target material. This unit was operated at $T \approx 1050$ °C which might have caused shorter extraction times, sufficiently for extracting ^{9}C. Furthermore bad vacuum and high intenisties of stable $^{12}CO^{+}$ ($I_{CO^{+}} = 410$ nA) and $^{12}CO_2^{+}$ ($I_{CO_2^{+}} = 44$ nA) (without proton bombardment) were measured after initial heating of the target unit.
The production of calcium oxide usually takes place by decomposition of calcium carbonate $CaCO_3$ to CaO and CO_2. This reaction is reversed if CaO is in contact with air and therefore CO_2 Therefore the possible presence of $CaCO_3$ combined with high operational temperatures assured the availability of oxygen and a sufficiently fast extraction of short lived ^{9}C.

The results suggest that the extraction of short-lived carbon isotopes as carbon oxide is limited by three major factors. These factors are losses on the heated tantalum surface, particularly if temperatures exceed $T = 1000$ °C, chemical reactions and adsorption on the hot molybdenum of the ion source delaying the extraction and a shortage of oxygen for the formation of molecules.
These problems might be tackled as follows

- Shortage of oxygen:
  - High operational temperature to decompose the target material
  - Injection of reactive species (e.g. CF_4) to substitute oxygen by fluorine and hence release oxygen
- Losses on tantalum of target container:
  - Coverage of the container with chemically inert material (e.g. Al_2O_3, SiO_2, compare [51])
  - Operational temperature below $T = 1000$ °C
- Delay due to adsorption on molybdenum in ion source and other materials:

- Replace FEBIAD ion source with RF ion source, (e.g. HELICON[33])
- utilization of target materials with low ΔH, e.g. Y_2O_3, Al_2O_3

3 Extraction of Short Lived Boron Isotopes

Up to now no beams of radioactive boron were extracted from ISOL targets. The reasons are similar as in the case of short lived carbon isotopes. Boron has a tendency to form various stable bonds with materials present in targets as for example metals. Furthermore the high boiling point requires an extraction as a more volatile molecule. Formation of boron fluorides by injection of fluorine containing gases (e.g. CF_4, SF_6) was suggested in [43]. This technique has been successfully applied for other refractory elements [[73], [74]].
Recently ^{8}B has been extracted with yields of 7 ions per second at KVI [75] and 200 ions per second at IGISOL [76] respectively. For experiments at ISOLDE, yields of post accelerated radioactive ^{8}B ($t_{1/2} = 770$ ms) of $5 \cdot 10^3$ $^1/_{\mu C}$ are requested. These experiments aim to investigate the structure of ^{8}B as ^{8}B is expected to possess a proton halo in its ground state [77]. Furthermore a successful extraction would allow to investigate the high lying resonances of ^{9}C by resonant elastic scattering on a thick proton target, aiming for a better insight into the poorly known nuclear structure of ^{9}C [78]. Besides studies in the field of nuclear physics, the availability of ^{8}B would allow a sophisticated study of diffusion in group IV semiconductors (Si, Ge, Diamond). For the production of semiconductor devices boron is the most used p-type dopant. However investigations on the position and diffusion behavior after the implantation of boron into semiconductor wafers are difficult or lack the needed sensitivity. Intended experiments aim to investigate the behavior of boron using alpha emission channeling [78].

Although potential target materials for the extraction of radioactive boron were studied [42] [79], no beams of boron have been extracted at ISOLDE. The difficulty in the case of boron is to find a target material that offers high production rates and fast diffusion while not competing in the reaction with injected fluoride.
Investigations performed within this work focus on the selection of materials, that obtain the necessary properties for a successful extraction of boron from ISOLDE targets. Besides simulations on the in-target production and calculation of the chemical equilibrium of boron with potential target materials, diffusion of boron in these materials was investigated. This was done using the high neutron capture cross section of stable ^{10}B. Furthermore the dependency of extractable currents of boron fluorides on target parameters such as temperature, ion source settings and amount of injected gas was studied.
Finally, a full prototype target unit combining MWCNT[1], SF_6 injection, a cold line and a VADIS ion source was tested.

Equation 1.1 shows the single parameters of the extraction process:

$$N = N_0 \cdot exp(-\lambda \cdot (t_{diff} + t_{Ads} + t_{eff})) \cdot \epsilon_{diff} \cdot \epsilon_{transport} \cdot \epsilon_{formation} \cdot \epsilon_{ion} \tag{3.1}$$

The following factors of formula 1.1 are studied within this chapter:

- N_0
  - Calculation of in-target production of boron isotopes, using EPAX, ABRABLA and FLUKA
- $\epsilon_{diffusion}$
  - Study of diffusion of boron in target materials via the reaction $^{10}B(n,\alpha)^7Li$
- $\epsilon_{formation}$

[1] Multi Wall Carbon Nano Tubes

Material	M $[g/mole]$	Density $[g/cm^3]$
CaO	56	3.35
Y_2O_3	226	5.01
Al_2O_3	102	3.95
HfO_2	210	9.68
CaF_2	78	3.18
Graphite	12	2.23

Table 3.1.: Densities and molar masses of target materials

  - Calculation of chemical equilibrium between boron and potential target materials

- $\epsilon_{transport}$
  - Calculation of chemical equilibrium between boron fluorides and structural materials

- $\epsilon_{ionization}$
  - Study of ionization behavior of BF_3 and BF_2 in a VADIS ion source - dependency of $\epsilon_{ionization}$ on U [V] and comparison with theoretical cross sections

- $\epsilon_{formation} \cdot \epsilon_{transport} \cdot \epsilon_{ionization}$
  - Study of the release of BF_3^+ and BF_2^+ from a target and ion source system depending on temperature and material composition

3.1 Isotope Production in Target Materials

Similar as in the case of carbon, the production cross sections of boron isotopes in target materials were calculated. For Al_2O_3, Y_2O_3, CaO and CaF_2 this was done using EPAX [14] and ABRABLA [13]. As it was seen in the simulation of the production cross sections of carbon, the results from EPAX give a higher cross section for the production of exotic isotopes compared to ABRABLA. Figure 3.1 shows the results for comparison for the case of Al_2O_3. The results obtained with EPAX show a production of ^8B which is more than one order of magnitude higher than the production cross section obtained with ABRABLA. Since results obtained with ABRABLA showed a good matching with measured currents of radioactive isotopes, all further discussion is limited to these results. For Graphite, additional calculations with FLUKA [15] were carried out. The results of all three calculations are shown in figure 3.2. The figures of all calculated cross sections can be found in appendix A.2.

Figure 3.3 presents all isotope production cross sections for boron for potential target materials. Using formula 2.3 allows to calculate the number of produced isotopes in the target per μC protons. The used target material densities are summarized in table 3.1. The calculations show that for the theoretical densities a production of ^8B between $2*10^9$ $^1/_{\mu C}$ and $1*10^{10}$ $^1/_{\mu C}$ nuclei can be expected. As one desired property of target materials is a high open porosity and therefore lower density, these numbers have to be scaled with the real density of the target materials. Production cross sections for the desired ^8B are comparable to those of ^{15}C which was extracted in molecular form with yields of up to $1.5 \cdot 10^5$ $^1/_{\mu C}$ from ISOLDE targets.

3.2 Diffusion of Boron in Target Materials

As described in 1.2.2, the diffusion of produced isotopes from the bulk target material to its surface is one of the determining processes during radioactive ion beam production.
Therefore the choice of a target material which allows a fast and efficient diffusion is crucial for the

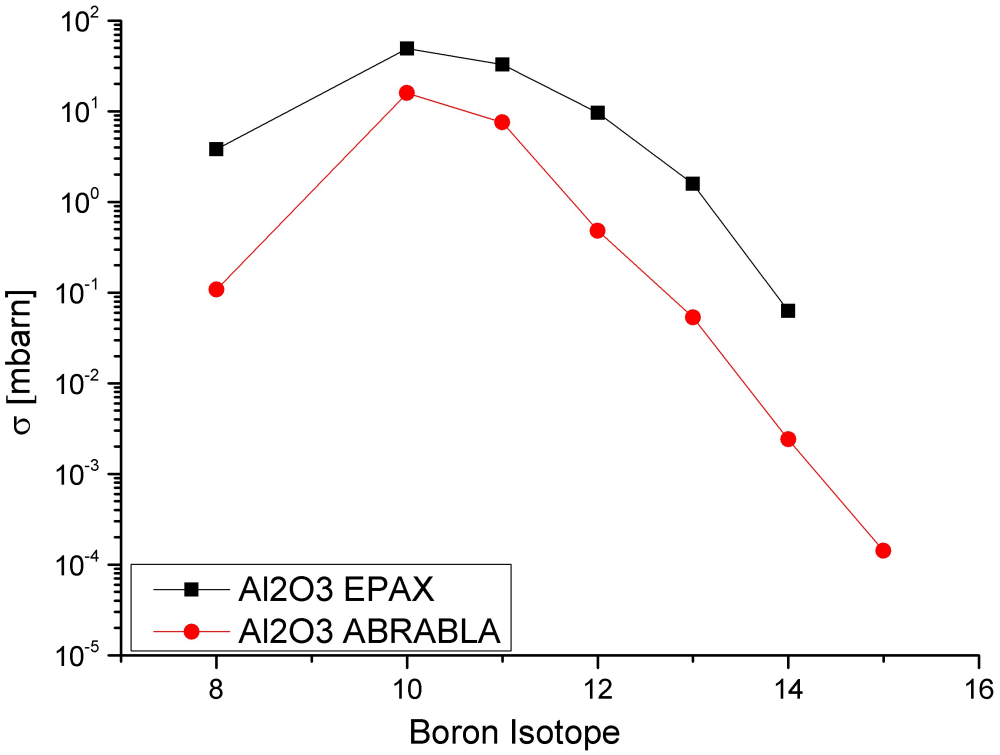

Figure 3.1.: Comparison of derived isotope production cross sections for the production of boron isotopes in Alumina, using ABRABLA and EPAX.

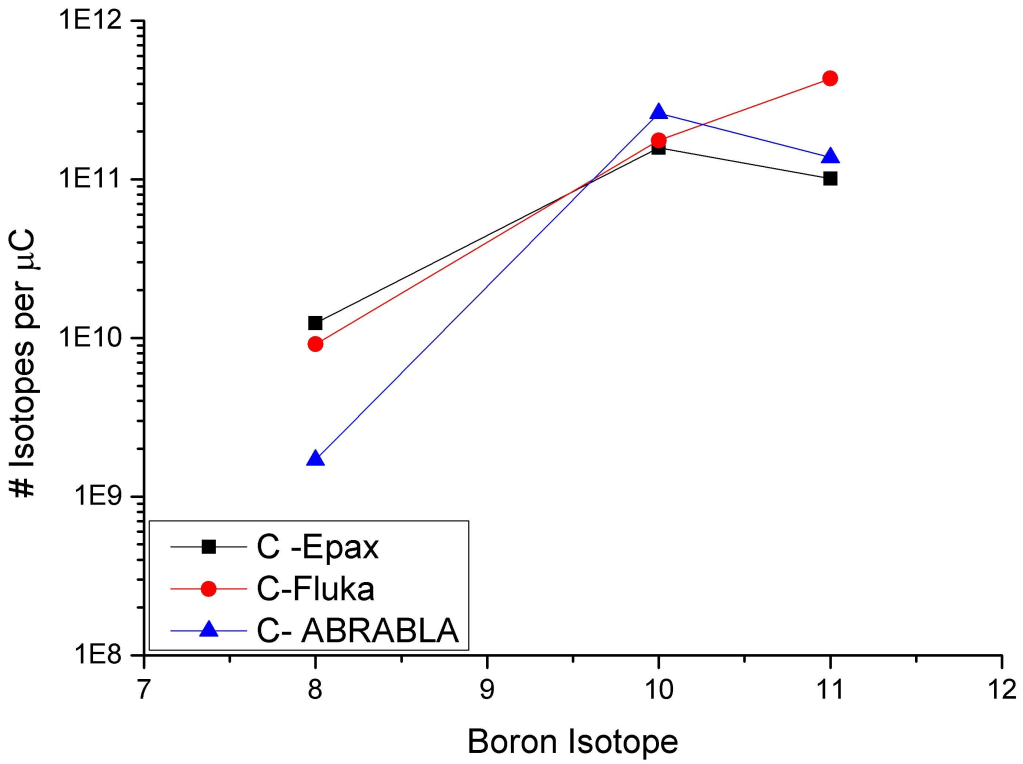

Figure 3.2.: Comparison of derived isotope production cross sections for the production of boron isotopes in Graphite, using Fluka, ABRABLA and EPAX.

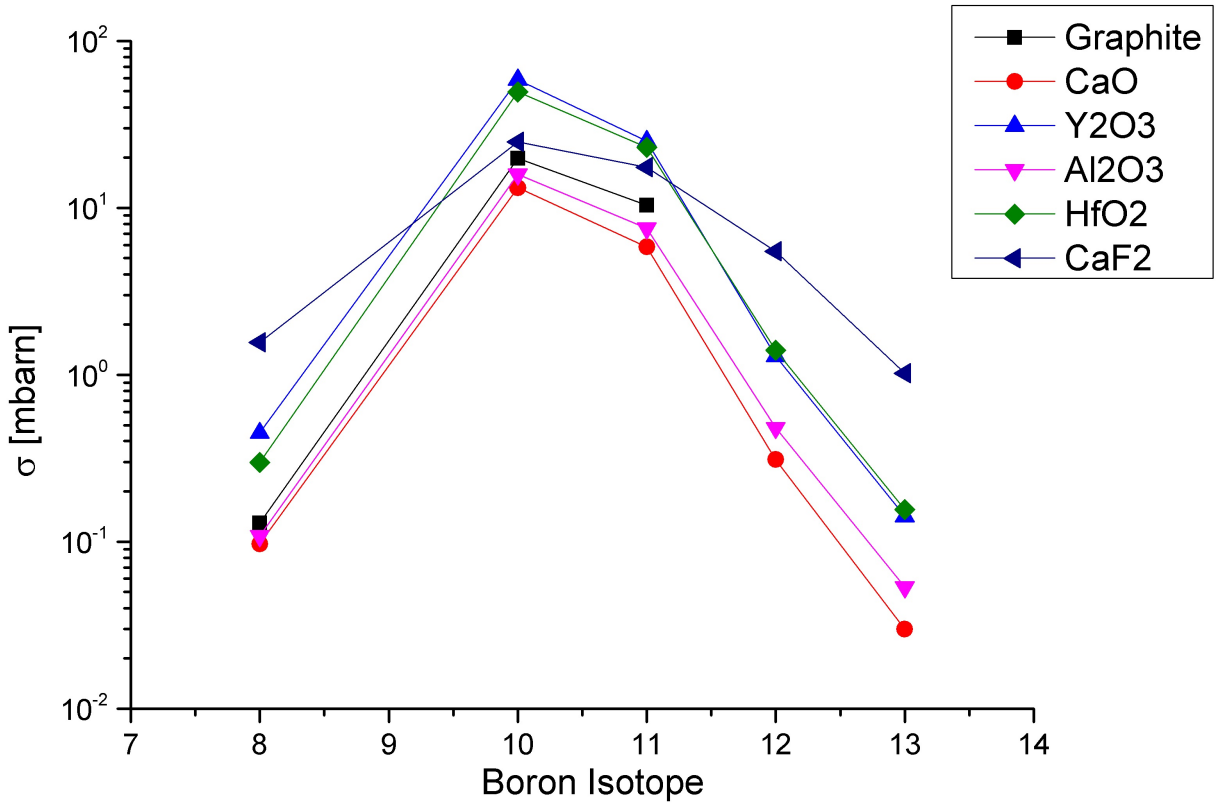

Figure 3.3.: Derived isotope production cross sections of boron isotopes in different target materials, using the ABRABLA code.

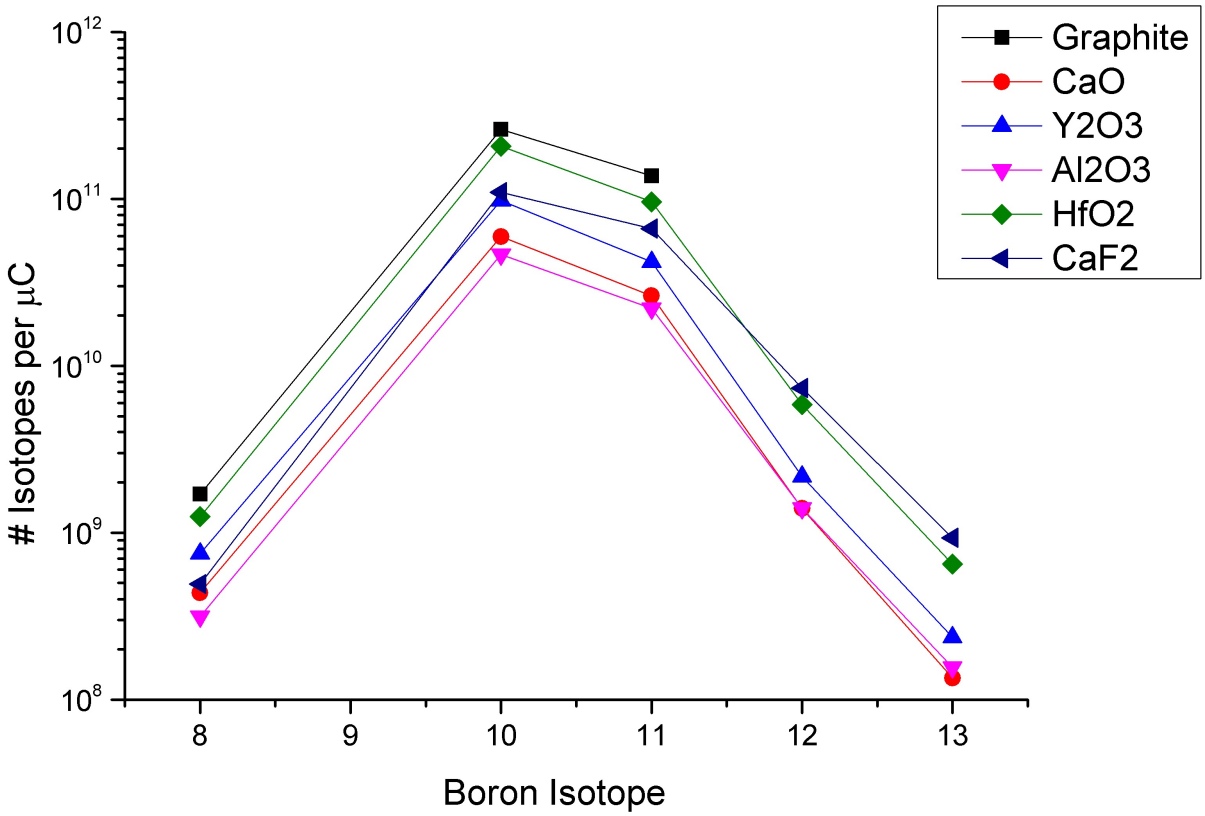

Figure 3.4.: Derived In-Target production of boron isotopes in different target materials, using ABRABLA.

extraction of exotic isotopes. In this work the diffusion of boron in potential target materials was studied.
Natural boron appears as ^{10}B with an abundance of 20% and ^{11}B with an abundance of 80%. An elegant way to investigate diffusion characteristics of boron is to use the extraordinary high neutron capture cross section of ^{10}B of up to $\sigma_{n_{th}} = 3840$ barn [80] for thermal neutrons. If a ^{10}B atom captures a neutron it decays via the reaction $^{10}B(n,\alpha)^{7}Li$ into an alpha particle and ^{7}Li via two different channels [81]:

$$\begin{aligned} &^{10}B + n_{th} \\ &\rightarrow 0.840\ MeV\ ^{7}Li + 1.470\ MeV\ \alpha + 0.478\ \gamma\ MeV\ [94\%] \\ &\rightarrow 1.015\ MeV\ ^{7}Li + 1.777\ MeV\ \alpha\ [6\%] \end{aligned} \tag{3.2}$$

In order to investigate the diffusion, boron was produced as a $^{10}BF_2{}^+$ ion beam from an ISOLDE target unit and implanted into target material samples. These samples were later on irradiated with thermal neutrons and the resulting alpha particles detected. The measurement process can be divided into the following steps

1. Implantation of ^{10}B as $^{10}BF_2{}^+$ into target material samples
2. Measurement of the initial distribution and amount
3. Heating of the sample to trigger diffusion
4. Measurement of ^{10}B distribution and remaining amount
5. Repeating step 2 to 4

The first step, the preparation of the samples, takes place at the in-house offline mass separator. Here ^{10}B is extracted with 50 kV as $^{10}BF_2{}^+$ and implanted into samples of target materials of Graphite, multi walled carbon nano tubes (MWCNT) and Yttria. The details of the sample production are described in section 3.2.1 and 3.4.
After the implantation, the samples are placed in a setup for alpha detection and irradiated with moderated neutrons, coming from a Pu-Be source. Alpha particles, originating from the reaction $^{10}B(n,\alpha)^{7}Li$, are detected and their energy measured. This measurement allows to determine the relative amount of boron inside the sample. The experimental setup for the alpha energy measurement is described in section 3.2.2
During step three samples are heated stepwise in order to promote diffusion. After each heat treatment the distribution of boron as well as the amount with respect to the initial implantation is checked by repeating step three. The analysis of these measurements and the results are presented in 3.2.3.

3.2.1 Sample Preparation

The samples were prepared at the ISOLDE off-line mass separator using the same target setup introduced in section 2.6. After the mass separator magnet a sample holder was installed which allowed to position the target material sample in the beam (see figure 3.5). The mass separated beam of $BF_2{}^+$ was collimated by a 8 mm collimator right before the sample position. The acceleration of the molecular ions was done with an applied extraction voltage of 50 kV on the target position. Tests with aluminum samples (compare figure 3.24) covered with a thin film of ^{10}B showed a reasonable separability of alpha peaks from the $^{10}B(n,\alpha)^{7}Li$ reaction to the background, occurring during irradiation with neutrons. The amount of ^{10}B on the used aluminum foils is known to be $4 \cdot 10^{16}$ on a beam spot with a radius of $r = 1.5$ mm.

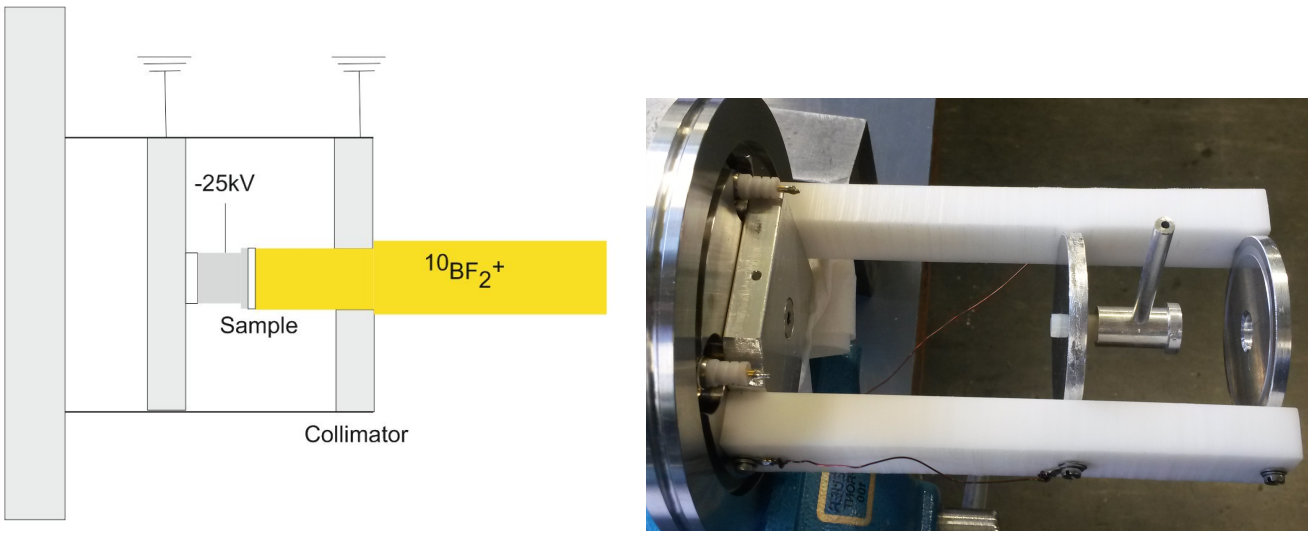

Figure 3.5.: Sample holder for the implantation of $^{10}BF_2^+$ into target materials. The sample is on a potential of -15 kV to increase the energy of the molecule and therefore the implantation depth.

Material	Density $[g/cm^3]$	Crystal structure
Graphite	2.23	mono crystalline
MWCNT	0.4	poly crystalline
Y_2O_3	3.16	poly crystalline

Table 3.2.: Investigated materials

With average currents of $^{10}BF_2^+$ of 50 nA on the sample position, implantation took approximately 36 hours per sample to achieve an amount of implanted atoms close to $4 \cdot 10^{16}$.

Table 3.2 summarizes the investigated materials and their densities. For the case of Yttria and CNT the material was pressed into pills. The density of the pills is not the same as the theoretical density as these materials are poly-crystalline and highly porous.

3.2.2 Measurements and Analysis

Detection of the alpha particles coming from the samples was realized with an Ortec Alpha Aria spectrometer. Inside of an evacuated chamber the sample is placed in a distance of $d = 5$ mm to a silicon detector (450 mm^2, 100 μm depletion layer) and irradiated with neutrons coming from a Plutonium-Beryllium (1.85TBq, $10^8 n/s$ @ 4π) source. Since the neutron capture cross section of ^{10}B is highest for thermal neutrons, the high energy neutrons [82][83]coming from the source were moderated. This was realized with 7 cm polyethylene (PE), placed in front of the detector. To reduce background, additional 15 cm of lead were placed between the source and the polyethylene block. Figure 3.6 shows a sketch of the setup.

Although a strong neutron source was utilized for irradiation of the samples, observable count rates were very low with approximately $1.6 \cdot 10^{-3}$ Hz. This low count rate required measurement times of approximately 50 hours per data point, in order to acquire sufficient statistics. Due to a high background in the detector only the most abundant alpha peak with $E_\alpha = 1481$ keV was observable. Therefore all

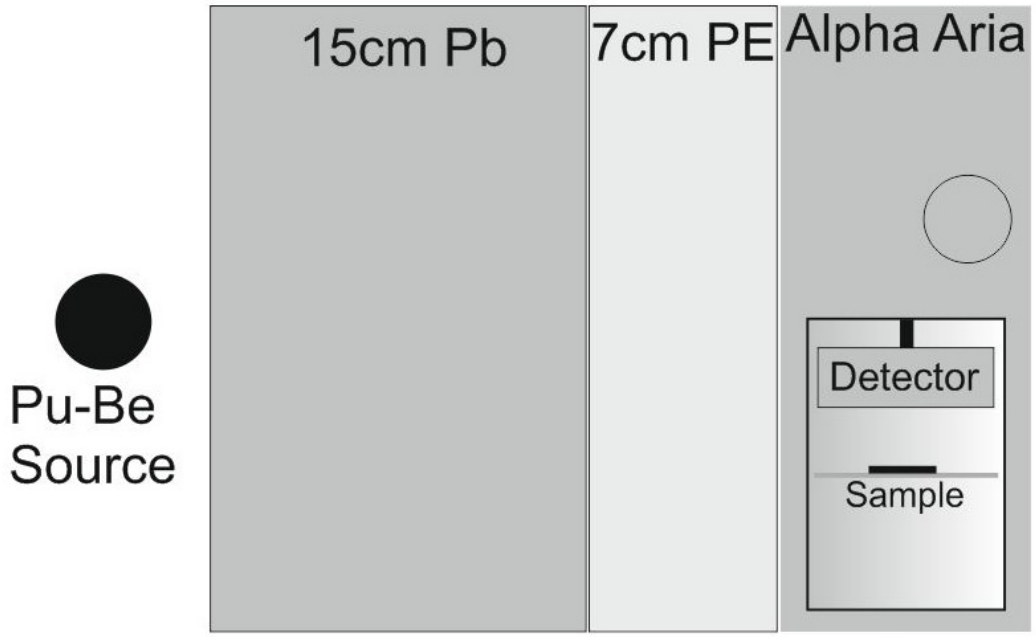

Figure 3.6.: Set up for detection of alpha particles coming from the $^{10}B(n,\alpha)^{7}Li$ reaction. In order to moderate the neutrons coming from the Pu-Be source, 7 cm of PE are placed in front of the Ortec Alpha Aria detector. Additional 15cm of lead help reducing the background in the measurement.

analysis are based on the position of the peak and it's area. These values were determined by fitting a function of the form

$$y = y_0 + \frac{A}{w \cdot \sqrt{\pi/2}} * exp(-2 * (\frac{x - x_0}{w})^2) \tag{3.3}$$

where A is the area under the peak, x_0 the position of the peak and w its width. Figure 3.7 shows an example of a measurement with a fitted function.

To promote the diffusion of the implanted boron in the target material samples, samples were heated in a modified ISOLDE target. Each heat treatment consisted of heating of the sample for 30 minutes with an increase and decrease of the temperature within 3 minutes. After each heat treatment, samples were irradiated with thermalized neutrons and emitted alpha particles detected. In order to determine the change in the amount of present boron and the migration in the sample, measured spectra are compared to the spectra taken after the initial implantation. The fractional activity is calculated via

$$\beta = \frac{A_i \cdot t_0}{A_0 \cdot t_i} \tag{3.4}$$

where A_0 is the area under the fit and t_0 the measurement time of the measurement after initial implantation. A_i and t_i are the corresponding values after heat treatment. The error of the fractional activity $\Delta\beta$ is given by the errors of the fit and calculated by Gaussian error propagation:

$$\Delta\beta = \sqrt{\left(\frac{t_0}{t_i \cdot A_0}\right)^2 \cdot \Delta A_i^2 + \left(\frac{t_0 \cdot A_i}{t_i \cdot A_0^2}\right)^2 \cdot \Delta A_i^2} \tag{3.5}$$

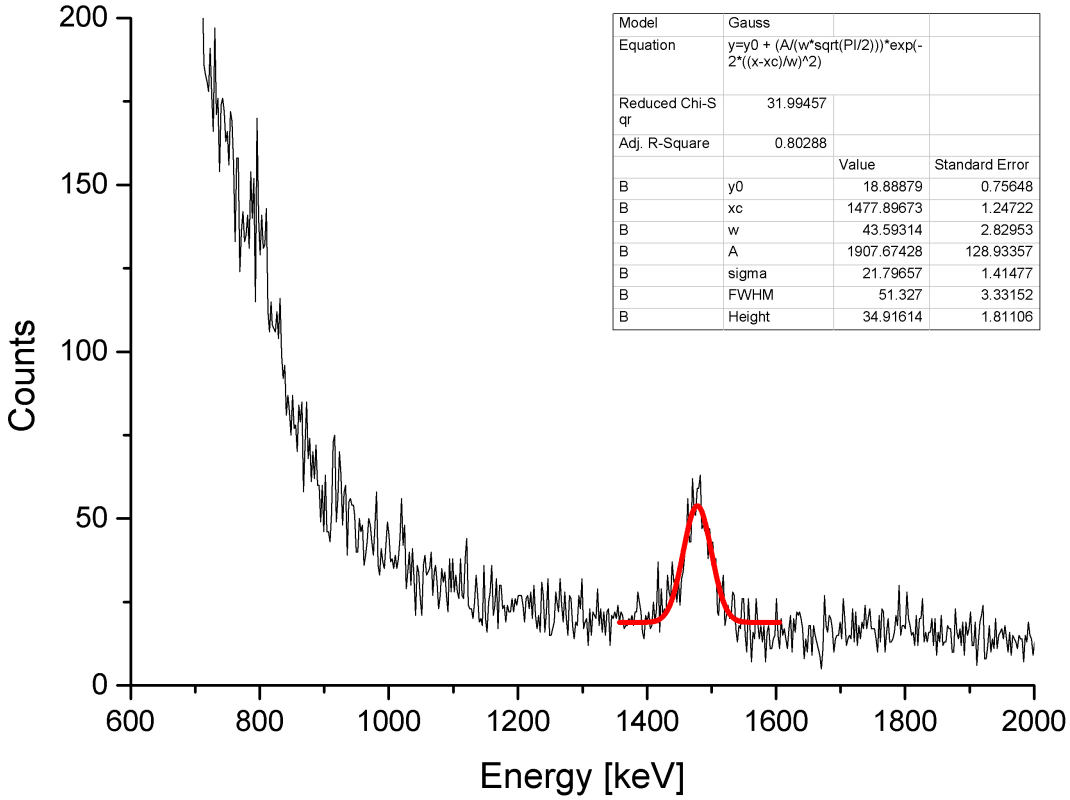

Figure 3.7.: Measured alpha spectrum resulting from $^{10}B(n,\alpha)^{7}Li$ reaction of investigated Graphite sample. The plot shows the region between 600 keV and 2000 keV. The 840 keV ^{7}Li peak is covered by the high background and thus analysis are limited to the most abundant alpha peak of 1481 keV. The measured time was $t = 27.2$ h.

3.2.3 Results and Discussion

In this section the diffusion characteristics of boron in potential target materials was investigated. Therefore an amount of approximately $4 \cdot 10^{16}$ ^{10}B was implanted as $^{10}BF_2^+$ into samples of Graphite, Carbon-nano-tubes and Yttria. Diffusion was investigated using the extraordinary high neutron capture cross section of ^{10}B. Samples were irradiated with moderated neutrons coming from a Pu-Be source and the particles originating from the reaction of $^{10}B(n,\alpha)^7Li$ were detected. To identify suited materials for the extraction of radioactive boron, similar studies were carried out in the past for MgF_2, Carbon and Pt [42]. However only the results from MgF_2 were published [79].

Due to high background levels in the detector, only the 1481 keV alpha peak could be used to analyze the measurements. The detection limit for ^{10}B in the sample is $2 \cdot 10^{15}$ atoms. To investigate the diffusion behavior, samples were heated for 30 minutes in 5 (4 for CNT) steps, from room temperature to approximately 2000 $°C$. After each step, samples were irradiated for approximately 50 hours and the emitted alpha particles detected. Figure 3.8 shows the evolution of the amount of boron, present in the sample in dependency of temperature. To ease comparison, measurements are normalized to the initial implantation of each sample. The measurements show a big difference for the diffusion of boron in the different materials. Diffusion coefficients of boron in Graphite are known to be high with $2.2 \cdot 10^{-5} \frac{cm^2}{s}$ at 2200 $°C$ [84] if diffusion happens between the atomic carbon layers. This is reflected in the results shown in figure 3.8: from 700 $°C$ the amount of boron in the Graphite sample drops from almost 100% to about 50% of the initially implanted amount. Heating the Graphite sample to 1300 $°C$ causes an additional drop of remaining boron to 30 %. Increasing the temperature further does not change the remaining amount significantly that suggests that the remaining boron is physically or chemically confined in the Graphite.

The situation for carbon nano-tubes (WMCNT) is slightly different. Similar as for Graphite significant fractions are released at relatively low temperatures with a decrease of present boron to approximately 65% after heating to a temperature of 300 $°C$. Further heating shows a faster decrease of present boron in comparison to Graphite. After heating to 1700 $°C$ no remaining boron could be detected during measurements.
While diffusion in between and through the walls of the nano tubes should be the same as for graphite, additional diffusion and effusion along the surface and through the capillaries of the tubes can be expected. This is probably the reason for the faster decrease of boron in the material.

In the case of Yttria almost no change can be observed up to 1300 $°C$. The remaining amount of boron at this temperature is close to 100 % of the initially implanted. However heating the sample to 1700 $°C$ shows a drop of 50%. After subsequent heating to 1900 $°C$ no remaining boron was detectable during irradiation with neutrons.

The width and the position of the measured alpha peaks remained constant for each material. If boron would diffuse deeper into the material a broadening of the measured peaks due to the additional energy loss of the emitted alpha particles would be expected. The fact that the amount of boron is decreasing while the peak energy and width remains constant, indicates that the loss of boron is due to diffusion to the surface of the sample with subsequent evaporation.
Based on these results carbon nano tubes (MWCNT) were chosen as a target material for the extraction of radioactive ^{8}B during an online experiment 2014.

3.3 Chemical Equilibrium of Boron with Target Materials

In contrast to carbon, boron was never extracted from a thick ISOL target. Therefore it is not possible to refer to former online runs to identify the process hindering its extraction.
The high reactivity and the high boiling point of boron ($T_{boil} = 3927$ $°C$) and therefore low vapor pressures at operational temperatures of ISOL units make it necessary to extract boron as a more volatile molecule. Obvious options are oxides (e.g. B_2O_3) and halides (BX_n, X=Cl,F,Br; n=2,3). As

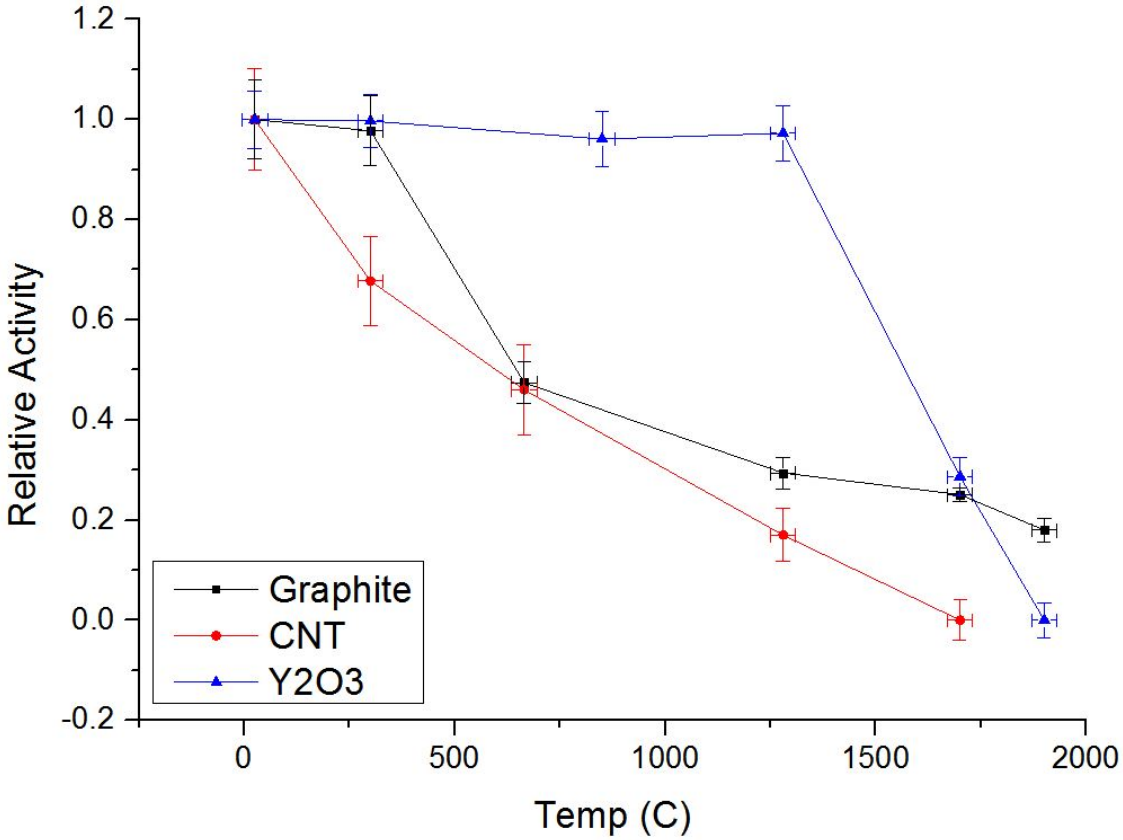

Figure 3.8.: Diffusion characteristics of Boron in different potential target materials. Shown is the relative activity for the reaction $^{10}B(n,\alpha)^{7}Li$

halides are more volatile (eg $T_{Boil}^{BF_3} = -100.3\ °C$, $T_{Boil}^{BCl_3} = 12.6\ °C$) than oxides ($T_{subl}^{B_2O_3} = 1860°C$), extraction of boron as a halide is intended.
In this thesis the extraction of boron as a fluoride (BF_2, BF_3) has been investigated. Following the same approach as in the case of carbon, a target made of a metal fluoride would be the obvious choice. Possible choices are CaF_2 ($T_{melt} = 1418\ °C$) or MgF_2 ($T_{melt} = 1263\ °C$).
If non-fluoride target materials are chosen, gases containing fluorine like CF_4 or SF_6 have to be injected into the target unit to allow the formation of boron fluorides. In this case, the chosen target material has to have a lower affinity to fluorine than boron. In order to identify suitable candidates, calculations of the chemical equilibrium were performed. Again two different cases are considered:

1. Formation of boron fluorides in target materials under the presence of tantalum as the target container material. When target materials are not fluorides, SF_6 is added for the calculation. These calculations help to identify candidate target materials that allow the formation and subsequent extraction of boron as BF_3.

2. Chemical equilibrium of the formed BF_3 with structural materials such as Ta, Re, Mo and Cu. These calculations allow to identify if a formed molecule reacts with the target environment. This is important in order to estimate where losses during the transport process take place.

3.3.1 Formation of BF_3

To asses the formation of BF_3 the chemical equilibrium for 5 different materials was calculated. The considered materials are Alumina Al_2O_3 and Yttria Y_2O_3 as oxides, MgF_2 and CaF_2 as fluorides and graphite.
Using MgF_2 and CaF_2 as a target material might have the advantage that fluorine is provided by the target material and no further injection is necessary. During investigation on carbon it was found, that even if metal oxides are used as target materials, the supply of oxygen for the reaction of carbon to carbon oxide, can not be guaranteed in all cases. Therefore it has to be tested experimentally if MgF_2 and CaF_2 provide fluorine for the reaction of boron to boron fluorides.
The high diffusion coefficient of boron in graphite of $2.2 \cdot 10^{-5} \frac{cm^2}{s}$ [84] together with the availability of carbon in very favorable forms such as carbon nanotubes or nanometric graphite powder (carbon black) make this material an interesting candidate. The high porosity of carbon nanotubes likely allows a fast effusion of volatile species trough the open porosity.
Figure 3.9 shows the results of the equilibrium calculation. The equilibrium composition between tantalum, the potential target material, boron and SF_6 in a ratio of 10:10:1:1 was calculated.
In order to increase readability of the resulting plots, only species that contain boron are shown.
The results show a wide spread of possible phase compositions. A common result for all cases is that fluorine has to be available in excess. If this is not the case tantalum borides are formed.
In the case of Alumina, volatile molecules of BF_3 and BOF are formed in relatively narrow temperature ranges. BF_3 can be expected from 800 $°C$ to 1400 $°C$, BOF from 1400 $°C$ to 2100 $°C$. Furthermore calculation show the formation of aluminum borides. The equilibrium with Yttria shows a dominant formation of BOF starting from 1500 $°C$. Below this temperature no volatile boron species is formed.
For both of calcium fluoride and magnesium fluoride MgF_2 and CaF_2 formation of boron fluoride takes place. Unfortunately the temperature at which formation of BF_3 starts is in both cases higher than the boiling point of the material. For MgF_2 gaseous BF_3 appears above approximately 1400 $°C$, for the case of CaF_2 above 1600 $°C$.
The calculation of the chemical equilibrium between carbon and boron indicates that the extraction of boron as a fluoride is feasible. Given a sufficient presence of fluorine, formation of boron fluorides, mainly BF_3, is taking place from room temperature to approximately 2000 $°C$. The results obtained from calculation of the chemical equilibrium suggest, that graphite is the favorable material for the extraction of boron fluorides.

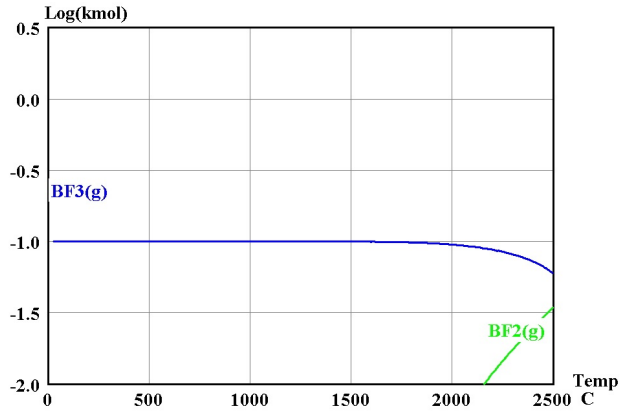

Ta+C+B+SF_6

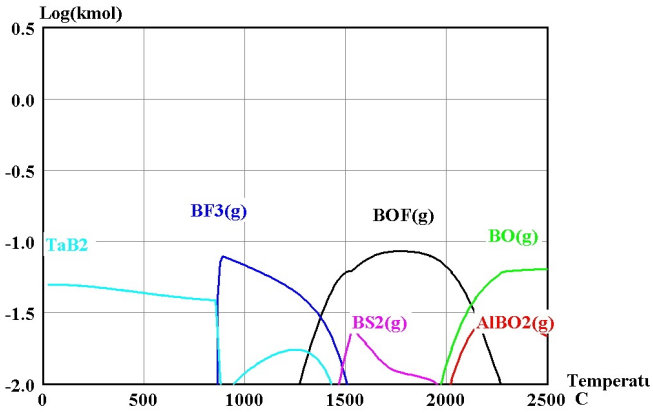

Ta+Al_2O_3+B+SF_6

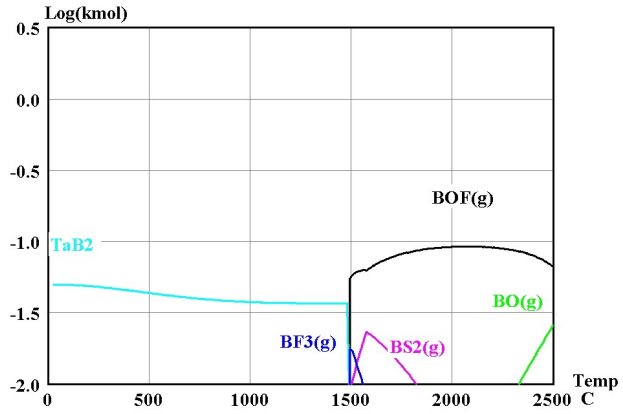

Ta+Y_2O_3+B+SF_6

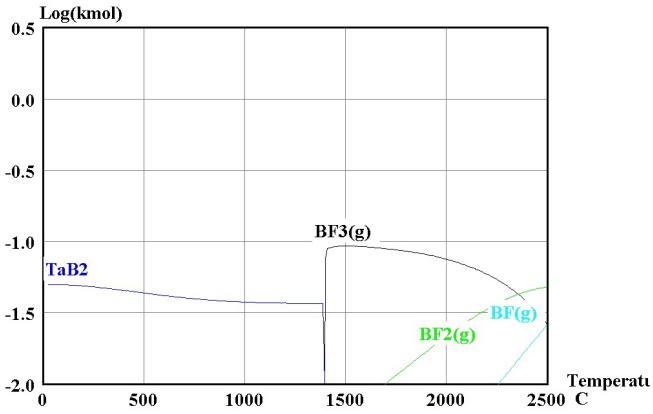

Ta+MgF_2+B

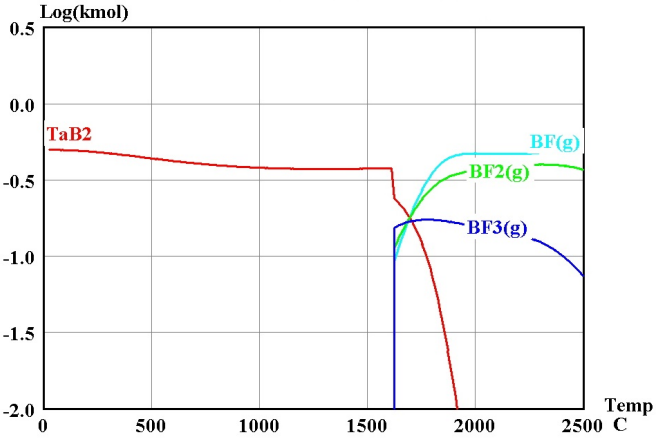

Ta+CaF_2+B

Figure 3.9.: Chemical equilibrium of B with possible target materials. To assure a better readability of the figures, only species containing boron are shown.

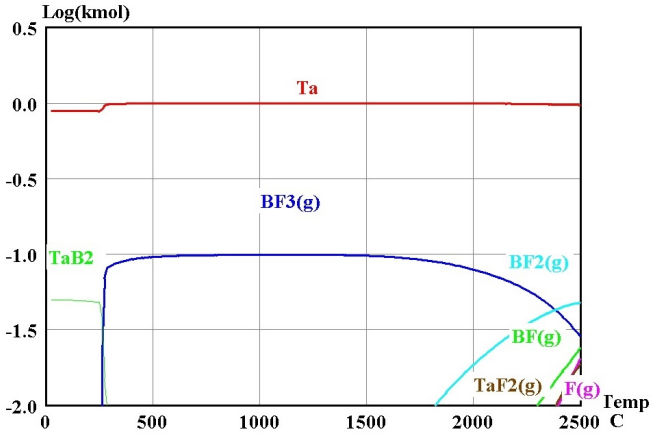

Ta+BF3

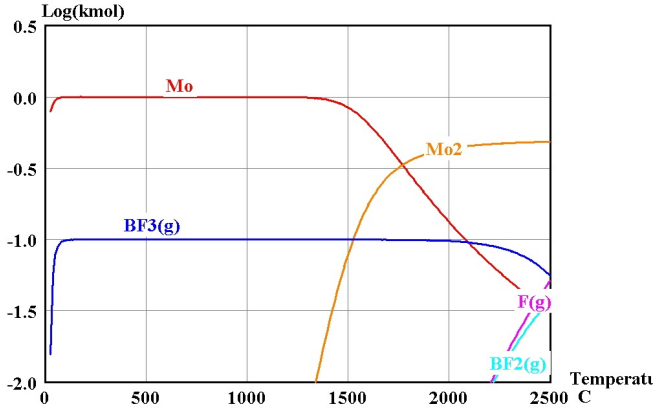

Mo+BF3

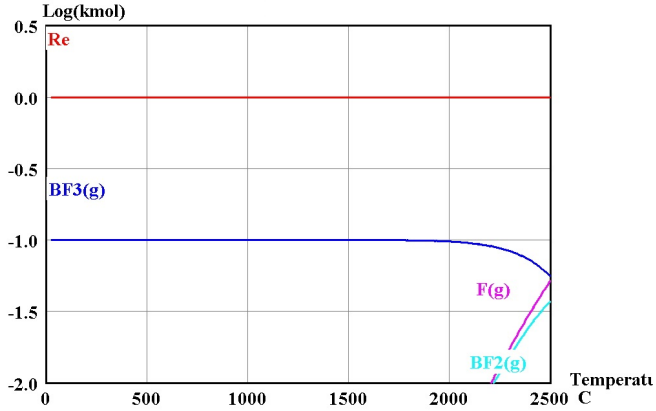

Re+BF3

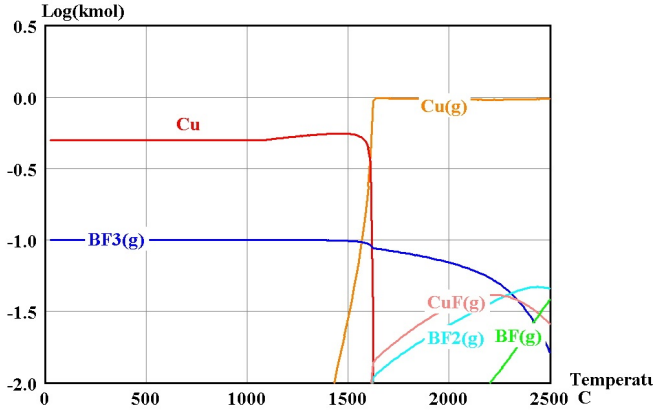

Cu+BF3

Figure 3.10.: Chemical equilibrium of BF_3 with structural materials. To assure a better readability of the figures, only species containing boron are shown.

3.3.2 Extraction of BF_3

In order to evaluate if a once formed molecule persists in the target environment, calculations of the chemical equilibrium with BF_3 and constructional materials were performed. The considered materials are tantalum, rhenium, molybdenum and copper. These materials are usually found inside the target container, the transfer line or the ion source. Apart from cold copper transfer lines, which are water cooled and operated at around $50°C$, materials are usually heated to temperatures between $1200°C - 2000°C$. The results of the simulation show (see figure 3.10), that once formed boron fluoride remains for temperatures between $500\ °C$ and $1900\ °C$ for all materials. If the temperature exceeds $2000\ °C$ transformation of BF_3 into BF_2 is taking place. It can be concluded that assuming a surplus of fluorine formation of boron fluoride is favored over the formation of borides with present materials and thus extraction should be possible. The formation and extraction of boron fluorides in a target system was tested experimentally and the calculations confirmed. The results are shown in the next section.

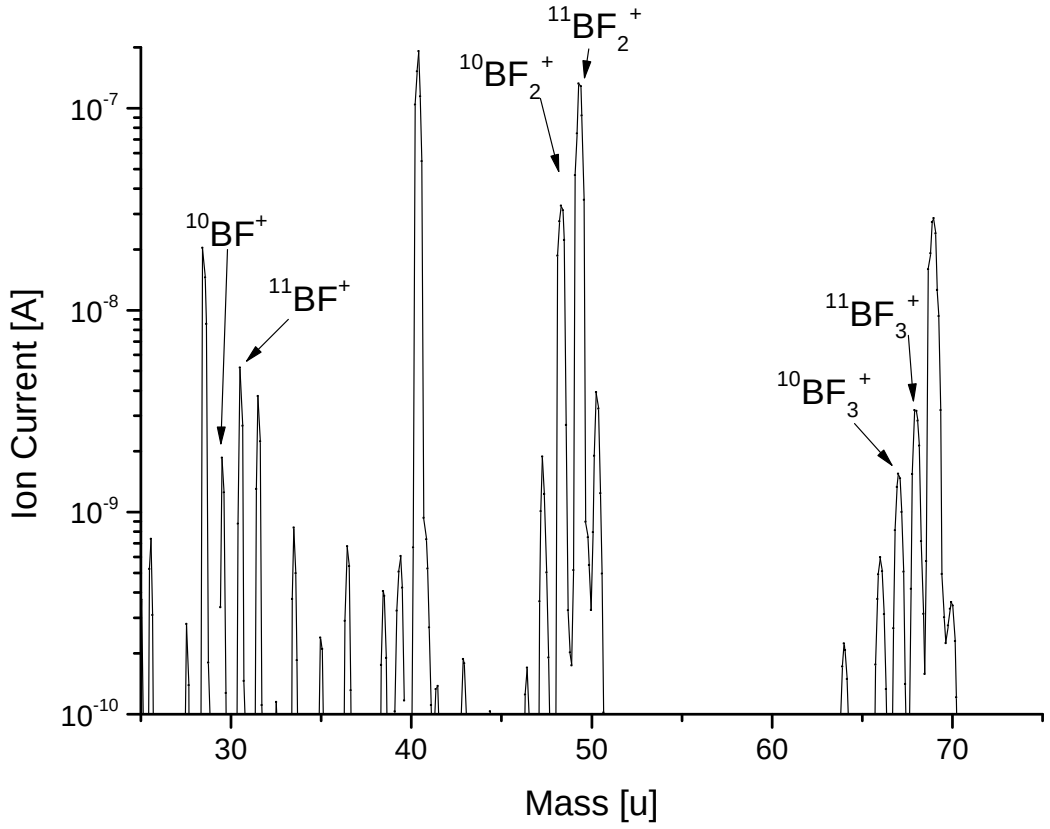

Figure 3.11.: Mass scan showing the peaks of boron fluorides molecular ions. The dominance of BF_2^+ is due to dissociative ionization of BF_3 in the ion source.

3.4 Extraction of Boron from ISOLDE targets

In this section the extraction of boron in atomic and molecular form from ISOLDE targets is investigated. In order to determine extraction characteristics atomic boron in powder form was inserted into a target container and the container gradually heated. The container was connected via a cold transfer line to a VADIS ion source.
To promote the formation of molecular sidebands, SF_6 was injected via a calibrated leak of $5 \cdot 10^{-5}\ \frac{mbar \cdot l}{s}$ (measured for air) into the container.
After the study of the temperature dependence, the impact of injected amounts of SF_6 on the release of boron fluorides was studied. Figures 3.12 and 3.13 show the results of these measurements.

Thermodynamical calculations of the chemical equilibrium show, that the formation of BF_3 is expected from a mixture of tantalum, boron and SF_6 (compare figure 3.12). Different from the results of the equilibrium calculation, mass spectra show that the dominantly extracted species is BF_2^+ instead of BF_3^+ (see figure 3.11). This observation can be explained with the higher dissociative ionization cross section of BF_3 to BF_2^+ compared to the cross section for direct ionization to BF_3^+ and will be addressed in section 3.4.1.
Assuming that the observed BF_2^+ is produced mainly from the dissociative ionization of BF_3, the measured BF_2^+ can be regarded as BF_3 prior its dissociative ionization. A comparison of the behavior of the measured ion currents to the theoretical expectations [compare fig 3.12] shows similarities: the ion yield rises from approximately $T \approx 100°C$ and drops at elevated temperatures from $T \approx 1600°C$. The maximum of the ion current was observed at $T \approx 1500°C$. Although suggested by the calculation of the

chemical equilibrium no plateau can be seen in the extracted currents.
Possible reasons that might lead to the difference in the measured spectra are:

- At lower temperatures the extraction happens before the system reaches equilibrium. The kinetics of this reaction is unknown.
- Ion source characteristics: superposition of ionization of BF_2 and dissociative ionization of BF_3
- Impurities affecting the equilibrium

Nevertheless the results confirm, that taking the previous comments into consideration, information obtained from calculations of the chemical equilibrium apply to ISOLDE targets.
Combining these results with calculations performed in section 3.3 shows that a target utilizing graphite as a target material at a temperature between $1300-1600\ °C$ should allow the extraction of boron as BF_2^+. As it was shown in section 3.2, this is as well the temperature range, where fast diffusion of boron in Graphite can be expected.

Besides the dependency of the extracted current of boron fluorides on temperature, the dependency on the amount of injected SF_6 was studied. The results are shown in figure 3.13. From equilibrium calculations a linear dependency of the formation of BF_3 to available fluorine is expected. This correlation is confirmed in the measurements: an increase of injected fluorine leads to an increase of extracted boron fluorides. Consequently, a high flow of injected fluoride fosters an efficient extraction.

The known leakage rate of the calibrated gas leak allows to determine a combined efficiency for the formation, transport and ionization of boron from the target. The extraction of boron as BF_2^+ can roughly be divided into three steps:

1. Formation of the molecule
2. Migration to the ion source
3. Ionization

According to formula 1.1 each of these processes has an efficiency ϵ, here $\epsilon_{formation}$ for the formation of the molecule, $\epsilon_{transport}$ for the migration through the system and ϵ_{ion} for the ionization in the ion source. Assuming a formation of BF_3 via the process

$$2B + SF_6 \rightarrow 2BF_3 + S \tag{3.6}$$

and followed by ionization to BF_2^+ the release efficiency can be determined via the known leakage rate of the calibrated leak and hence the supply of SF_6. The analysis of measured data leads to a combined release efficiency of

$$\epsilon_{BF2} = \epsilon_{transport} \cdot \epsilon_{formation} \cdot \epsilon_{ion} = 1.5\%$$

.

3.4.1 Ionization Characteristics of Noble Gases, BF_2 and BF_3

In order to guarantee an efficient extraction of atoms and molecules from ISOLDE targets, it is crucial to operate ion sources in a mode where the electron energy matches the maximum ionization cross section of the species to be ionized. In chapter 2.7 the dependency of extractable currents of carbon oxide on the anode voltage and with that electron energy was studied. The results were compared to theoretically and experimentally obtained ionization cross sections found in literature. A discrepancy between

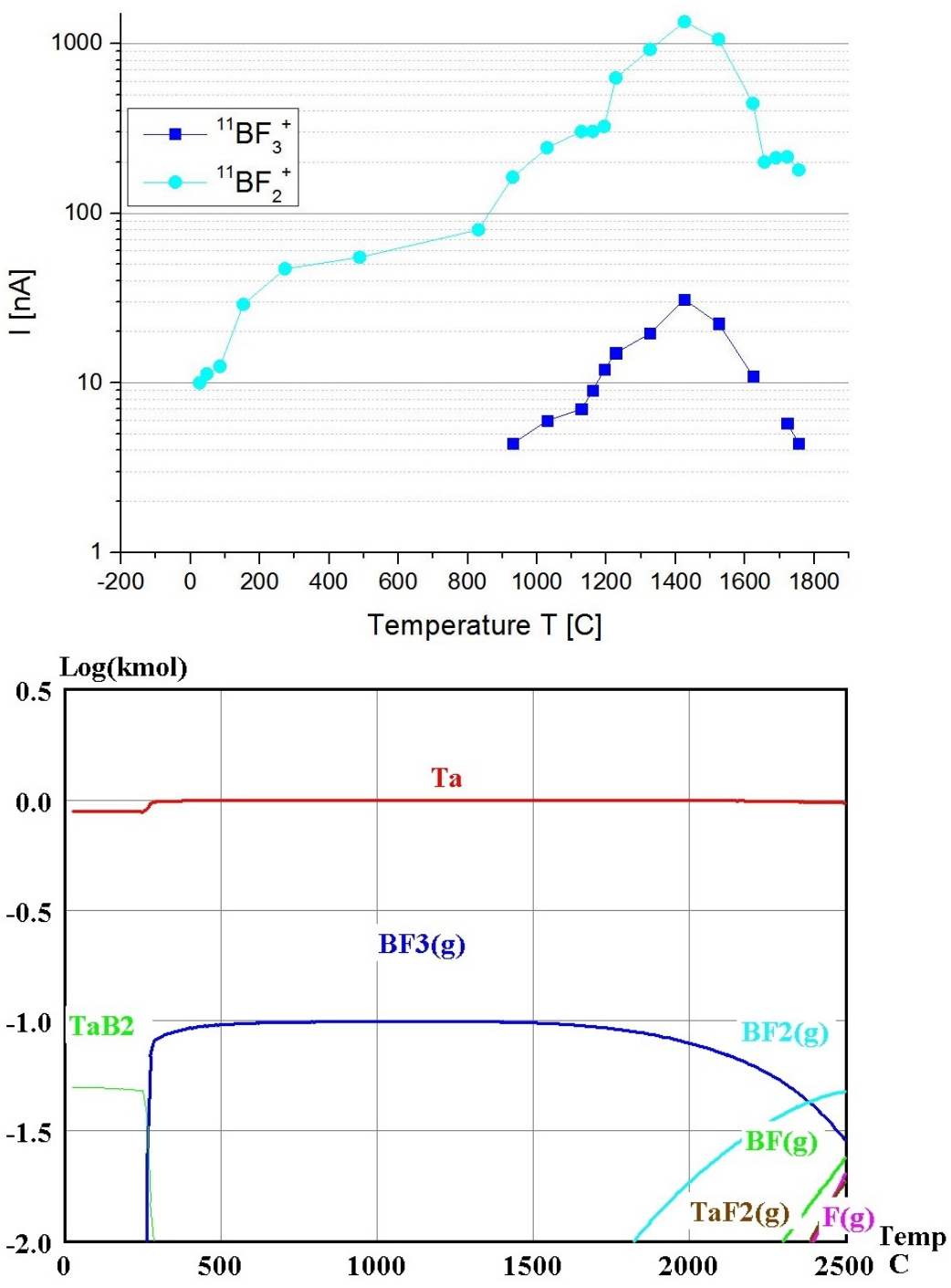

Figure 3.12.: Dependency of the BF_2^+ ion current on the target temperature in comparison with calculated chemical equilibrium of tantalum, sulfurhexafluoride and boron.

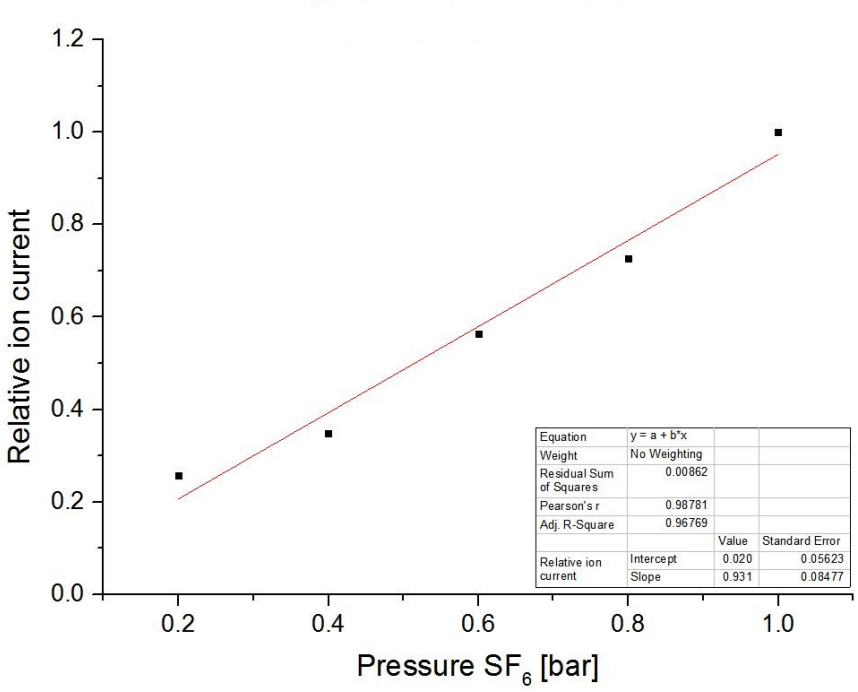

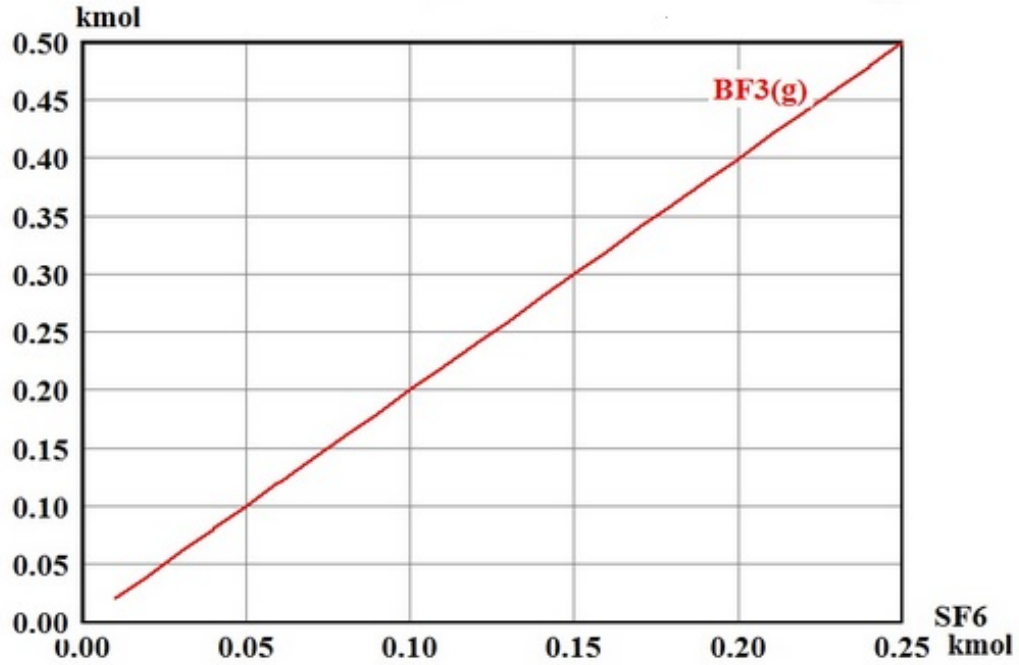

Figure 3.13.: Dependency of the BF_2^+ ion current on the amount of injected SF_6 in comparison with calculated chemical equilibrium.

the expected and the measured ionization behavior was observed. While ionization begins at electron energies close to the Ionization potential I_p, a mismatch can be observed for higher electron energies.
To further investigate the characteristics of the ion source, measurements are extended to noble gases (Ar,Kr,Xe) and boron fluorides (BF_2 and BF_3).
Due to their chemical inertness noble gases are well suited to investigate ion source characteristics. In addition to that is the ionization process for atoms not as complex as for molecules where additional degrees of freedom such as rotation and vibration are present and additionally dissociative ionization can occur.

During the measurements the anode voltage of the source and, with that, the energy of the electrons was varied and the resulting current of $^{11}BF_2^+$ and $^{11}BF_3^+$ as well as $q = +1$ ions of argon, krypton and xenon coming from the target was monitored. After each change of the anode voltage a mass scan was performed and the peak maximum in the mass spectra determined. In this way possible changes of the peak position due to changes in the extraction energy caused by the anode voltage are taken into account. To ease comparison, measured data and the theoretical cross section are normalized to the maximum. The results of all measurements are listed in table 3.3.

3.4.2 Ionization of Ar,Kr and Xe

To better understand the ionization characteristics of the used VADIS ion source, noble gases were injected into the target container. As noble gases don't undergo chemical reactions with the environment, the resulting current of $q = +1$ ions is only dependent on the ionization. The noble gases used are neon, argon, krypton and xenon. The results for Ne^{+1} ions are not presented, as contamination of Ar^{+2} ions were present on the same mass. The ionization of noble gases was studied intensively, e.g. [85],[86]. Values for comparison are taken from [85]. Figure 3.14 to 3.16 show the results of the measurements for xenon, argon and krypton.

3.4.3 Ionization of Boron Fluorides

From calculation of the chemical equilibrium (see section 3.3) of boron with fluorine containing gases like SF_6, the production of BF_2 and BF_3 is expected. Indeed mass spectra, measured from a target containing atomic boron in which SF_6 is injected, show the presence of these molecules as $q = +1$ ions. As opposed to the equilibrium calculation for neutral molecules, BF_2^+ molecular ions are present in a much higher amount than BF_3^+ ($I_{BF_2^+}/I_{BF_3^+} \approx 35$).
Figure 3.17 and 3.18 show the result of these measurements together with the theoretical cross section for ionization. To ease comparison the measurements and the theoretical cross sections are normalized.

The ionization behavior of BF_3 in the VADIS ion source is very similar to other species measured before. In other experiments the ionization potential of BF_3 was found to be 16.5 eV [69] and 16 eV [87] respectively while the maximum ionization cross section was found for an electron energy of 125-130 eV [69] and 120-170 eV [87].
The results obtained in this work show BF_3^+ first occurring (detection limit: $I_{min} = 1$ pA) in the mass spectra at $U = 25.9 \pm 1.7$ V. The maximum current was extracted for an anode voltage of $U = 160$ V which is agreement of the values obtained in [87]. Furthermore, a slower increase in the ionization behaviour can be observed for measured values in comparison to theoretical predictions.

To the best of our knowledge no experimentally obtained values of the ionization cross section of BF_2^+ are published. Hence the only available values are those calculated with the BEB model. A comparison of the results from the performed measurements with the calculated cross sections from [69] shows a bigger discrepancy for the case of BF_2^+ than in other cases. The reason for that can be found in the origin of measured BF_2^+. BF_2^+ can be produced via three reaction channels:

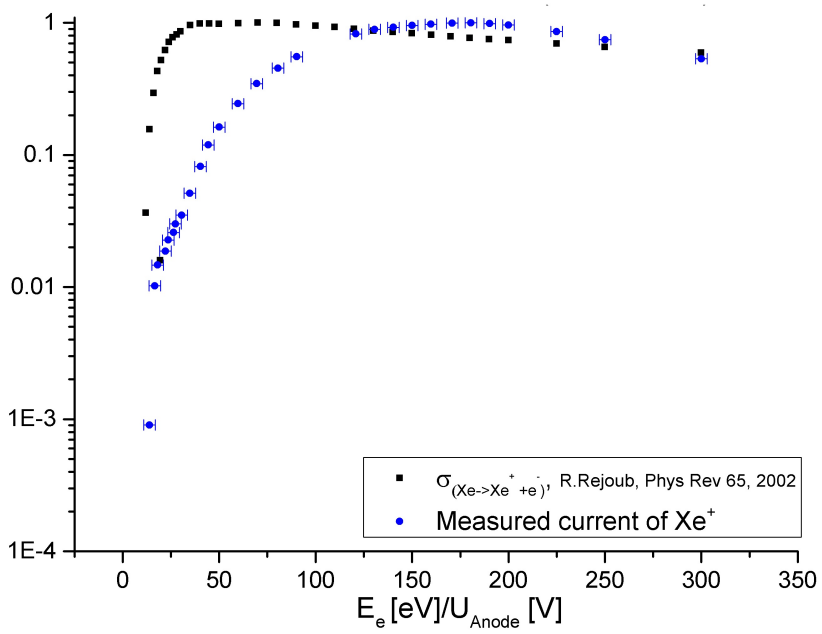

Figure 3.14.: Comparison of ionization cross section for xenon and measured ion currents in dependency of anode voltage. Cross section values are taken from [85].

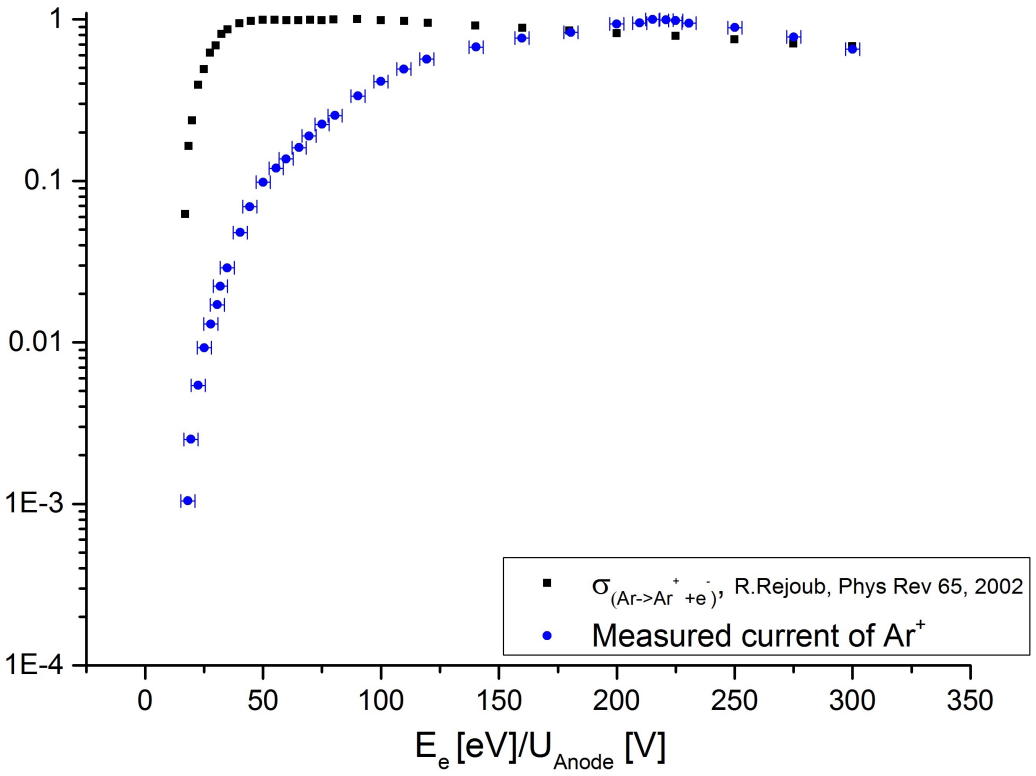

Figure 3.15.: Comparison of ionization cross section for argon and measured ion currents in dependency of anode voltage. Cross section values are taken from [85].

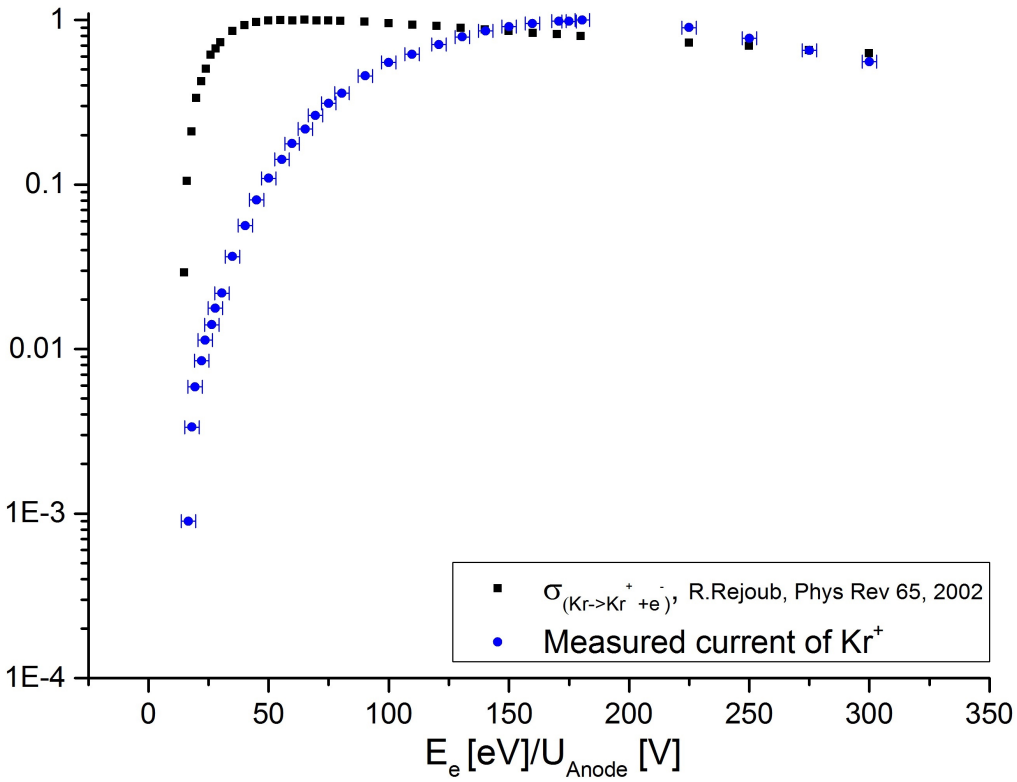

Figure 3.16.: Comparison of ionization cross section for krypton and measured ion currents in dependency of anode voltage. Cross section values are taken from [85].

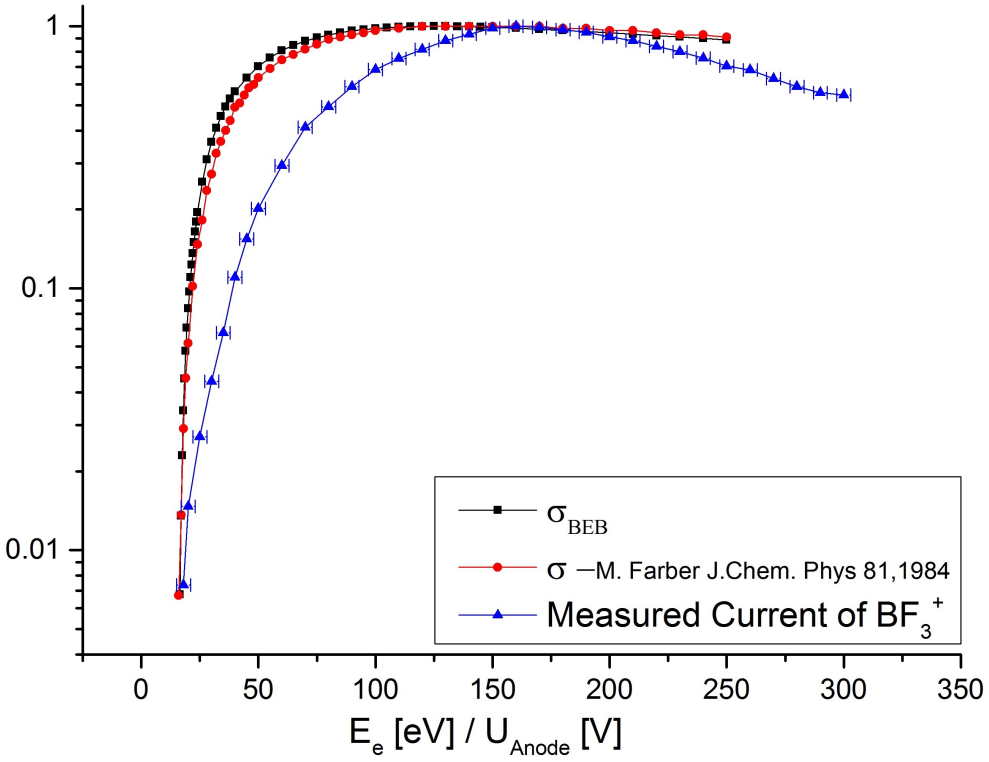

Figure 3.17.: Comparison of normalized ion current of $BF_3{}^+$ coming from a VADIS ion source with normalized ionization cross section for the process $BF_3 \rightarrow BF_3{}^+ + e^-$.

- Direct ionization of BF_2: $BF_2 \rightarrow BF_2{}^+ + e^-$
- Dissociation ionization of BF_3: $BF_3 \rightarrow BF_2{}^+ + F^+ + 2e^-$
- Thermal dissociation of $BF_3 \rightarrow BF_2 + F$ and later on direct ionization of BF_2: $BF_2 \rightarrow BF_2^+ + e^-$

Literature [87] indicates that the main production process of $BF_2{}^+$ is thermal dissociation of BF_3 with add-on ionization of BF_2 and dissociative ionization of BF_3. It was found in [87] that the cross section for dissociative ionization of BF_3 to $BF_2{}^+$ is 10 times higher than the direct ionization of BF_3 at an electron energy of $E_e = 70$ eV.
The same publication stated that thermal dissociation cross section at 1800 K is in the order of $2.26 \cdot 10^{-16}\ cm^2$, compared to $5.56 \cdot 10^{-16}\ cm^2$ for dissociative ionization of BF_3 found in [88]. Since the ion source temperature is approximately 2300 K, thermal dissociation becomes as important as dissociative ionization. Comparing the ionization cross section of BF_3 with the measured current of $BF_2{}^+$ shows indeed a better match than for the ionization of BF_2. This also confirms the prediction from calculation of the chemical equilibrium, that BF_3 is the dominantly produced species.

3.4.4 Discussion

Comparison of the results obtained in this section for some noble gases and boron fluorides with former results for CO and CO_2 [section 2.7] shows an accordance in the ionization behavior. All measurements show discrepancies in comparison to experimentally and theoretically obtained values found in literature. For comparison the measured values and values for the ionization potential I_p found in literature and maximum ionization $E_{\sigma_{max}}$ are summarized in table 3.3. In most cases the anode voltage where ionization

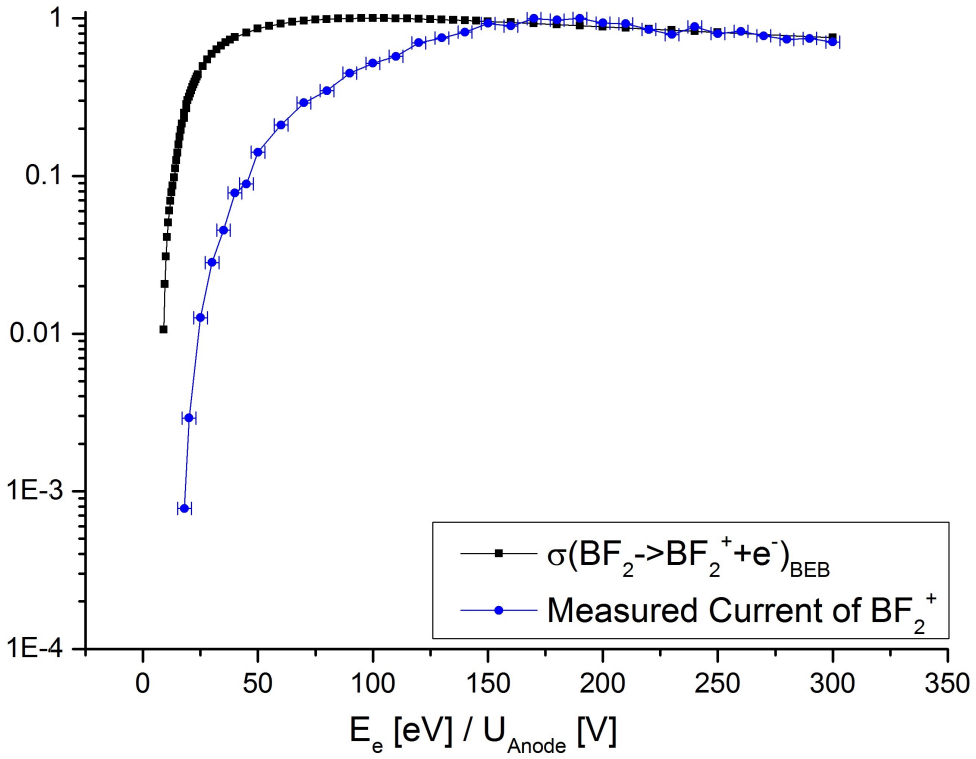

Figure 3.18.: Comparison of normalized ion current of BF_2^+ coming from a VADIS ion source with normalized ionization cross section.

first occurs $I_{p,exp}$ is close to the values $I_{p,theo}$ found in publications for noble gases. Comparing the values for maximum ionization $E_{\sigma_{max}}^{theo}$ and $E_{\sigma_{max}}^{meas}$ shows a big discrepancy for most investigated species. Furthermore all measured curves show a different slope especially for the region up to $U = 150$ V. In [32] the resulting field in the VADIS ion source for an applied anode voltage of $U = 150$ V was calculated. These calculations considered the effect of electrons and ions to the resulting field. It was found that the potential in the source varies between 110 V and 149 V. However no resulting average electron energy was given. Nevertheless these calculations show that the average electron energy in the ion source can be expected to be smaller than given by $E = e \cdot U$.
If calculations were extended to lower voltages, the measured results obtained in this work would allow to verify the theoretical result.

Species	I_p theo [eV]	I_p exp [eV]	$E_{\sigma_{max}}$ theo [eV]	$E_{\sigma max}$ exp [eV]	$\Delta E[eV]$
CO	14	20.7 ± 1.5	105	200	95
CO_2	14.5	31.1 ± 7.3	95	80-120	≤ 25
BF_2	8.45	20.8 ± 4.2	100	190	90
BF_3	16	25.9 ± 1.7	125-170	160	0
Ar	17	17.9 ± 2.3	90	215	145
Kr	15	15.7 ± 0.9	65	180	115
Xe	18	11.9 ± 1.7	70	180	110

Table 3.3.: Comparison of measured and theoretical threshold of ionization I_p and electron energy with maximum cross section for molecules and noble gases

Results obtained within this work suggest that the extraction of ^{8}B ($t_{1/2} = 770ms$) as $^{8}BF_2{}^{+}$ is feasible. The most promising material seems to be carbon in the form of carbon nanotubes (MWNCT). Simulations of the production cross section (compare section 3.1) and the in-target production of ^{8}B show that rates of $1 \cdot 10^{9} \frac{1}{\mu C}$ to $1 \cdot 10^{10} \frac{1}{\mu C}$ can be expected if graphite is utilized as a target material. If carbon nano tubes are chosen as a target material, the lower density of $\rho = 0.4 \frac{g}{cm^3}$ will result in a production of $2 \cdot 10^{8} \frac{1}{\mu C}$ of ^{8}B.
Results obtained from diffusion measurements presented in section 3.4.4 show, that for this choice diffusion of boron can be expected to be fast. As these measurements do not allow a quantitative analysis, diffusion efficiencies have to be accessed during on-line runs.
During offline studies with a VADIS ion source (compare section 3.4) a combined efficiency for the formation of BF_3, transport and ionization to BF_2^{+} of $\epsilon = 1.5\%$ was found. This was for an empty target container in which a source of atomic boron was inserted and SF_6 injected through a calibrated leak of $5 \cdot 10^{-5} {}^{mbar \cdot l}/_{s}$. The maximum extracted current was observed for $T = 1500\ ^{\circ}C$.
An unknown factor during online operations is the effect of carbon nano tubes on the formation and extraction of boron fluorides. Although calculation of the chemical equilibrium show (section 3.3), that the formation of BF_3 is favored over the formation of carbon fluorides, the dominating amount of carbon combined with the extraordinary high surface area of CNT might hinder the formation and/or extraction. This might affect the extraction time t_{extr}, the formation efficiency $\epsilon_{formation}$ and the transport efficiency $\epsilon_{transport}$.
Yields of $I = 5 * 10^{3}\ {}^{1}/_{\mu C}$ of post-accelerated ^{8}B are requested [77]. For stable CO to C^{+6} a combined charge breeding and transmission efficiency through the low energy part of the REX post accelerator of 2.7% was measured [89]. Assuming a similar efficiency for boron allows to calculate lower limits for the combined value of extraction time t_{extr} and diffusion efficiency ϵ_{diff}. With equation 3.7 follows that a combined decrease due to extraction time and diffusion efficiency should not exceed a factor of $\frac{1}{15}$. This would for instance be the case for $t_{extr} = 1.5$ s and $\epsilon_{diff} = 0.25$. The real values for these parameters have to be determined during on-line operation.

$$\begin{aligned} N_{max} &= N_0 \cdot e^{-\lambda \cdot t_{extr}} \cdot \overbrace{\epsilon_{REX}}^{2.7 \cdot 10^{-2}} \cdot \overbrace{\epsilon_{formation} \cdot \epsilon_{transport} \cdot \epsilon_{ionization}}^{1.5 \cdot 10^{-2}} \cdot \epsilon_{diff} \\ &= 2 \cdot 10^{8} \cdot e^{-\frac{ln(2)}{0.77} \cdot 1.5} \cdot 2.7 \cdot 10^{-2} \cdot 0.015 \cdot 0.25 \\ &\approx 2.94 \cdot 10^{4} \frac{1}{\mu C} \end{aligned} \tag{3.7}$$

The desired current of $5 \cdot 10^{3} \frac{1}{\mu C}$ after post acceleration corresponds to an intensity of $N_{BF_2^{+}} = 1.9 \cdot 10^{5} \frac{1}{\mu C}$ of expected molecular ions before post acceleration.
In most cases the release of isotopes from ISOLDE targets is determined with a setup called a tapestation. This setup is located in the beam line of ISOLDE and allows to collect the extracted beam on a tape. After collection, the tape is moved from the in-beam position to a position where it is surrounded by gamma and beta detectors. This combination allows for most cases to determine the amount of radioactive species and distinguish between isobars by detection of specific gamma emission. A problem that is common for radioactive isotopes of light elements is the lack of gamma emission or only such with very high energies where detector efficiencies are very low.
In the case of ^{8}B no gamma lines are known and thus a separation from isobars is difficult. Possible isobars are ^{8}C, ^{8}Li, ^{8}Be and ^{8}He. As ^{8}C is extremely short lived and ^{8}Be unbound, only ^{8}Li ($t_{1/2} = 839.9ms$) and ^{8}He ($t_{1/2} = 119.1ms$) might be seen. However, as boron is expected to be extracted as $BF_2{}^{+}$ with $m(^{8}BF_2) = 46$ amu, isobaric contaminants on $m = 8$ amu will not affect the measurement. If carbon nanotubes are used as a target material no radioactive species with $m_X = 46$ amu or $m_X = 27$ amu as

Target material	Ion Source	U_{anode} [V]	T_{target} [$°C$]	Gas injection
CNT	VADIS	160	$\geq$ 1500	SF_6 or CF_4

Table 3.4.: Suggested combination of target material, ion source and operational parameters for the extraction of radioactive boron as $^8BF_2$. During off-line studies a cold transfer line was used.

XF^+ ions will be produced. Furthermore the formation of $^8LiF_2{}^+$ is in principle not possible and thus no contamination on mass $m = 46$ amu for the low energy beam or $m = 8$ amu for the post accelerated one have to be expected. Hence a measurement of the β^+ activity should allow a determination of extracted currents of $^8BF_2{}^+$
Table 3.4 summarizes the suggested target unit, choice of target material and operational parameters.

3.6 Online Measurement at ISOLDE

3.6.1 Target Setup

The release of radioactive boron from an ISOLDE target unit was tested during the online period 2014. Therefore a target prototype with the characteristics suggested in section 3.5 was built. The target unit (# 499) consisted of a standard tantalum target container, connected via a cold copper transfer line to a VADIS ion source. For the target material multi-walled carbon nano tubes (MWCNT) with a purity of 95% (Nanocyl S.A.m NC3100) were chosen. The same material was used for the study of diffusion of boron in chapter 3.2. A total amount of 15.1 g of MWCNT was pressed (8t) into 41 pellets (thickness $\approx$3 mm, $r = 7.5$ mm) with a density of 0.43 g/cm^3. All pellets were loaded into a rhenium boat and inserted into the target container. In order to promote the formation of boron fluorides a gas line with a calibrated leak of $0.37 \cdot 10^{-4} \frac{mbar \cdot l}{s}$ was connected to one side of the target container, allowing the injection of SF_6. The applied pressure of SF_6 on the calibrated leak varied between 0.5 bar and 1.8 bar.

3.6.2 Measurements and Results

Earlier studies showed that boron under a fluorine atmosphere is released mainly as BF_2^+ from ISOLDE targets (section 3.4.4). Therefore the release of radioactive boron fluoride and possible molecule fragments ($^8B^+$, $^8BF^+$, $^8BF_2{}^+$, $^8BF_3{}^+$) was measured to identify the most abundant ions. As the majority of the released stable beam consisted of CO^+ ($I_{max} = 6\mu A$) and CO_2^+ ($I_{max} = 400nA$) the release of radioactive species on the masses of $^8BO^+$, $^8BOC^+$ and $^8BOF^+$ was measured in addition. For all measurements the earlier described tape station [90] was used. This setup allows to monitor the gamma and beta activity of the extracted beam. The expected isobaric contaminant for ^8B ($t_{1/2} = 770ms$) is ^8Li ($t_{1/2} = 839.9ms$). To distinguish ^8B (β^+ emitter) from ^8Li (β^- emitter) the presence of the E= 511 keV gamma line, originating from annihilation of the emitted positrons with electrons, was used. The detection limit with this setup is $7.5 \cdot 10^1$ $1/\mu C$. The activity on the described masses was measured for three different target temperatures: $T = 1350°C$, $T = 1600°C$ and $T = 2000°C$.
Contrary to expectations no activity was found on the masses of boron fluorides $^8BF^+$, $^8BF_2{}^+$ and $^8BF_3{}^+$ or $^8BO^+$, $^8BOC^+$ and $^8BOF^+$. However for all three temperatures a beta activity on mass m= 8 amu with a maximum for $T = 2000°C$ of $1 \cdot 10^4$ $1/\mu C$ was measured. The half live of the extracted isotopes was determined to be approximately $t_{1/2} \approx 800 \pm 100$ ms. This half is very close to the half lives of ^8Li and ^8B The measured gamma activity on E= 511 keV suggests that 3% of the measured beta activity originates from a β^+ emitter. Since the presence of doubly charged β^+ emitting ions with m= 16 amu was excluded, it can be concluded that the measured isotope is most likely ^8B with a yield of $3 \cdot 10^2$ $1/\mu C$. It was intended to identify the isobaric composition using the ISOLTRAP MR-tof [91] setup with

a mass resolution power of $\Delta m = 2 \cdot 10^{-4}$ amu. The combination of the occurrence of activity only on mass m= 8 amu combined with low count rates did not allow to use this setup. Thus the final proof that the measured isotope is ^{8}B is still pending.

The absence of boron fluorides can be caused by several reasons. During offline studies SF_6 was injected into the target container over multiple days before the current of extracted BF_2^+ and BF_3^+ reached a constant maximum. Prior the online release measurements, injection of SF_6 into the target unit took place for only about 48 hours. A typical sign indicating a surplus of fluorine in the target is the presence of tantalum fluoride and tantalum oxo-fluoride ions in the extracted beam. These peaks were absent during the online measurement with the MWCNT target unit, indicating a lack of fluorine. Contrary to this theory is the presence of $^{19}F^+$ ions with $I_F = 7$ nA and SF_5^+ with $I_{SF_5} \approx 0.9$ nA in the stable beam. The applied pressure of SF_6 varied between 0.8 bar and 1.8 bar. A second reason why no boron fluoride peaks were formed might be given by the used MWCNT as a target material. Although not predicted by chemical equilibrium calculations, a reaction of carbon with the injected fluorine might take place. Contrary to this theory is the fact that the release of stable CF_n ($n = 1, 2, 3, 4$) was very little with currents in the order of pA.

To qualify MWCNT as a target material for the extraction of radioactive boron in the future, the release efficiency of stable boron as boron fluoride from a target using MWCNT should be determined during off-line experiments.

3.7 Sample Preparation for Experiments at the SARAF Facility

Besides the implantation of boron into possible target materials for ISOLDE, implantation into aluminum foils took place. This was done in the framework of a collaboration between n-tof/CERN, Paul Scherrer Institute (PSI), the Israel-US SARAF collaboration and ISOLDE. This collaboration intends to measure the cross section for the reaction $^{7}Be(n,\alpha)$ which might correct the difference between predicted and observed amount of primordial ^{7}Li and possibly solves the ^{7}Li problem [92].
While the relative abundances of $^{2}H/^{1}H$, $^{3}H/^{1}H$ and $^{4}He/^{1}H$ are predicted correctly by the Big Bang Nucleosynthesis theory (BBN)[93], the relative abundance of primordial $^{7}Li/^{1}H$ is predicted to be 3-4 times higher than it is observed (fig 3.19). Most of the primordial ^{7}Li is destroyed during the first 4-15 minutes after big bang via the $^{7}Li(p,\alpha)$ reaction.

The ^{7}Li which can be observed up to now is believed to be produced via the decay of ^{7}Be ($t_{\frac{1}{2}} = 53.29d$) by electron capture.
One possible reason for the deficiency of ^{7}Li might be the destruction of ^{7}Be via the $^{7}Be(n,\alpha)$ reaction during the first minutes after the big bang (10-15min). The calculation of this destruction rate relies on an extrapolation of the cross section to high (primordial) energies from measurements performed with neutrons at thermal energies [94].
The goal of the experiment is to measure the cross section for $^{7}Be(n,\alpha)$ at higher neutron energies (10-100keV) with a modern setup.
For the measurements, ^{7}Be, coming from the water-cooling loop of the SINQ neutron spallation source at the Paul-Scherrer Institute [95] will be implanted into Beryllium foils at ISOLDE during operations in 2015.
The extraction of ^{7}Be happens within the framework of the ERAWAST[2] project at PSI. Within this project several sources for radio nuclides are exploited, offering high amounts of desired exotic isotopes such as ^{7}Be, ^{44}Ti, ^{60}Fe and ^{53}Mn.
The measurement of the cross section will take place at the Soreq nuclear research center in Israel, with neutrons coming from a liquid lithium target which is irradiated with protons.
In order to test the experimental procedure and determine the energy distribution of the neutrons from

[2] Exotic Radionuclides from Accelerator WAste for Science and Technology

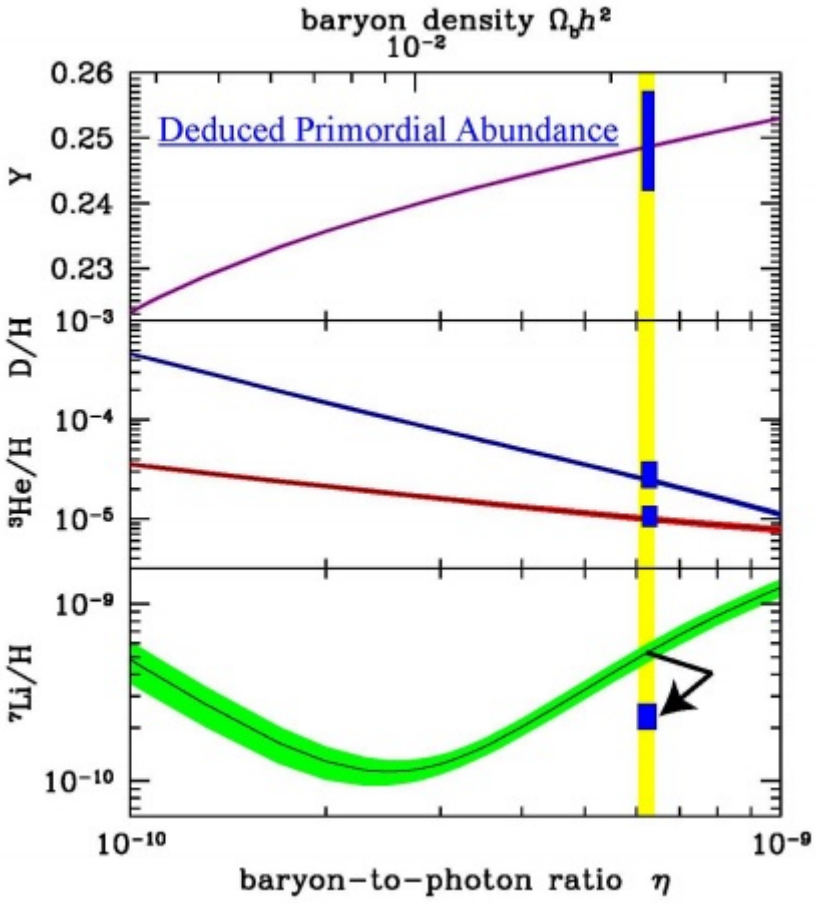

Figure 3.19.: Relative abundances of D, ^3He, ^4He (Y) and ^7Li to ^1H in dependency of the Baryon to photon ratio η. In the case of ^7Li the green line indicates the expected abundance while the blue square marks the observed. Picture taken from [92]

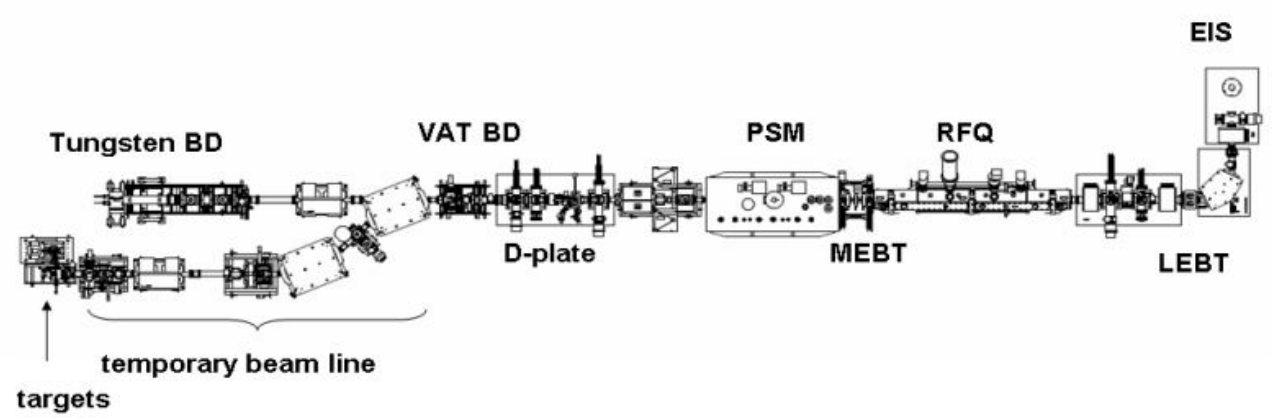

Figure 3.20.: Layout of SARAF during Phase I and the temporary beam line [96]

the liquid lithium target (LiLiT), an experiment with an aluminum foil with implanted ^{10}B, produced within this work, is planned beforehand the measurement of the cross section $\sigma(^7Be(n,\alpha))$.

3.7.1 SARAF and LiLiT

At SARAF protons and deuterons with currents up to 5 mA are accelerated via a RF superconducting linear accelerator [96] and directed onto a target. Figure 3.20 shows the setup of the accelerator during phase 1. The achievable energy can be varied up to 4 MeV for protons and 5 MeV for deuterons. For the production of neutrons, a proton beam of 1.91 MeV is directed on a liquid lithium target (LiLiT). The energy is chosen to be just above the threshold for the reaction $E_{^7Li(p,n)^7Be} = 1.8804$ MeV, in order to produce neutrons with low energies (10-100 keV).

Besides investigations on astrophysics, one target of SARAF is dedicated to investigate the feasibility of liquid lithium targets for neutron production, serving the treatment of cancer with the boron-neutron capture therapy (BNCT). Neutrons produced with a low proton beam of energies just above the reaction threshold for $^7Li(p,n)^7Be$ have the advantage that the energy of the resulting neutrons is close to the optimum energy for cancer treatment with the BNCT of $E = 1eV - 10\ keV$.
Neutrons coming from radioactive sources such as Pu-Be possess a much higher energy of about 5MeV [83] and thus need to be moderated.

The liquid lithium target at SARAF consists of a loop of molten lithium [97]. In order to keep the lithium in a liquid state, the loop is kept at $200°C$ ($T_{melt,Li} = 180.5°C$). A steady flow with up to $4m/s$ is assured by a electromagnetic pump. Figure 3.21 shows the target setup and its components.
The area where the proton beam interacts with the lithium is an open part of the loop, where the lithium flows through a narrow nozzle and a wide and thin stream of lithium is created. The liquid lithium has two tasks: first the production of neutrons via the reaction $^7Li(p,n)^7Be$. This happens in the first few μm of the lithium stream. Second, the high thermal power of 5 kW transported by the proton beam needs to be removed. The extraordinary high heat capacity of lithium of $C_p = 4350J/Kg \cdot K$ allows to transport the power to a heat exchanger.
The to be investigated samples (^7Be,^{10}B) will be located very close to the lithium target. Neutron yields at this position are estimated to be in the order of $10^{10}\ \frac{n}{s \cdot cm^2}$.

3.7.2 Sample Preparation

As in the case of studies of prospective target materials, ^{10}B was extracted as $^{10}BF_2^+$ and implanted into aluminum foils. Figure 3.23 shows the setup for the implantation into foils of aluminum with its 4

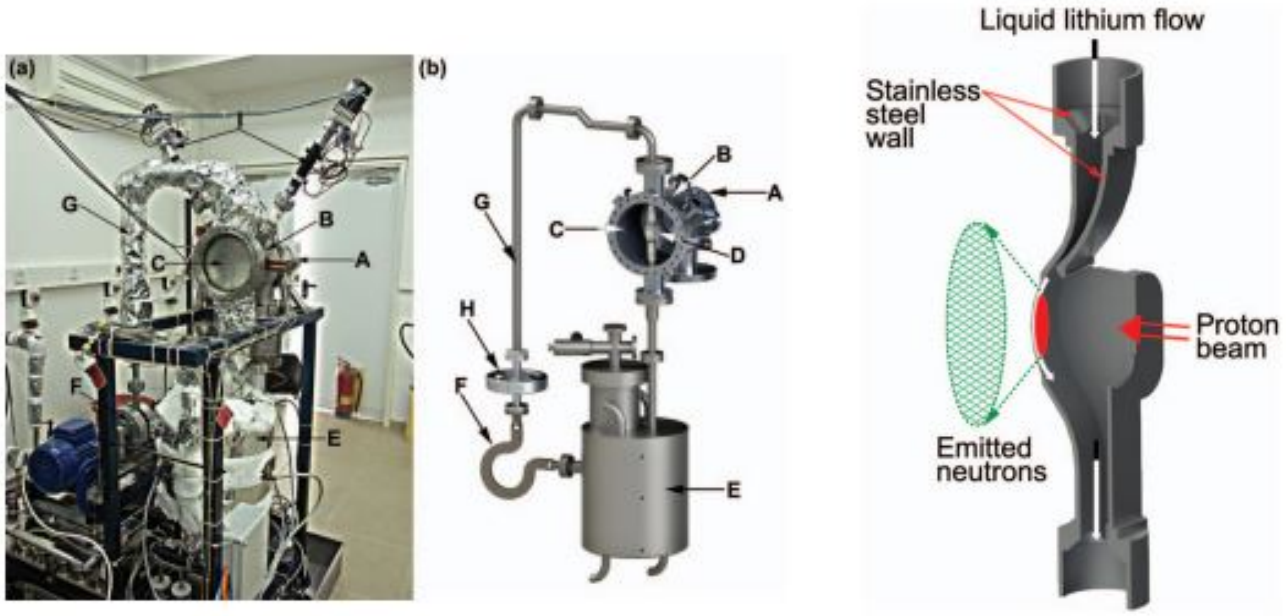

Figure 3.21.: The right side shows the LiLiT target loop with the target chamber (A-D), the lithium containment tank (E), the EM pump (F), loop line (G) an flow meter(H). The left side shows a zoom on the interaction zone. The lithium flows through a narrow nozzle, creating a steady stream where the proton beam impinges the lithium [96].

Particle	$-\frac{dE}{dx}$ $[\frac{keV}{nm}]$	$-\frac{dE}{dx}(x = 25nm)$ [keV]	$\overbrace{-dE(x = 715nm)}^{200\frac{\mu g}{cm^2}}$	$\overbrace{-\frac{dE}{dx}(x = 1825nm)}^{500\frac{\mu g}{cm^2}}$ [keV]
840 keV ^7Li	0.508	12.7	363	927
1481 keV α	0.298	7.45	213	543

Table 3.5.: Energy loss of the emitted alpha particles and lithium from the reaction $^{10}B(n,\alpha)^7Li$ in aluminum . The energies of the particles are the one of the most abundant reaction channel.

elements: the 2 elements surrounding the sample holder were kept on -500 V in order to repel secondary electrons. This is important as the total amount of boron needs to be known. Therefore the current of $^{10}BF_2{}^+$ on the sample was monitored with a micro ampere meter and later on integrated. The goal was to implant an amount of boron of $4 * 10^{16}$ atoms.
The beam of $^{10}BF_2{}^+$ was collimated to the desired beam spot size of 3 mm.The average current of $^{10}BF_2{}^+$ on the aluminum foil was approximately 12 nA. To achieve the desired amount of boron of $4 \cdot 10^{16}$ an implantation time of approximately 7 days was necessary per sample. In total three foils were produced with two different thicknesses. These are 200 $\frac{\mu g}{cm^2}$ which corresponds to a thickness of 740 nm and 500 $\frac{\mu g}{cm^2}$ which corresponds to a thickness of 1850 nm. The extraction of $^{10}BF_2{}^+$ took place with an applied high voltage of 32 kV. This corresponds to $\frac{m_{10_B}}{m_{10_{BF_2}}} \cdot 32keV = \frac{10}{48} \cdot 32keV = 6.67keV$ for ^{10}B. Simulations of the implantation depth, using the SRIM code show (fig 3.22), that the majority of implanted ^{10}B is located at a depth of 25 nm.

In the case of the 200 $\frac{\mu g}{cm^2}$ aluminum foil both, the alpha particle and the ^7Li can be detected at the same time. This allows to only count coincidentally events and therefore reduce the background from other sources. Table 3.5 shows the expected energy loss for the most abundant alpha and lithium particles for the used aluminum foils of 740 nm ($200\frac{\mu g}{cm^2}$) and 1850 nm (500 $\frac{\mu g}{cm^2}$) thickness.

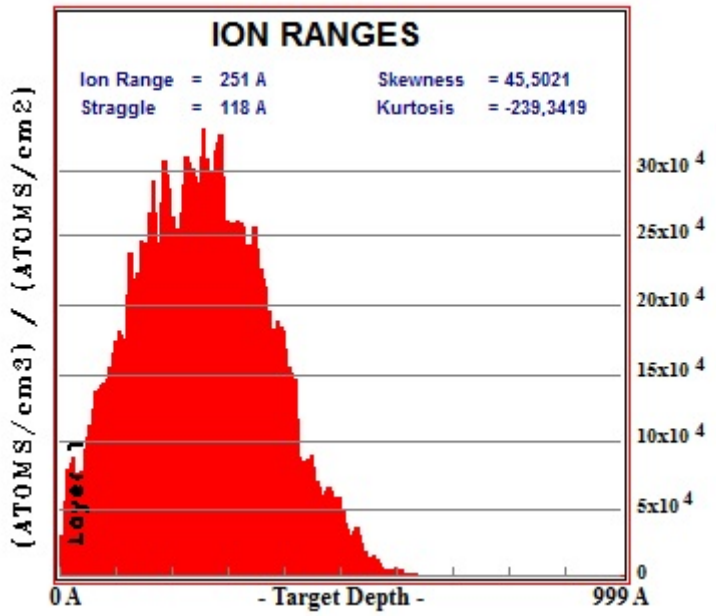

Figure 3.22.: Distribution of implanted boron in aluminum. Boron was extracted with a high voltage of 32kV as $^{10}BF_2$. This corresponds to an implantation of ^{10}B with 6.66 keV.

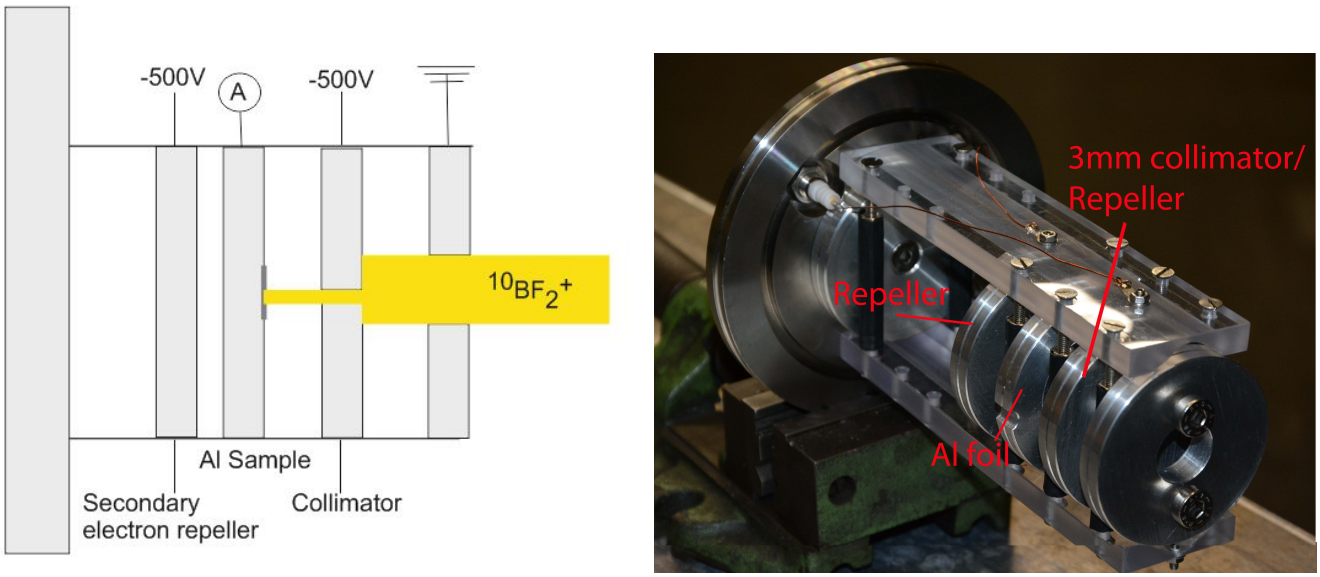

Figure 3.23.: Setup for the implantation of BF_2 into aluminum foil for SARAF

Sample	d_{beam} [mm]	thickness Al foil (μm)	Implanted $N_i(^{10}B)$	$\Delta N_i(^{10}B)$
Calibration	3	0.74	$4.0 \cdot 10^{16}$	$2 \cdot 10^{15}$
Sample 1	3	1.85	$3.88 \cdot 10^{16}$	$2.66 \cdot 10^{15}$
Sample 2	3	0.74	$1.07 \cdot 10^{16}$	$1.12 \cdot 10^{15}$
Sample 3	5	0.74	$2.59 \cdot 10^{16}$	$1.95 \cdot 10^{15}$

Table 3.6.: List of produced samples and amount of implanted boron. The calibration sample was used as a reference with a known amount of boron.

3.7.3 Determination of Implantation

In order to determine the implanted amount of ^{10}B, the produced sample was placed in front of the alpha detector described in section 3.2.2 and irradiated with thermal neutrons. The result of the measurement is compared to measurements with a calibration sample with a known amount of boron of $4{\cdot}10^{16}{\pm}2{\cdot}10^{15}$ atoms.

In order to determine the implanted amount, the more abundant alpha peak is fitted with a function of the form introduced in equation 3.3.

The amount of boron in the aluminum foil is determined by comparison of the peak areas of the calibration sample with the implanted foils. The used equations are similar as in section 3.2.2. The amount of implanted boron N_i is given by:

$$N_i = \frac{A_i \cdot t_0}{A_0 \cdot t_i} \cdot N_0 \tag{3.8}$$

where A_0 is the area of the peak of the calibration sample, t_0 the time measured, $N_0 = 4 \cdot 10^{16}$ is the amount of ^{10}B in the calibration sample, A_i the area of the peak of sample i and t_i the corresponding time.
The error of the implanted amount ΔN_i is given by the errors of the fit and calculated by Gaussian error propagation:

$$\Delta N_i = \sqrt{\left(\frac{t_0 \cdot N_0}{t_i \cdot A_0}\right)^2 \cdot \Delta A_i^2 + \left(\frac{t_0 \cdot A_i \cdot N_0}{t_i \cdot A_0^2}\right)^2 \cdot \Delta A_0^2 + \left(\frac{t_0 \cdot A_i}{t_i \cdot A_0}\right)^2 \cdot \Delta N_0^2} \tag{3.9}$$

Table 3.6 summarizes the results from these measurements and shows the derived amount of implanted boron.

3.7.4 Online Measurements at SARAF

In march 2014 the first proton beam, coming from SARAF hit the liquid lithium target. During this test, the combined operation of the accelerator and the lithium target was successfully tested. Also, a foil with implanted ^{10}B was placed close to the target position in order to be irradiated with produced neutrons, coming from the target. The sample was positioned in between two silicon detectors in order to detect alpha and lithium particles, resulting from the $^{10}B(n,\alpha)^7Li$ reaction, in coincidence. Due to a high radiation background in the detectors and a low event rate it was not possible to tune the data acquisition to allow the detection of emitted alpha and lithium particles within the short beam time.
For the future a different approach for the execution of the measurements will be followed. Instead of silicon detectors, measurements will take place using CR-39 plastic detectors. The detector is placed close to the sample during the irradiation with neutrons. Charged particles coming from the reaction $^{10}B(n,\alpha)^7Li$ enter the plastic, resulting in a visible damage. After irradiation the detectors will be

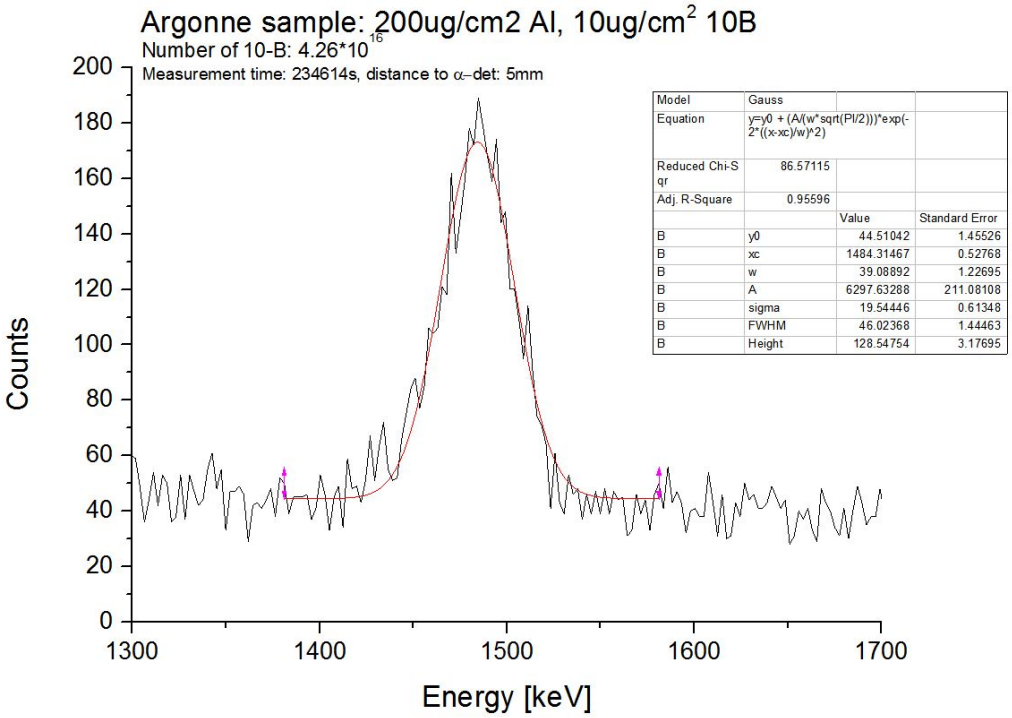

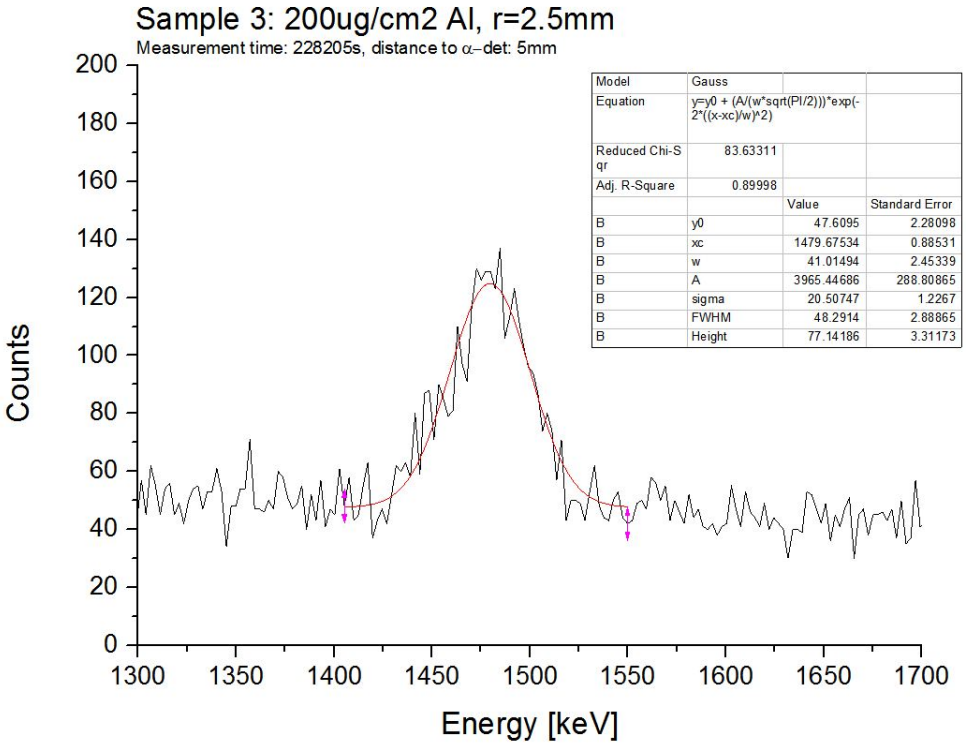

Figure 3.24.: Measurements and fit of the calibration sample and sample 3. Details see table 3.6.

extracted from the setup and the number of detected particles determined by counting dark spots on the surface. Depening on the structure of the spot it is possible to distinguish between different charged particles such as protons, alpha particles or lithium. If this setup is feasible to investigate the reactions of interest is currently studied by Emily Kading and Moshe Gai, University of Connecticut.

3.8 Summary

In this chapter the feasibility of extracting radioactive boron ^{8}B from an ISOLDE target unit was investigated. The high boiling point of boron requires the extraction in molecular form. The extraction as boron fluoride is favorable in comparison to other halides or oxygen as only one stable fluoride isotope exists and the low boiling point of boron fluorides. To identify target materials that allow the formation of boron fluorides in presence of CF_4 or SF_6, the chemical equilibrium between these elements was calculated. These calculations also allow to estimate where losses due to reactions with structural materials might occur. The results show that if a surplus of fluoride is present in the target container, the formation of boron fluorides is favored for all considered materials over the formation of e.g. metal borides. Furthermore, results suggest that graphite is the best suited target material. Although results of other considered target materials show that formation of volatile boron molecules is taking place, only the obtained results with graphite show a constant formation of boron fluorides over the majority of the considered temperature range from 25 $°C$ to 2500 $°C$.
The formation and extraction of boron fluorides from an ISOLDE target unit was tested experimentally. Therefore boron was inserted into a target container and SF_6 injected. The influence of operational parameters such as target temperature, ion source settings and amount of injected fluoride gas on the intensity of extracted boron fluoride was investigated. It was found that under optimum conditions a combined efficiency for formation, transport and ionization of 1.5 % can be achieved for the extraction of boron as BF_2^+ from an otherwise empty target container.
Beams extracted from this experiment were used to implant ^{10}B as $^{10}BF_2^+$ into samples of potential target materials to investigate the diffusion of boron and identify a material for the extraction of radioactive boron. Investigated materials are graphite, multi walled carbon nanotubes (MWCNT) and Yttria. The high neutron capture cross section of ^{10}B allowed to monitor the amount of boron in the samples before and after thermal treatment. Therefore the samples were irradiated with moderated neutrons and alpha particles originating from the reaction $^{10}\mathrm{B}(\mathrm{n},\alpha)^{7}\mathrm{Li}$ detected. The results show, that the fastest decrease of activity can be found for pellets made from MWCNT.
In the framework of a collaboration between ISOLDE, n-TOF, the Paul Scherrer institute and Saraf the same method was used to produce and characterize aluminum foils with implanted ^{10}B. The produced samples will be used to characterize neutrons, coming from the liquid lithium target (LiLiT) at the Saraf facility in Israel.
Results from off-line investigations were tested at ISOLDE during an online run 2014 with a dedicated target unit prototype. The prototype consisted of a standard target container using a cold transfer line and a VADIS ion source. The investigated multi walled carbon nanotubes were chosen as a target material. A special gas line allowed the injection of SF_6 directly into the target container to promote the formation of boron fluorides. Contrary to expectations no activity was found on masses of boron fluorides or other volatile boron molecules. However on mass $m = 8$ u a positron activity corresponding to $3 \cdot 10^2$ $1/\mu C$ was measured. Although other sources were excluded, the final proof that the measured activity originates from ^{8}B is still pending.

4 Other Molecular Beams

4.1 Titanium Fluoride

Within the ERAWAST[1] project different sources for radioactive isotopes are explored and exploited at the Paul Scherrer Institute (PSI) in Villigen. The sources that are used to extract isotopes are beam dumps and irradiated samples of e.g. stainless steel formerly used for material studies[98]. The PSI cyclotron accelerates protons up to 590 MeV with current up to 2.4 mA and hence production of exotic isotopes takes place wherever the high intensity beam is directed on material. With advanced radio chemical methods ^{44}Ti ($t_{1/2} = 60.4$ a) and ^{60}Fe ($t_{1/2} = 1.5 \cdot 10^6$ a) were extracted from a copper beam dump.
Furthermore ^{7}Be ($t_{1/2} = 53.29$ d)[95], produced by spallation of oxygen with fast neutrons in the cooling water of one of the experiments, is extracted. As mentioned in the last chapter the extracted ^{7}Be will be used to investigate the primordial ^{7}Li problem at SARAF (see section 3.7).

During the experimental phase 2012 a sample of extracted ^{44}Ti was used at ISOLDE to investigate the cross section for the reaction $^{44}Ti(\alpha,p)^{47}V$ aiming to gain a better understanding of physics processes triggering core collapse supernovae [73].
Due to the refractory nature of titanium, with a boiling point of $3287\ ^{\circ}C$ extraction had to take place in molecular form. Figure 4.1 shows the periodic table presented in section 1.4 where the extraction of titanium as a halide was suggested. Fluorine is the favorable element as it possesses only one stable isotope in contrast to chlorine and bromine. Furthermore, the relatively low boiling point favors the extraction as a fluoride (TiF_4: $T_{boil} = 377^{\circ}C$) over the oxide (TiO_2: $T_{boil} = 1843^{\circ}C$). The feasibility of extracting Ti as a fluoride was demonstrated in the past during offline tests.
Simulations of the chemical equilibrium show (fig 4.2), that the formation of titanium fluorides from ^{44}TiF to $^{44}TiF_4$ is expected, with $^{44}TiF_3$ as the dominant species.
The different fluoride molecules were visible in offline measurements prior the online experiment with different stoichiometries. The part of the measured mass spectra around 104 amu (figure 4.3) shows the peaks of natural titanium as $^{46-50}TiF_3^+$. For the offline measurements a target equipped with a hot transfer line and a VADIS ion source was used. Transfer line and container were heated up to 2000 $^{\circ}C$. During the later online measurements with the extracted sample from PSI an identification of the corresponding titanium peaks was much more difficult as the isotope abundances were unknown. Nevertheless sufficient extraction was achieved [73].

The used ^{44}Ti sample was extracted from a stainless steel sample and contained 50 MBq of activity which corresponds to $5 * 10^{18}$ atoms. The half life of ^{44}Ti is measured to be 60.4 years.
During online operations the extracted ion current was measured with Faraday cups at two positions. The first position was after the mass separator. Here the yield of low energetic $^{44}TiF_3^+$ was measured. The second measurement was after the REX-ISOLDE post-accelerator [99] where singly charged molecules are dissociated and ionized further by charge breeding. There the current of Ti^{13+}, the most abundant ion after charge breeding, was monitored. The measurements of both Faraday cups are shown in figure 4.4. Integration of the measured currents shows an extraction efficiency for ^{44}Ti from the target of 0.01% and a transmission efficiency through REX ISOLDE of 0.3%. Hence a total amount of approximately $2 * 10^{12}$ ions was delivered to the experiment.

[1] Exotic Radionuclides from Accelerator WAste for Science and Technology

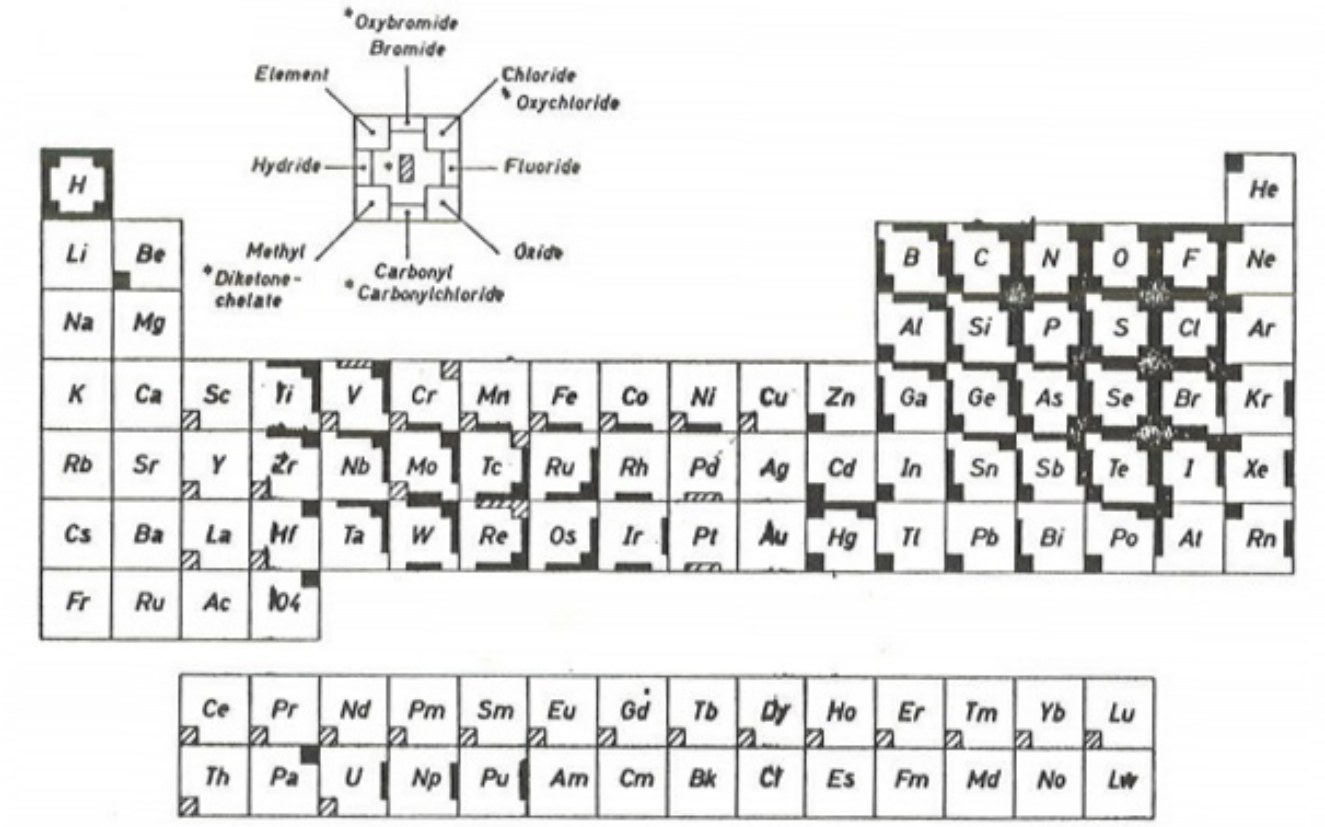

Figure 4.1.: Periodic table with suggestions on how refractory elements can be extracted by formation of molecules. Taken from [43]

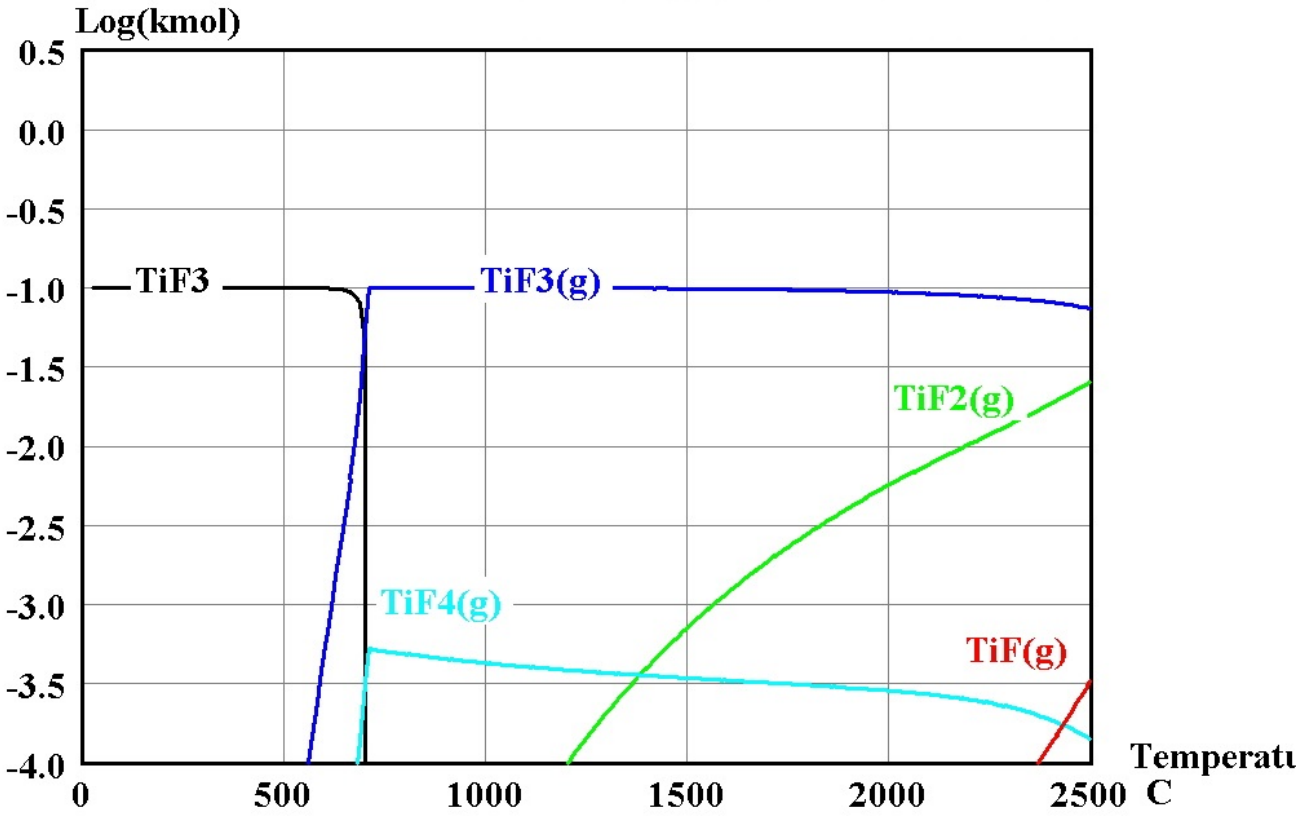

Figure 4.2.: Chemical equilibrium of Titanium with carbon tetrafluoride CF_4 in presence of tantalum.

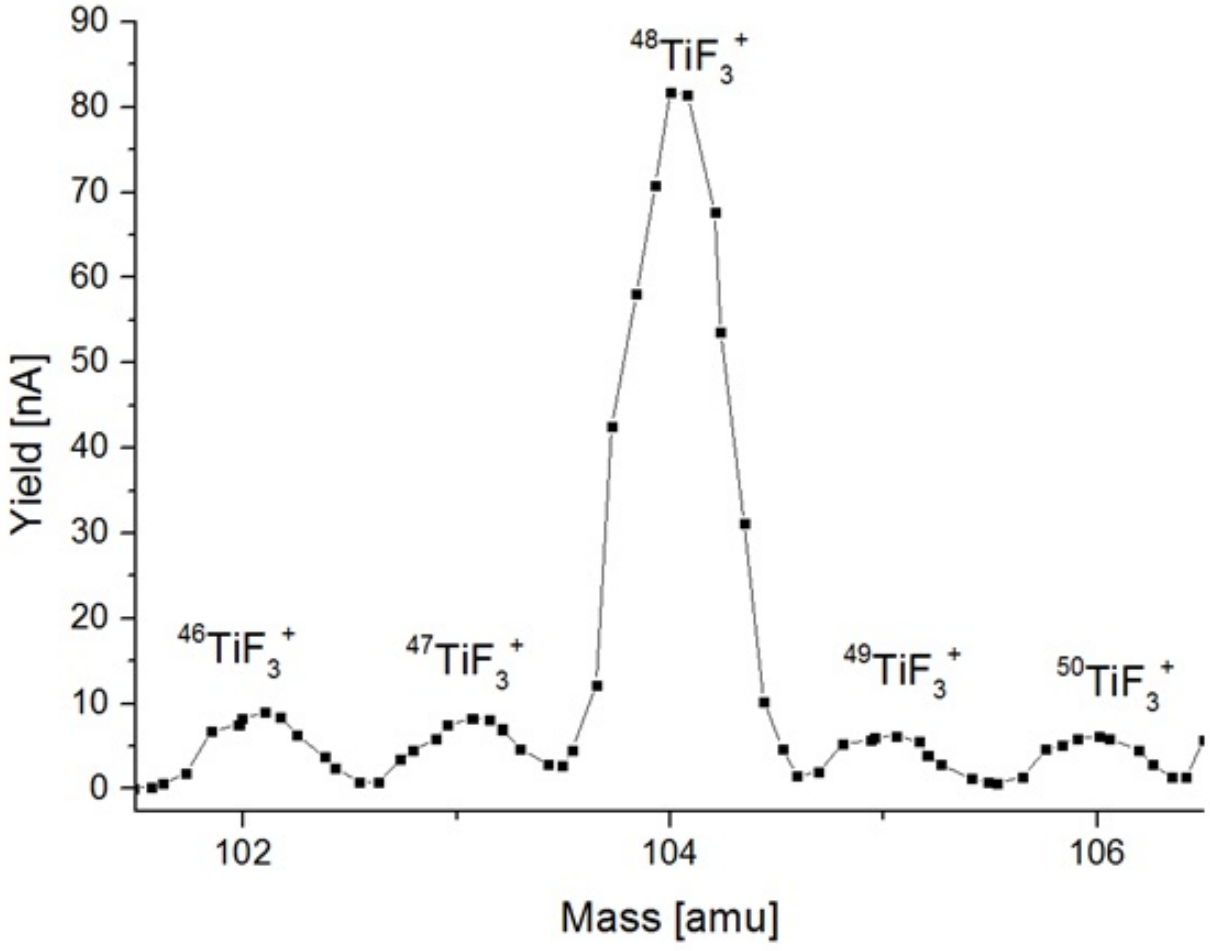

Figure 4.3.: Mass scan in the mass range of TiF_3^+. The isotope distribution of natural titanium is nicely visible ($^{46}Ti : 8\%, ^{47}Ti : 7.3\%, ^{48}Ti : 73.8\%, ^{49}Ti : 5.5\%, ^{50}Ti : 5.0\%$)

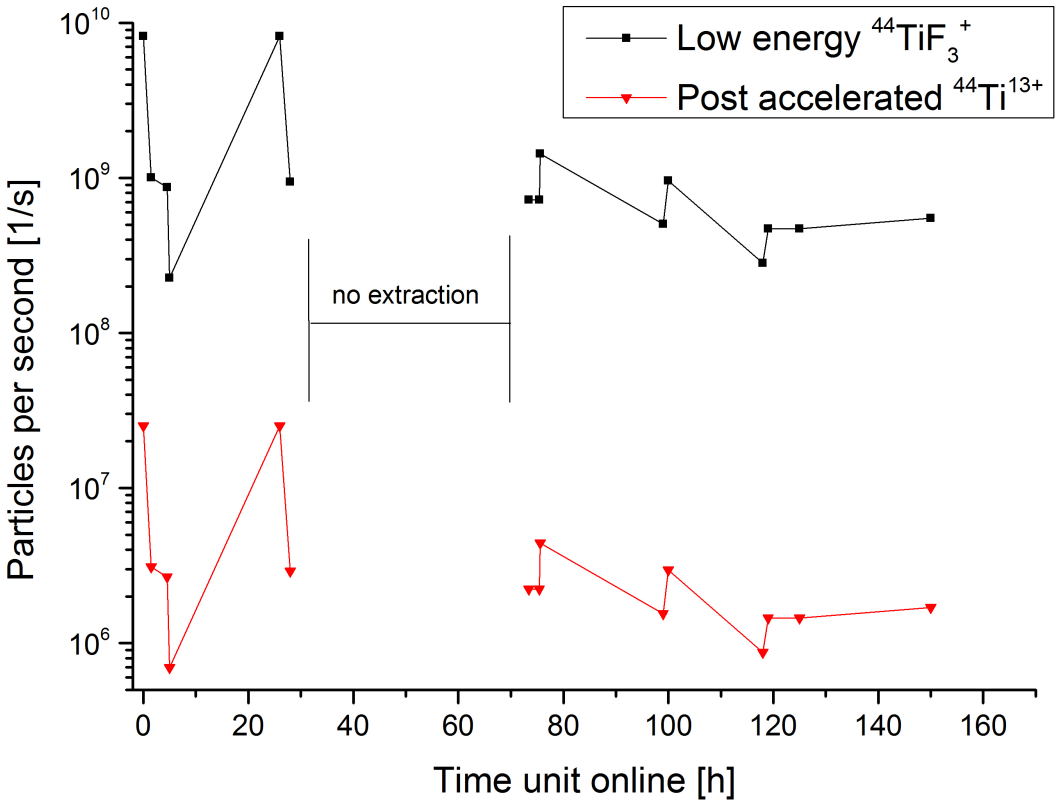

Figure 4.4.: Extracted yield of radioactive titanium ions. Plotted are the yields of $^{44}TiF_3^+$ and post accelerated $^{44}Ti^{+13}$ after REX-ISOLDE. During the charge breeding process molecules are dissociated [99].

4.2 Extraction of Tantalum

The extraction of radioactive isotopes of refractory metals such as tantalum, rhenium or tungsten from ISOL targets is confronted with similar problems as in the case of carbon and boron. High boiling points and chemical reactivity requires the extraction in molecular form. Radioactive isotopes of tantalum were extracted from a target using LuF_3 as tantalum fluoride and oxo-fluorides in 1982 at the ISOCELE facility [100] and the used technique of fluorination was further discussed and applied in several cases (e.g. [47] and [45]). However up to now no beams of radioactive tantalum were extracted at ISOLDE. Tantalum shares the refractory nature and chemical reactivity with other elements discussed within this thesis and in addition a relatively low number of potential target materials are suitable for its production. The extraction of TaF_n from a target utilizing $50\mu m$ tungsten foil was investigated in [42] but it was found that diffusion times are very long ($\approx 2h$).
Within the LIEBE [101] project a new target system for ISOLDE using an eutectic of lead and bismuth is currently under development. As both lead and bismuth are heavier than tantalum the production of radioactive tantalum is possible.
Calculations of the chemical equilibrium between lead, bismuth, tantalum and CF_4 show, that the formation of TaF_n is favored over the formation of lead- or bismuth-fluorides (compare figure 4.5). The calculation was carried out with a ratio of Ta:Pb:Bi:CF_4 of 1:100:100:10 at a pressure of 10^{-3} mbar.
Figure 4.5 shows that besides TaF_n lead fluorides are produced. This production takes place if a surplus of fluorine compared to tantalum is present in the target.
The dominantly formed lead fluoride species PbF_2 has a melting point of $824°C$ under normal conditions compared to operational temperatures of approximately $600°C$ of the target. The result of the calculation shows however that from approximately $600°C$ PbF_2 will transform to gaseous PbF_4. The precise behavior of liquid lead in combination with fluorine in an ISOLDE target system has to be investigated experimentally to make an extraction of radioactive tantalum feasible.

The same setup (compare 2.6) that was used to investigate the release of carbon oxides was used to study the response of the target system to injections of CF_4. The observation of several tantalum molecules, created by the reaction of CF_4 lead to the investigation on their release characteristics. Figure 4.6 shows the extracted amount of tantalum oxo-fluorides and CO, COF depending on the temperature of the target container. Molecules of TaF_n with n=1,2,3,4 were present as well, although in a lower amount.
In the present case formation of oxo-fluorides is favored, likely due to the presence of Ta as Ta_2O_5 on the container surface.

Besides measurements on the quantity, the time structure of the release was investigated. The results are presented in figure 4.7. The long release time for all molecules suggest that chemical reactions with relatively slow kinetics take place. Interesting is that release of the heavy ions $TaOF_2^+$ and $TaOF_3^+$ is much faster than the release of CO^+ and COF^+.
The reason for this difference is probably that the heavy tantalum molecules are an intermediate stage of a multistage chemical reaction from Ta_2O_5 and CF_4 to the reaction products.
Although times for molecule formation are long in comparison to other cases, a target unit designed for relatively quick diffusion of tantalum could allow the extraction of $^{168-186}Ta$ with half lives longer than 2 minutes as fluorides or oxo-fluorides.

4.3 Sulfur and Phosphorus

Sulfur and Phosphors have similar properties in terms of chemical reactivity as carbon and boron. Therefore the extraction from ISOL targets is very difficult. So far radioactive sulfur at ISOLDE is documented with $8 \cdot 10^3 \frac{1}{\mu C}$ ^{38}S only from a unit utilizing ZrO_2 fibers.
Phosphorus was extracted at GANIL after spallation of ^{36}Ar on a graphite target. The longer lived isotope

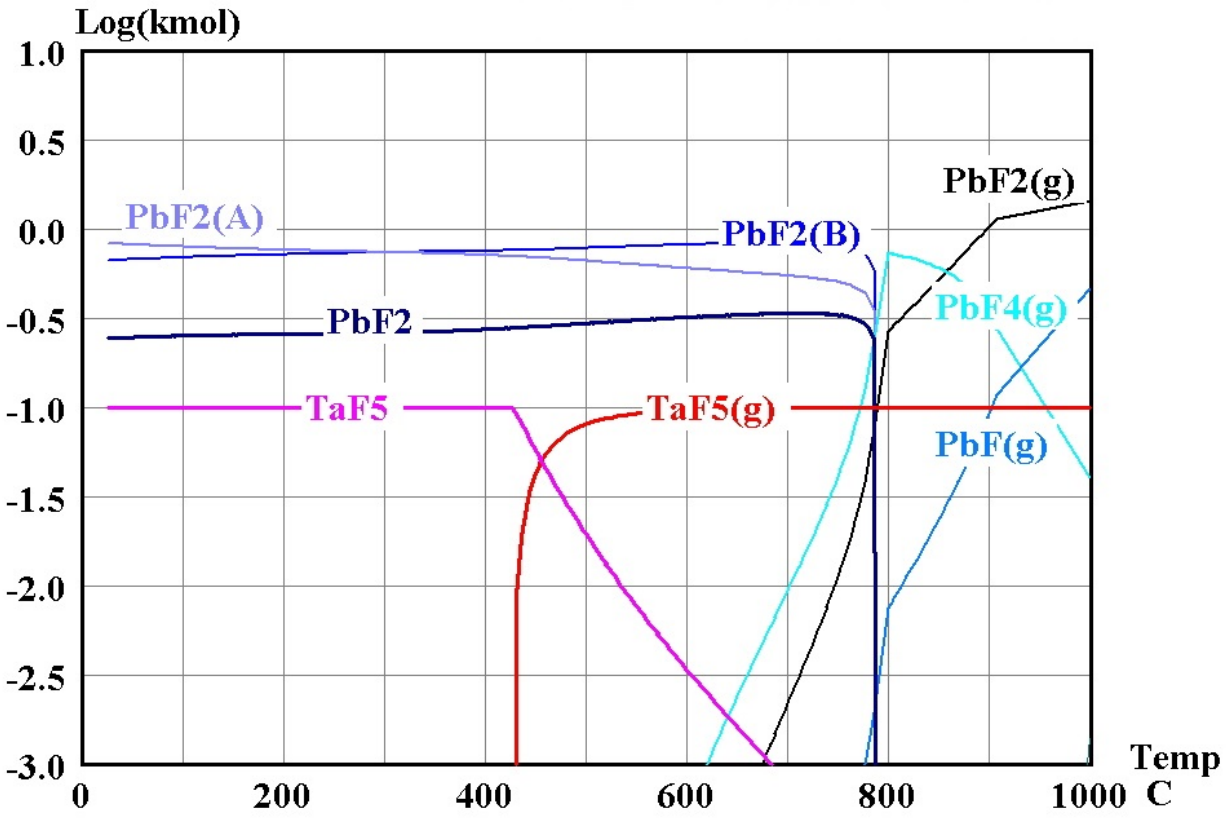

Figure 4.5.: Chemical equilibrium of Ta, Pb, Bi and CF_4 with ratios of 1:100:100:10. Although PbF_n molecules are shown, is the production of TaF_n favored. This is clear as all added Ta (here 0.1 kmole)can be found as fluoride. Only then lead fluorides starts to form.

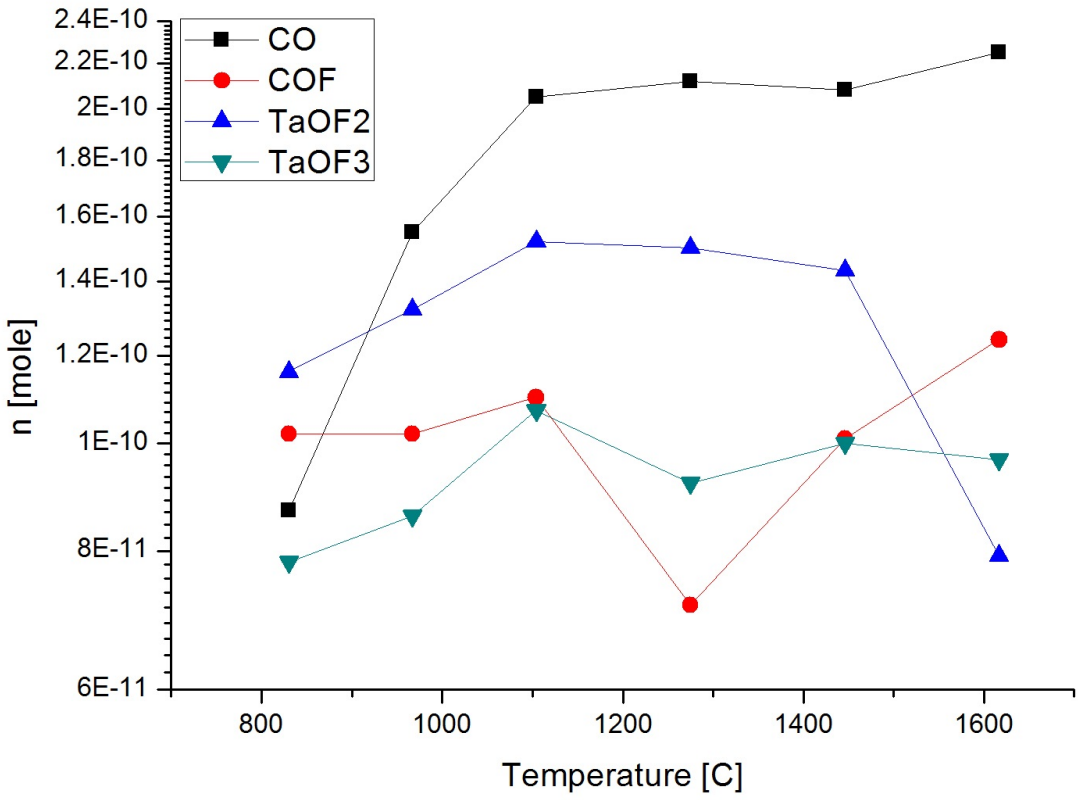

Figure 4.6.: Yields of $Ta_nO_mF_k$ molecules depending on target temperature.

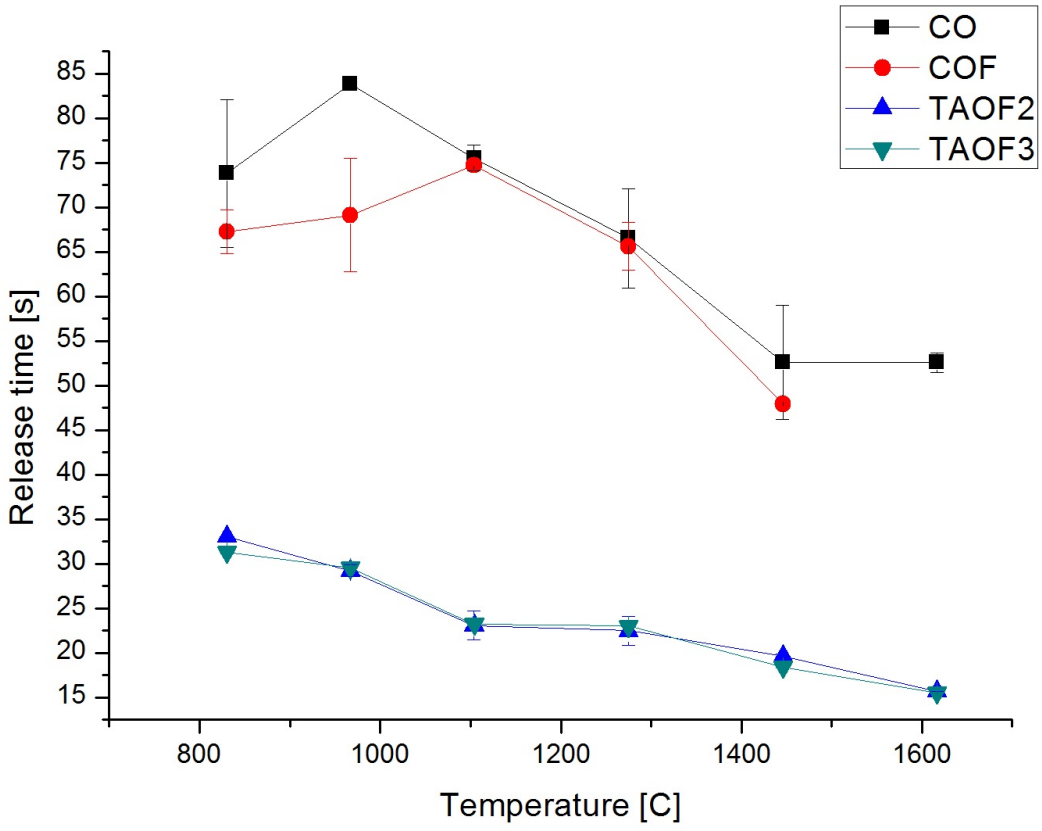

Figure 4.7.: Release time of tantalum and carbon molecules from an empty target container after the injection of CF_4.

Material	Formation of SO_2 ?	Comment
CaO	x	Formation of CaS
TiO_2	(✓)	Formation of TaS_2
Y_2O_3	x	Formation of TaS_2 and Y_2S_3
ZrO_x	x	Formation of TaS_2 and Zr_nS_m

Table 4.1.: Potential target materials for the extraction of sulfur. The chemical equilibrium between tantalum, sulfur and the target material was simulated for a temperature range of $T = 25°C$ to $2500°C$.

Material	Formation of PF_n ?	Formation of P_mO_n ?	Comment
CaF_2	x		
YF_3	x		
CaO		x	Formation of Ca_3P_2
Y_2O_3		x	
TiO_2		x	
ZrO_2		x	

Table 4.2.: List of considered target materials for the extraction of phosphorus as fluoride or oxide. The chemical equilibrium between tantalum, phosphorus and the target material was simulated for a temperature range of $T = 25°C$ to $2500°C$.

^{30}P ($t_{1/2} = 2.49$ min) with a current of $4.7 \cdot 10^6$ pps as $^{30}P^+$ and with a current of $3 \cdot 10^5$ pps as $^{30}PH^+$. Furthermore, ^{29}P with a half life of $t_{1/2} = 4.14$ s was extracted with a current of $2 \cdot 10^4$ pps as $^{29}P^+$ [102].

To produce beams of phosphorus and sulfur at ISOLDE, the extraction of molecules of these elements might be beneficial. For sulfur the extraction as SO_2 with a boiling point of $T_{boil} = -10°C$ seems to be a potential candidate.
In order to estimate which target materials would allow the extraction, calculations of the chemical equilibrium of oxides of Ca, Ti, Y and Yr with traces of sulfur were performed (see table 4.1).
The calculations show that from the considered materials only TiO_2 allows the extraction of S as SO_2. This however is only the case if no tantalum is present. Hence a substitution or coverage of the reactive tantalum surface with e.g. Alumina seems to be the only possibility for the extraction of sulfur isotopes.

Phosphorus forms bonds with fluoride and oxygen with relatively low boiling point compared to operational temperatures of ISOLDE targets. These molecules are PF_3 with a boiling point of $T_{boil} = -101.8°C$ and depending on the availability of oxygen P_2O_3 with $T_{boil} = -175.3°C$ and P_2O_5 with a boiling point of $T_{boil} = 360°C$.
Therefore possible target materials are metal oxides for the production of phosphorus oxides and fluorides for the extraction of phosphorus as a fluoride. The results are compiled in table 4.2. Unfortunately none of the calculated chemical equilibrium of the considered target material show a formation of phosphorus oxides or fluorides.

5 Summary and Outlook

In this work important phenomena for the extraction of carbon and boron in molecular form from ISOLDE target units were studied. The studies have been combined with former results.
The in-target production of carbon and boron was simulated using the EPAX [14], ABRABLA [13] and Fluka [15] code. Comparison of the results showed, that the production of exotic isotopes ^{9}C and $^{17-20}C$ is up to two orders of magnitude lower than formerly believed to be possible [51]. The same difference between the results of the two codes was found for the production of short lived isotopes of boron.
In order to succeed in the extraction of exotic carbon and boron the chemical reactivity of these elements needs to be considered. Therefore calculations of the chemical equilibrium between carbon, boron and materials used in ISOLDE targets were carried out using the HSC 7 [37] code. These calculations enable evaluation of materials and conditions that allow formation and extraction of carbon as carbon oxides and boron as boron fluorides. It was found that some oxide target materials (Y_2O_3, HfO_2) that have been used in the past for the production of beams of short lived carbon isotopes, do not allow a sufficient formation of carbon oxides. On the contrary, some other materials (CaO, TiO_2) were identified where the chemical equilibrium favors the formation of carbon oxides at operational temperatures. The results from the calculations of the chemical equilibrium explain measured yields of radioactive carbon oxide during former online measurements. While currents from units utilizing CaO are very high (e.g. ^{10}C: $I \approx 10^7\ 1/\mu C$) is the release from a similar setup but Y_2O_3 as a target material rather low (e.g. ^{10}C: $I \approx 10^4\ 1/\mu C$). The only difference between these units were the used target material and the operational temperature.

The results from the chemical equilibrium calculations were tested experimentally at the ISOLDE off-line mass separator. A target unit was equipped with a gas line, allowing the injection of gases into the target container. To test the impact of different materials on the release efficiency the inner side of the tantalum target container was covered with Re and Al_2O_3. It was found that the release efficiency of $^{13}CO_2{}^+$ originating from injected $^{13}CO_2$ varied between $7 \cdot 10^{-2} - 1 \cdot 10^{-4}$% for the plain tantalum container, $3 \cdot 10^{-2} - 1 \cdot 10^{-4}$% for the container covered with rhenium and $7 \cdot 10^{-2}$% for the container covered with alumina (Al_2O_3). Furthermore, the results indicate that released $^{13}CO^+$ originates from a chemical reaction of $^{13}CO_2$ with the molybdenum present in the ion source and subsequent ionization of ^{13}CO.
The same setup was used to test the formation and extraction of boron fluorides. Boron in the form of powder was inserted into the container and SF_6 injected through a calibrated leak. It was found that the combined efficiency for formation of BF_3, transport to the ion source and dissociative ionization to $BF_2{}^+$ is up to 1.5%. The extraction of $BF_2{}^+$ was used to implant ^{10}B as $^{10}BF_2{}^+$ into samples of target materials. The high neutron capture cross section of ^{10}B of $\sigma_{n_{th}} = 3840$ barn allowed studies of the diffusion of boron in the samples by monitoring alpha particles occurring from the reaction $^{10}B(n,\alpha)^7Li$ under irradiation with thermal neutrons. These measurements allowed the identification of multi-walled-carbon-nano-tubes as a suited material for the extraction of radioactive ^{8}B.
The same method was used to implant ^{10}B into aluminum foils which will be used for experiments at the SARAF facility in Israel.
Results from chemical equilibrium calculations, diffusion studies and release measurements for boron resulted in an on-line measurement where the extraction of radioactive ^{8}B was tested. The results indicate the first ever extraction of ^{8}B with $3 \cdot 10^2\ 1/\mu C$ at an ISOL facility. The relatively low yield and the absence of gamma emission from ^{8}B did not allow the definite identification of the isotope. This has to be done in the future by experimental setups sensitive to alpha or β^+ particles emitted from ^{8}B.

The experimental setup used for investigation of the dependency of the release efficiency on temperature and materials was also used to investigate the ionization behavior of carbon oxides, boron fluorides and noble gases in the equipped VADIS [32] ion source. The measurements confirmed results from simulations of the electron energy distribution inside the ion source.
The technique of extracting refractory elements as molecules was used for the production of a titanium fluoride beam. A sample of radioactive ^{44}Ti ($t_{1/2} = 63.3a$), produced at the Paul Scherrer Institute in Villigen, was inserted into an ISOLDE target unit. Injection of CF_4 allowed the formation and extraction of titanium as $^{44}TiF_3^+$, and a pure beam of $^{44}Ti^{+13}$ at REX-ISOLDE after break up of the molecule in the REX-Trap.

For the extraction of refractory species from ISOLDE target, the in-target and ion source chemistry seems to be one of the most important factors. In this work the chemistry of carbon oxides and boron fluorides with the target environment was studied. In the future release measurements from ISOLDE targets should include target materials. Doping a target material with the element of interest will allow to determine the impact of the target material on the molecule formation and test results from calculations of the chemical equilibrium. Investigating the formation of carbon oxides with CaO and Y_2O_3 would help to further understand results obtained during on-line measurements. Furthermore would tests of the formation and release of boron fluorides from carbon-nano-tubes under the injection of SF_6 allow to clarify if the absence of boron fluorides during the performed online measurements is caused by the used target material.
A precise knowledge of the electron energy distribution in the VADIS ion source would allow to exploit the source as a tool for the measurement of ionization potentials and ionization cross sections.

A Production cross sections

A.1 Carbon

Production cross section of carbon isotopes in target materials, calculated with EPAX [14] and ABRABLA [13] codes.

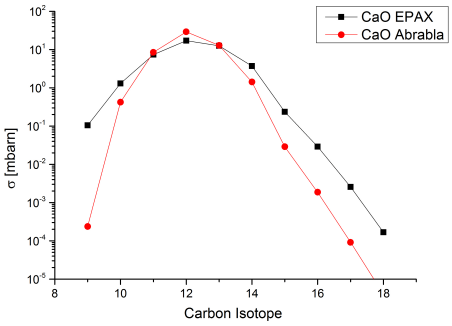

(a) CaO

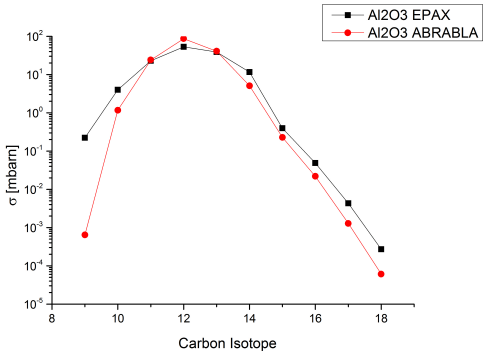

(b) Al2O3

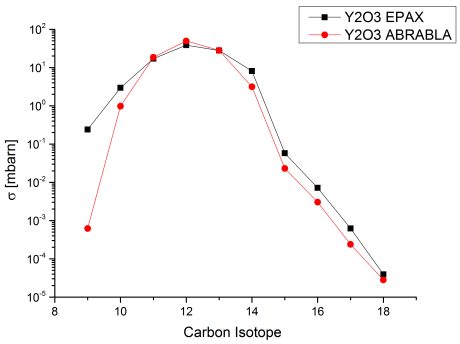

(c) Y2O3

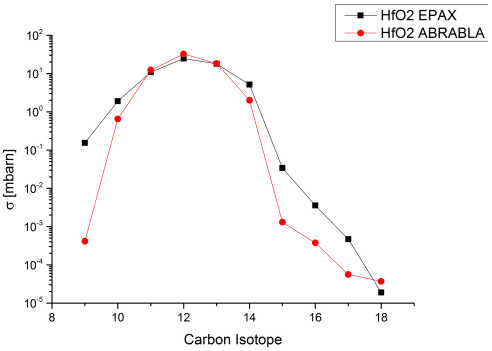

(d) HfO2

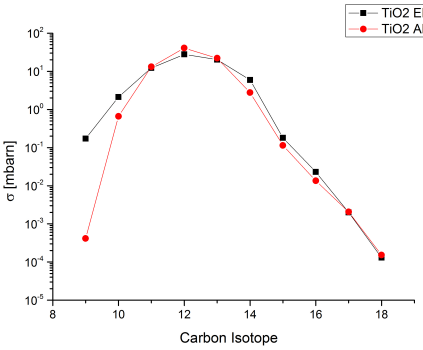

(e) TiO2

A.2 Boron

Production cross section of boron isotopes in target materials, calculated with EPAX [14] and ABRABLA [13] codes.

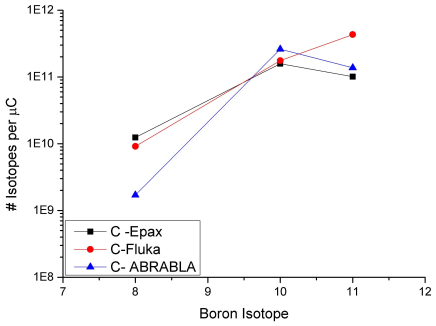

(a) Graphite

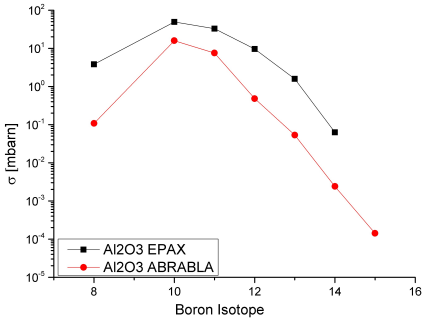

(b) Al2O3

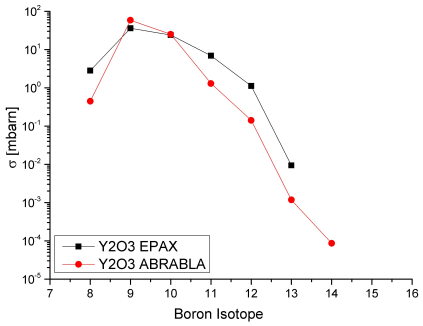

(c) Y2O3

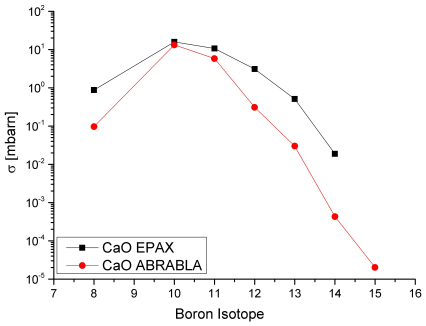

(d) CaO

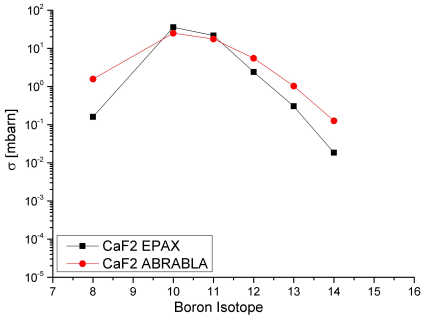

(e) CaF2

B Pressure dependency of chemical equilibrium calculations

Figure B.1 shows the result of the calculation of the chemical equilibrium between calcium oxide and carbon at three different pressures A: $p = 10^{-1}$ mbar,B: $p = 10^{-3}$ mbar and C: $p = 10^{-6}$ mbar.

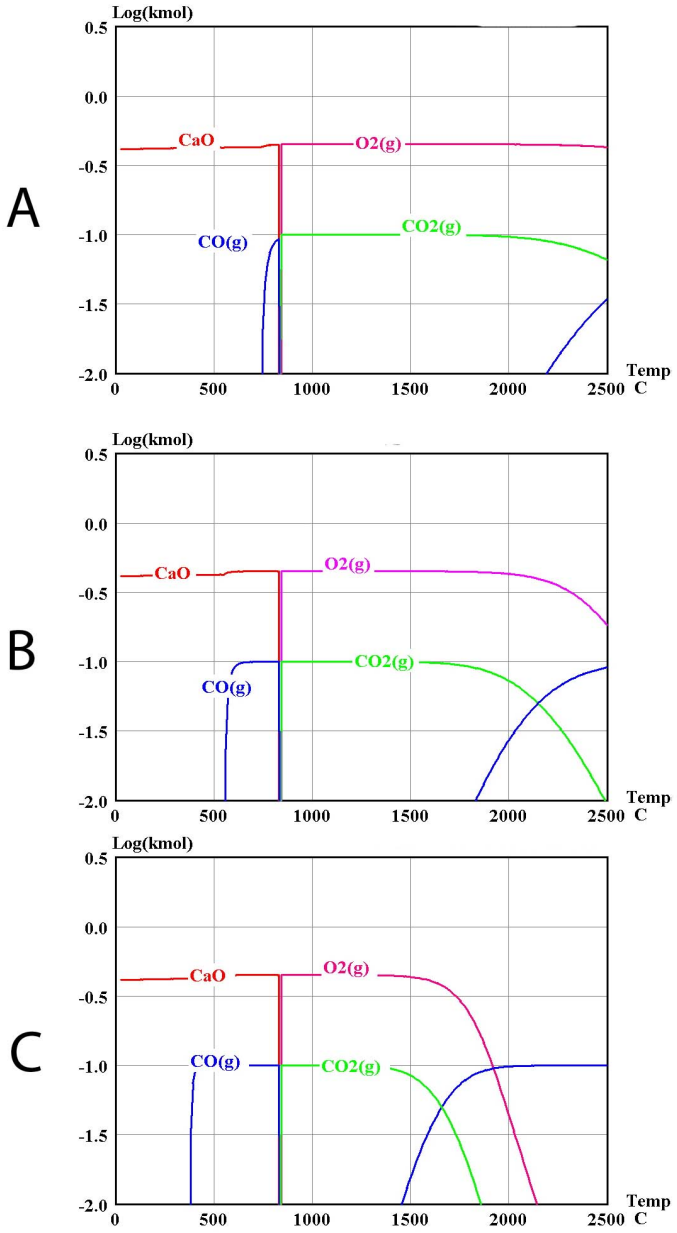

Figure B.1.: Results of chemical equilibrium calculation of CaO and carbon for A: $p = 10^{-1}$ mbar,B: $p = 10^{-3}$ mbar and C: $p = 10^{-6}$ mbar.

C Results Ionization Measurements and Linear Fit

Measurements of ionization behavior of different gases in a VADIS ion source and fit of the low energy part.

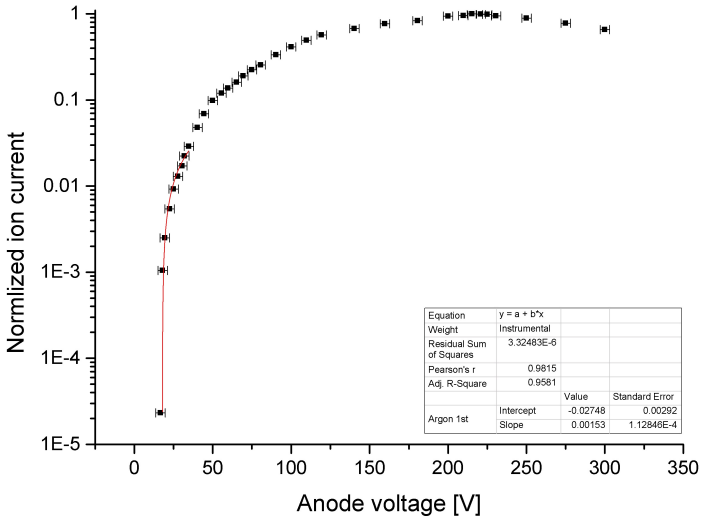

Figure C.1.: Argon

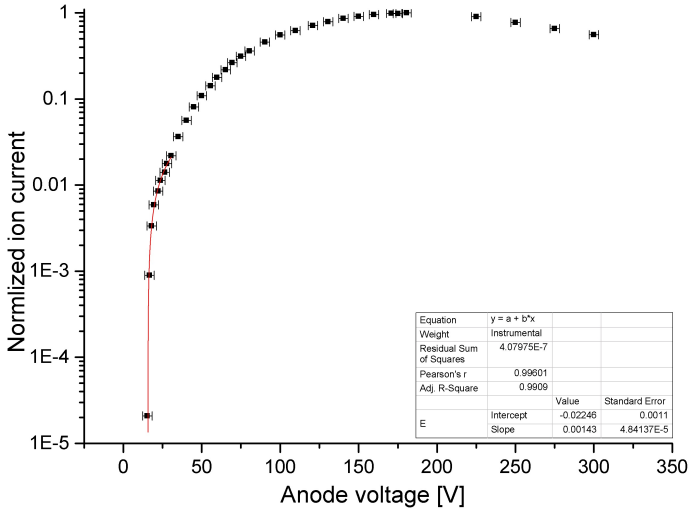

Figure C.2.: Krypton

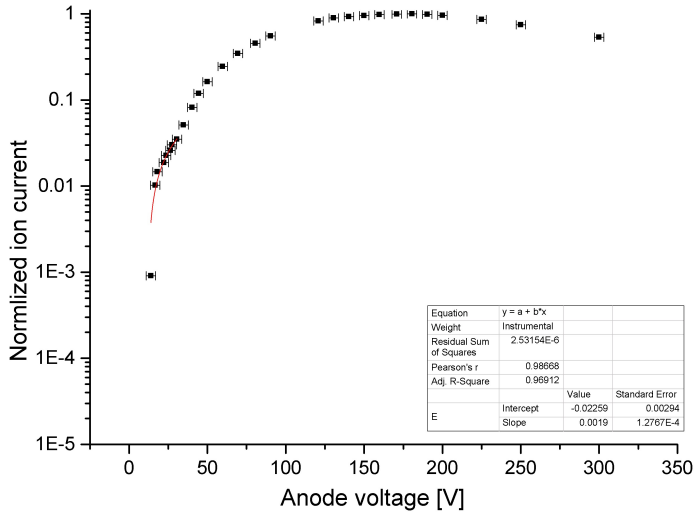

Figure C.3.: Xenon

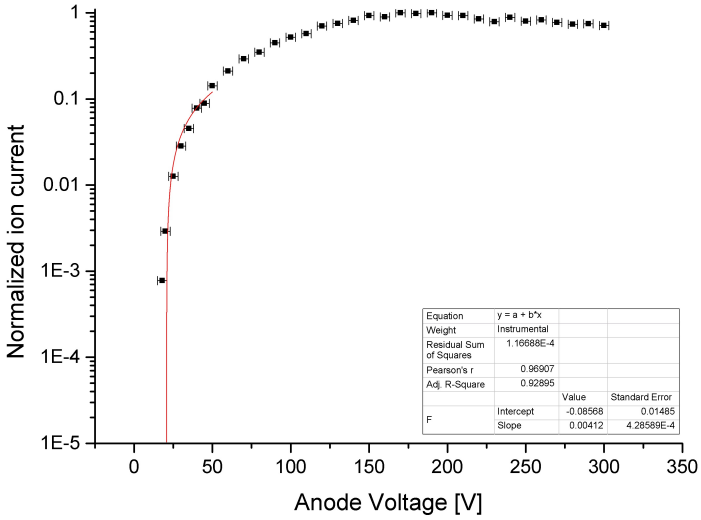

Figure C.4.: BF_2

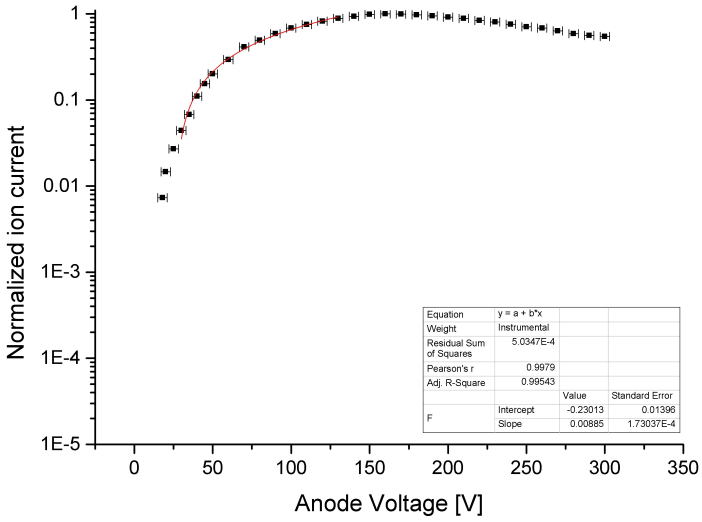

Figure C.5.: BF_3

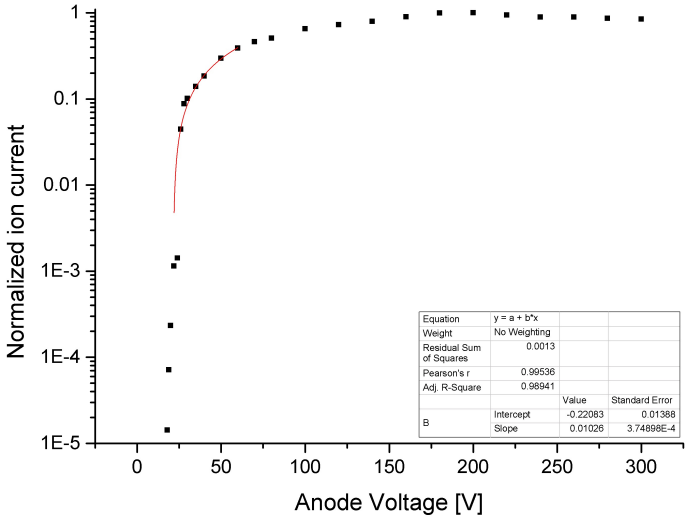

Figure C.6.: CO

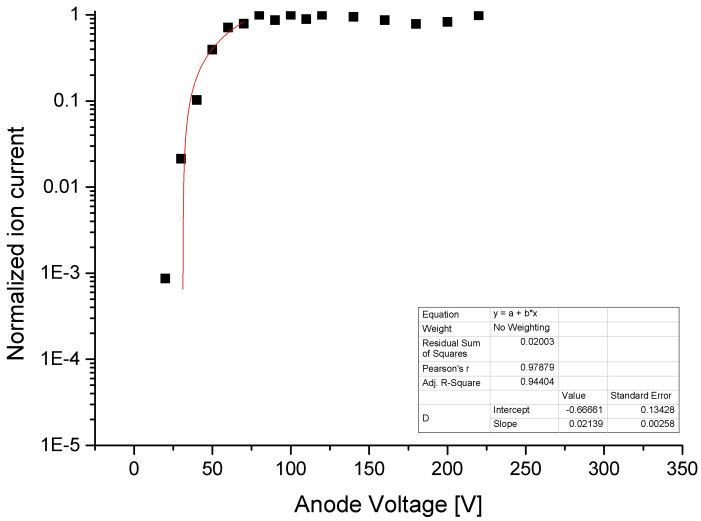

Figure C.7.: CO_2

Bibliography

[1] L. Dauer et. al. Radiation Safety Considerations for the Use of $^{223}RaCl_2$ in Men with Castration-resistant Prostate Cancer. Health Physics, 106, 2014.

[2] Y. Blumenfeld et. al. Facilities and methods for radioactive ion beam production. Physica Scripta, T152, 2013.

[3] Peter Dendooven. The development and status of the IGISOL technique. NIM B, 126:182–189, 1997.

[4] Juha Aysto. Development and applications of the IGISOL technique. Nuclear physics A, 693:477–494, 2001.

[5] M.A. Fraser. Status of the HIE-ISOLDE Project at CERN. Proceedings HIAT conference, 2012.

[6] R. York et. al. Technical Challanges in Design and Construction of FRIB. Proceedings of 2011 Particle Accelerator Conference, New York, NY, USA, pages 2561–2565, 2011.

[7] A.H.M. Evenson et. al. Release and yields from thorium and uranium targets irradiated with a pulsed proton beam. Nim B, 126:160–165, 1996.

[8] U. Köster. ISOLDE target and ion source chemistry. Radiochemica Acta, 89:749–756, 2001.

[9] U. Köster et. al. Oxide fiber targets at ISOLDE. NIM B, 204:303–313, 2003.

[10] G D Alton et. al. Criteria for selection of target materials and design of high efficiency release targets for radiactive ion beam generation. NIM A, 1999.

[11] O Alyakrinskiy et. al. Influence of grains size and porosity on the release of radioactive isotopes from target materials with high open porosity. NIM B, 267:2554–2558, 2009.

[12] E.Bouquerel et.al. Beam purification by selective trapping in the transfer line of an ISOL target unit. NIM B, 266:4298–4302, 2008.

[13] J.-J. Gaimard et. al. ABRA - improved version of the abrasion model for peripheral and mid-peripheral collisions of relativistic heavy ions. Nucl. Phys. A, 710, 1991.

[14] K. Sümmerer et. al. Target fragmentation of Au and Th by 2.6 Gev protons. Phys. Rev. C, 42:2546, 1990.

[15] www.FLUKA.org.

[16] V.Devanathan. Nuclear Physics. Alpha Science International Ltd, 2011.

[17] Brian Martin. Nuclear and Particle Physics: An Introduction. John Wiley & Sons, 2009.

[18] W.G. Lynch. Nuclear Fragmentation in Proton-and-Heavy Ion Induced Reaction. Ann. Rev. Nucl. Part. Sci, 37(493-535), 1987.

[19] Roque Malherbe. Adsorption and Diffusion in Nanoporous Materials. CRC Press, 2007.

[20] Julo de paula Peter Atkins. Physical Chemistry, 9th edition. Oxford University Press, 2010.

[21] Sandrine Fernandes. CERN-THESIS-2010-170. PhD thesis, 2010.

[22] Richard I. Masel. Adsorption and Reaction on solid surfaces. John Wiley & Sons, 1996.

[23] M. Santana-Leitner. A Monte Carlo code to optimize the production if radioactive ion beams by the ISOL technique. PhD thesis, TU Catalonia, Barcelona, 2005.

[24] Bilheux J.-C. et. al. Simulabeam of the effusive flow of reactive gases in tubular systems: radioactive ion beam applications. AIP Conf. Proc., 576:285, 2001.

[25] R Kirchner. On the thermoionization in hot cavities. NIM A, 292:203–208, 1990.

[26] Bernhard Wolf. Handbook of Ion Sources. CRC Press, 1995.

[27] http://environmentalchemistry.com.

[28] B.A. Marsh et. al. New developments of the insource spectroscopy method at RILIS-ISOLDE. Nuclear Instruments, 317:550–556, 2013.

[29] V. N. Fedosseev et. al. Upgrade of the resonance ioniozation laser ion source at ISOLDE on-line isotope separation facility: New lasers and new ion beams. Rev. Sci. Instruments, 83, 2011.

[30] Sebastian Rothe. Poster INPC: A complimentary Laser system for ISOLDE-RILIS, 2010.

[31] S. Sundell et. al. Ion source with combined cathode and transfer line heating. NIM B, 70:160–164, 1992.

[32] L. Penescu et. al. Development of high efficiency Versatile Arc Discharge Source at CERN-ISOLDE. Review of scientific instruments, 81, 2010.

[33] M.Kronberger et. al. Production of molecular sideband radioisotope beams at CERN-ISOLDE using a Helicon-type plasma ion source. EMIS contribution, 2012.

[34] Simon J. King et. al. Electron Ioniozation of CO_2. International Journal of Mass Spectrometry, 272:154–164, 2008.

[35] R. Locht et. al. The dissociative electroionization of carbon dioxide by low-energy electron impact. The C^+, O^+ and CO^+ dissociation channels. International Journal of Mass Spectrometry, 144:105–129, 1995.

[36] H.D. Smyth et. al. The Ionization of Carbon Dioxide by Electron Impact. Phys Rev, 36:472, 1930.

[37] http://www.hsc-chemistry.net.

[38] C.C.R.S. Rossi et.al. Gibbs free energy minimization for the calculation of chemical and phase equilibrium using linear programming. Fluid Phase Equilibria, 278(1–2):117 – 128, 2009.

[39] Ph. Dam et. al. A compact tape transport station for on-line studies of short-lived nuclides. NIM A, 161:427–430, 1979.

[40] R Kirchner. On the Release and ionization efficiency of catcher ion sources systems in isotope separation on-line. NIM B, 70:186–199, 1992.

[41] J. Lettry et. al. Pulse shape of the ISOLDE radiactive ion beams. NIM B, 126:130–134, 1997.

[42] U. Köster et. al. (Im)-possible ISOL beams. Eur. Phys special Topics, 150:285–291, 2007.

[43] K. Bächmann. Chemical Problems of the On-Line Separation of Short-Lived Nuclides. Forschungsbericht K70-28, BMBK-FB-L70-28, 1970.

[44] H.L.Ravn et. al. Target Techniques for the ISOLDE Online Isotope Separator. Nucl. Instr. Meth, 123:131–144, 1975.

[45] P Hoff et. al. Production of molecular ions in the integrated target/ion source of an isotope separation on line system. Nuclear instruments and methods, 172:413–418, 1980.

[46] Y. Kawase et. al. Fluorination method for the surface ionization of Sr and Ba with a helium-jet type ISOL. NIM B, 70:146–149, 1992.

[47] A. Kronenberg et. al. Molecular sideband of refractory elements for ISOL. NIM B, 266:4252–4256, 2008.

[48] R.Kirchner. Release studies of elementary and metal-fluoride ions at the GSI on-line mass separator. NIM B, 126:135–140, 1997.

[49] Yoichi KAWASE et. al. The Oxidation Technique for Efficient Ionization of Lanthanides by a Helium-Jet Loaded On-Line Isotope Separator. NIM B, 37-38:116–119, 1989.

[50] H.L.Ravn et. al. Bunched Release of Gaes from Oxide Targets. NIM B, 126:176–181, 1997.

[51] H. Franberg. Production of exotic, short lived carbon isotopes in ISOL-type facilities. CERN Thesis 2008-084-27-10-2008, 2008.

[52] T.M. Mendonca et. al. Production and release of ISOL beams from molten fluoride salt targets. NIM B, 329:1 – 5, 2014.

[53] U.C. Bergmann et. al. On the β decay of ^{9}C. Nuclear Physics A, 692:427–450, 2001.

[54] J.P Ramos et. al. Intense $^{31-35}Ar$ beams produced with a nanostructured CaO target at ISOLDE. NIM B, 320:83–88, 2014.

[55] M.Alcorta et. al. Experiments with the newly available Carbon beams at ISOLDE. Cern INTC 2006-011, 2006.

[56] M.N Rahaman. Ceramic Processing and Sintering. ISBN 0-8247-0988-8.

[57] A. Chrysanthou. The behaviour of tantalum in the presence of CO and CO/CO_2 mixtures at elevated temperatures. Materials Science & Engineering, 194:L11–L14, 1995.

[58] T.W. Haas et.al. Adsorption on Niobium(110), Tantalum (110), and Vanadium (110) Surfaces. The Journal of Chemical Physics, 46:3025–3033, 2007.

[59] V.D.Belov et. al. Cabon monoxide and Carbon Dioxide Interaction with Tantalum. Surface Science, 72:390–404, 1978.

[60] Badchenke S.G. et. al. High Temperature Reaction of Tantalum with Carbon Monoxide. Combusition, Explosion and Shock Waves, 26:726–731, 1991.

[61] Yasuo Fukuda et. al. XPS,UPS And TDS Study of Adsorption, Oxidation and Hydrogenation of CO on Rhenium. Surface Science, 93:338–350, 1980.

[62] John T. Yates et. al. Chemisorption on Rhenium: N_2 and CO. J. Chem. Phys., 51:334, 1969.

[63] Ch. Steinbruechl and R. Gomer. The Adsorption of CO on the (110) Plane of Tungsten: LEED, XPS, and Auger Measurements. Surface Science, 67:21–44, 1977.

[64] A.Degras and J. Lecante. Capture of carbon monoxide on nickel (110) and polycrystalline tungsten. Nuovo Cimento Suppl., 5:408–419, 1967.

[65] H.E. Farnsworth K. Hyek and R.L. Park. Interaction of oxygen, carbon monoxide and nitrogen with (001) and (110) faces of molybdenum. Surface Science, 10:429–445, 1968.

[66] Roman Bulanek et. al. Study of adsorption sites hetergeneity in zeolites by means of coupled microcalorimetry with volumetry. J. therm. Anal. Calorim., 105:443–449, 2011.

[67] Roman Bulanek et. al. Microcalorimetric and FTIR study of the adsorption of carbon dioxide on alkali-metal Exchanged Zeolites. Top. Catal., 53:1349–1360, 2010.

[68] D. Brennan et. al. The adsorption of Carbon Monoxide on Evaporated Metal Films. Physical Sciences, 258(1089):347–373, 1965.

[69] Y.K. Kim et. al. BEB. 2nd int Conf on Atom. Molec. Data and Their Applications, 543.

[70] www.nist.gov.

[71] I.Kanik et. al. Total Electron Scattering and ElElectron State Excitations Cross Sections for O_2, CO and CH_4. Journal of Geophysical Research, 98:7447–7460, 1993.

[72] Yukikazu Itikawa et. al. Cross Sections for Electron Collisions With Carbon Dioxide. J. Phys. Chem., 31:749–767, 2002.

[73] V. Margerin et. al. Study of the $^{44}Ti(\alpha,p)^{47}V$ reaction and implications for core collapse novae. Physical Letters B, 731:358–361, 2014.

[74] U. Koester et. al. Isol beams of hafnium isotopes and isomers. Eur. Phys. Jorunal on special Topics, 150:293–296, 2007.

[75] T.Roger et. al. Precise Determination of the Unpertubed ^8B neutrino Spectrum. PRL, 108, 2012.

[76] O.S. Kirsebom et. al. Precise and accurate determination of the ^8B decay spectrum. Phys Rev C, 83, 2011.

[77] A. Di Pietro et. al. Reaction mechanisms in collisions induced by a low energy ^8B beam. CERN-INTC 2010-063 / INTC I 126, 2010.

[78] M.G. Pellegriti et. al. Study of ^9C state by Inverse Kinematics Inelastic Scattering. ISOLDE INTC, 2010.

[79] J. Vacik et. al. On Boron Diffusion in MgF_2. Appl of Accl. in Research and Industry, 20th int conference, 2009.

[80] R.B. Sutton et. al. The Capture Cross Section of Boron for Neutrons of Energies from 0.01 eV to 1000 eV. Phys Rev, 71, 1972.

[81] F.J.Hambusch et. al. The $^{10}B(n,\alpha)^7Li$ and $^{10}B(n,\alpha\gamma)^7Li$ Li alpha-particle angular distributions, branching ratios and cross-sections measurements for $E_n \leq 3$ MeV. J. Phys.: Conf. Ser., 2010.

[82] M.E. Anderson and R.A. Neff. Neutron energy spectra of different size ^{239}Pu-Be neutron sources. Nuclear Instruments and Methods, 99(2):231 – 235, 1972.

[83] M. Edward Anderson and William H. Bond Jr. Neutron spectrum of a plutonium-beryllium source. Nuclear Physics, 43(0):330 – 338, 1963.

[84] Yu. V. Novak. Solid Fuel Ch, 16, 1982.

[85] R.Rejoub et. al. Determination of the absolute partial and total cross section for the electron-impact ionization of the rare gases. Phys Rev, 65, 2002.

[86] E. Krishnakumar et. al. Ionization cross sections of rare-gases atoms by electron impact. Journal of Physics B, 21, 1988.

[87] M. Farber et. al. Electron and Thermal dissociation of BF_3(g). J. Chem. Physics, 81, 1984.

[88] M.V. Kurepa et. al. Total Ioniozation and Dissociative attachement cross-sections of boron trifluoride by electron impact. J.Phys.D: Appl. Phys., 9, 1976.

[89] https://rex-isolde.web.cern.ch.

[90] M.Turrion et. al. Management of ISOLDE yields. NIM B, 266, 2008.

[91] R.N. Wolf et. al. ISOLTRAP's multi-reflection time-of-flight mass separator/spectrometer. International Journal of Mass Spectrometry, 349-350:123 – 133, 2013.

[92] D. Berkovits et. al. Measurements of Neutron Interactions With ^7Be and the Primordial ^7Li Problem. UConn-40870-00XX/, 2013.

[93] Claus Grupen. Astroparticle Physics. Springer, 2005.

[94] R.V. Wagoner. On the Synthesis of the Elements at Very High Temperatures. Astrophysical Journal, 148, 1967.

[95] Dorothea Schumann et. al. Radiochemical separation of ^7Be from the cooling water of the neutron spallation source SINQ at PS. Radiochim. Acta, 101, 2013.

[96] L.Weissmann et. al. The Status of the SARAF Linac Project. Proceedings of linear accelerator conference LINAC2010, 2010.

[97] S.Halfon et. al. High-power liquid lithium jet target for neutron production. Review of scientific instruments, 84, 2013.

[98] Rugard Dressler Marin Ayranov Schumann, T. Stowasser. Possibilities for the preparation of exotic radionuclide samples at PSI for scientific experiments. Radiochimica Acta, pages 501–508, 2013.

[99] O Kester et. al. Accelerated radioactive beams from REX-ISOLDE. NIM B, 204:20–30, 2003.

[100] C.F. Liang et. al. Selective On-Line Separation of new Ta, Zr and Sr Isotopes. Z. Phys A. -Atoms and Nuclei, 309, 1982.

[101] T. Stora. Recent developments of target and ion sources to produce ISOL beams. EMIS contribution, 2012.

[102] P. Jardin et. al. Latest results obtained at GANIL with new target-source systems dedicated to radioactive ion production. Review of scientific instruments, 75, 2004.

I would like to thank my supervisors Prof. Dr. Thorsten Kröll and Dr. Thierry Stora for accepting me as a PhD student and the supervision and guidance throughout the last years.
Alexander Gottberg, for a countless number of discussions and the help with the writing of this thesis.
The ISOLDE collaboration, especially Ricardo Dos Santos Augusto, Michal Czapski, Matthias Kronberger, Bruce Marsh, Tania Mendonca, Joao Pedro Ramos, Ralf Rossel, Sebastian Rothe and Frank Wienholtz.
Moshe Gai, for the interesting collaboration and the help with the experiment.
The members of the ISOLDE workshop and other specialists for their help, Ermanno Babero, Berhard Crepieux, Christophe Mitifiot, Michal Owen and Julien Parra-Lopez.
The radio protection team, DGS/RP-DC, for hosting my experimental setup and giving me the possibility to use the radioactive sources: Pierre Carbonez, Alix Chantelauze and Gilles Lagneau.
The Wolfgang-Gentner-Programme and Michael Hauschild, for the financial support. An dieser Stelle möchte ich meiner Familie für die Unterstützung während meines Studiums und der anschliessenden Promotion danken. Besonderer Dank gilt dabei meiner Mutter Ursula für die mentale Unterstützung und meinem Vater Wilfried, nach dessen Vorbild ich mich für ein naturwissenschaftliches Studium entschied.
I would like to thank all my friends, especially those at CERN, who made the time here such a great one.
Last but not least I would like to thank my girlfriend Lene for the support on various levels during the PhD and the great times we shared in the mountains. I am looking forward to the upcoming adventures with you.

Curriculum Vitae

Personal Information

Name:	Christoph Seiffert
Address:	An der Heppenmauer 17, 63619 Bad Orb
Date of Birth:	09.06.1983
Place of Birth:	Bad Nauheim, Germany
Nationality:	German
Email:	Christseiffert@Gmail.com
Parents:	Wilfried Seiffert
	Ursula Seiffert, née Häfner

Education

2011-2015:	PhD student at ISOLDE-CERN and TU Darmstadt Thesis Title: "Production of radioactive molecular beams for CERN-ISOLDE" Supervisors: Prof.Dr. Thorsten Kröll, TU Darmstadt, Dr. Thierry Stora, ISOLDE-CERN
2003-2010:	Studies in physics at University of Mainz Degree: Diplom Physiker Thesis Title: "Aufbau und Charakterisierung eines Triggerhodoskopes für das COMPASS Experiment" Supervisor: Prof.Dr. Michael Ostrick, University of Mainz
1999-2001:	Upper secondary school, Ludwig-Geissler-Schule Hanau